

國立交通大學

生物科技研究所

碩士論文

重組金屬乙炔苯酸紫質之人工肌紅蛋白系統對於光激發電子轉移機制的研究與其在生物性太陽能電池的應用

**Photo-Induced Electron Transfer Study of Free-base and Metallo Carboxyphenylethynyl Porphyrins Based Artificial Myoglobin Systems and Their Biosolar Cell Application**

研究生：胡禕庭

指導教授：吳東昆 博士

中華民國九十八年七月

重組金屬乙炔苯酸紫質之人工肌紅蛋白系統對於光激發電子轉移機制的研究與其在生物性太陽能電池的應用

**Photo-Induced Electron Transfer Study of Free-base and Metallo Carboxyphenylethynyl Porphyrins Based Artificial Myoglobin Systems and Their Biosolar Cell Application**

研究生：胡禕庭

Student: Yi-Ting Hu

指導教授：吳東昆 博士

Advisor: Prof. Tung-Kung Wu Ph.D



國立交通大學  
生物科技研究所  
碩士論文

A Manuscript of Dissertation  
Submitted to Department of Biological Science and Technology College of  
Biological Science and Technology  
National Chiao Tung University  
in partial Fulfillment of the Requirements for  
the Degree of Master of Philosophy  
in  
Biological Science and Technology Hsinchu,  
Taiwan, Republic of China

July, 2009

中華民國九十八年七月

# 重組金屬乙炔苯酸紫質之人工肌紅蛋白系統對於光激發電子轉移機制的研究與其在生物性太陽能電池的應用

## 中文摘要

肌紅蛋白是一個很適合用來了解光物理以及探討光催化電子轉移機制的生物系統，因為肌紅蛋白的血色素基口袋可以有效穩定中間輔基的氧化或還原態。而將人工合成的輔基重組進入肌紅蛋白中是一個嶄新的方式為蛋白質注入新的功能。為了模擬光合作用的機轉，我們設計一個更簡單的系統來模擬光合作用。我們將一系列不同金屬的光敏劑 metallo-5-(4-carboxy-phenylethynyl)-10,20-biphenylporphines (簡稱 MtPE1)重組到肌紅蛋白中防止自身聚集的現象以及延長在激發態的生命期。我們進行紫外光-可見光光譜、循環伏安法、螢光光譜、時間-解析螢光光譜、光化學還原法、光電流等的研究。在螢光生命期的比較，ZnPE1-Mb 以及 H<sub>2</sub>PE1-Mb 在緩衝溶液中的生命期比起在有機溶劑四氫呋喃 (THF) 中的 ZnPE1、H<sub>2</sub>PE1 有些微的增加。光化學還原是利用以肌紅蛋白重組 MtPE1 做為光敏劑，TEA 做為電子提供者，NADP<sup>+</sup> 為電子接受者所組成的簡單系統來比較不同金屬 MtPE1 以及 MtPE1-Mb 的轉換效率。在將 NADP<sup>+</sup> 還原成 NADPH 的效率上，以 H<sub>2</sub>PE1 與 ZnPE1 重組的肌紅蛋白相對於只以 H<sub>2</sub>PE1 與 ZnPE1 為光敏劑的轉換效率來說，約可提升兩倍的效率，我們推測蛋白質能有效穩定光敏劑的激發態並延長處於激發態的時間而提高轉換效率。我們也利用循環伏安法確認重組之 MtPE1-Mb 具有和 TEA 及 NADP<sup>+</sup> 可適當轉移電子的能階。最後，也試著建構一個以 MtPE1-Mb、TiO<sub>2</sub> 導電玻璃、電解液組合成能將光能轉成電能的生物太陽能電池。

# **Photo-Induced Electron Transfer Study of Free-base and Metallo Carboxyphenylethynyl Porphyrins Based Artificial Myoglobin Systems and Their Biosolar Cell Application**

## **Abstract**

Myoglobin (Mb) is a suitable model to understand the photophysical properties and photoinduced electron transfer mechanism, because of the heme pocket of Mb can stabilize the reduced and oxidized state of the prosthetic group. Reconstitution of an artificial prosthetic group into apo-myoglobin (apo-Mb) is a unique method for introducing a new chemical function into the protein. To mimic the function of photosynthetic system, we design a simple system. A series of different metallo-5-(4-carboxy-phenylethynyl)-10, 20-biphenylporphyrins, denoted as MtPE1 (used as photo-sensitizers) were reconstituted with apo-Mb to avoid self-aggregation and extend the lifetime of excited state. The photophysical properties of reconstituted Mb were examined by UV-Vis, CV, fluorescence spectra, time-resolved fluorescence spectroscopy, photochemical reduction, and photocurrent study. Fluorescence decay profiles of ZnPE1-Mb and H<sub>2</sub>PE1-Mb showed slightly increase by comparing with ZnPE1 and H<sub>2</sub>PE1 in THF. Photochemical reduction of nicotinamide adenine dinucleotide phosphate (NADP<sup>+</sup>) was studied by using MtPE1 reconstituted myoglobin (MtPE1-Mb) as a photosensitizer, and triethanolamine (TEA) as a sacrificial donor. This simple model system can let us to compare the conversion efficiency of MtPE1 and MtPE1-Mbs. H<sub>2</sub>PE1-Mb and ZnPE1-Mb exhibited 2-folds of photo-induced electron transfer efficiency than H<sub>2</sub>PE1 and ZnPE1 for converting NADP<sup>+</sup> to NADPH. The results showed that MtPE1 reconstituted with apo-Mb can stabilize the excited state and increase the conversion efficiency. We also confirmed that MtPE1-Mb have well-matched energy level of TEA and NADP<sup>+</sup> by CV analysis. At last, we try to combine MtPE1-Mb, TiO<sub>2</sub> film, and electrolyte to construct a biosolar cell with solar-electric energy converting ability.

## 謝誌(Acknowledgement)

首先，要感謝我的指導教授-吳東昆博士，在實驗的邏輯及觀念上給我許多啟發，以及給予我們這麼充裕的設備以及研究環境，在這兩年使我了解科學所要的堅持，也許在研究的路上並不是一帆風順，經驗的累積是無形的財富。除此之外，十分感謝李耀坤老師、刁維光老師、林敬堯老師、鄭建中老師在百忙之中撥空參加學生我的口試以及審定論文，使我的論文更為完整。

此外我要感謝帶我的學長豪哥，這兩年在我實驗上的幫忙以及鼓勵真的讓我獲益良多。程翔以及裕國學長總能在我實驗低潮時給我鼓勵，以及感謝實驗室的博班學長姐們，媛婷學姊、晉源、小紅、文鴻、Mili在實驗上以及生活上的幫忙以及指教。感謝已畢業的學長姐，宏城、宏明、小高、文祥、采婷、小妹、大景、皓宇、文瑄學姊在實驗上的細心指教。而一起打拚兩年的同學天昶、育勳、亦諄有你們一起砥礪彼此，有你們真好！也感謝學弟妹奕齊、青山、小花、靜婷有你們實驗室歡樂許多，也感謝專題生，孟儒、俞靜，也感謝合作實驗室的學長姐，駱立揚學長、德茹學姊、羅振夫學長在實驗上的幫忙，有大家的陪伴使我的實驗室多采多姿，也才能順利完成論文以及研究。

最後要感謝我家人的支持與鼓勵，你們永遠是我受挫折時的避風港，有你們的支持與鼓勵是我堅持下去的動力來源，有你們我才能順利完成學業，邁向下個階段，在此，謹以此論文獻給他們。

# Table of Contents

中文摘要.....	I
Abstract.....	II
謝誌(Acknowledgement) .....	III
Table of Contents.....	IV
Table of Figures .....	VI
1. Introduction .....	1
1.1 The global energy crisis .....	1
1.2 Techniques for converting sunlight into electricity.....	2
1.3 Natural photosynthesis mechanisms.....	4
1.3.1 Bacterial photosynthesis -Purple bacteria .....	4
1.3.2 Plant photosynthesis .....	6
1.3.3 The importance of protein scaffold in photosystem .....	8
1.4 Artificial photosynthesis.....	8
1.5 Biosolar cell.....	9
1.6 Myoglobin .....	11
1.6.1 Why is myoglobin? .....	13
1.6.2 Pigment (MtPE1).....	13
1.7 The application of myoglobin in electron transfer study.....	14
1.7.1 Myoglobin based triads .....	14
1.7.2 Photochemical reduction of NADP <sup>+</sup> by Zn-Mb as simple model of photosystem I.....	18
2. Specific aims .....	19
2.1 Reconstitution of MtPE1 with wild-type apo-Mb .....	19
2.2 Optic assay of reconstituted MtPE1-Mb (UV-Vis, fluorescent and TCSPC) .....	20
2.3 Electrochemistry assay of reconstituted MtPE1-Mb (CV).....	20
2.4 Photoirradiation assay of reconstituted MtPE1-Mb .....	20
2.5 Photoelectronics assay of reconstituted MtPE1-Mb (IV).....	21

3.	Experimental materials and procedures.....	23
3.1	Experimental materials.....	23
3.2	Experimental apparatus .....	24
3.3	Obtain wild type apo-Mb from myoglobin by Methyl ethyl ketone method .....	25
3.4	Reconstitution of apo-Mb with MtPE1 .....	25
3.5	Steady-state spectral measurements .....	26
3.6	Picosecond fluorescence decays.....	26
3.7	CV analysis and differential pulse voltammetry (DPV).....	26
3.8	Photoirradiation experiment.....	27
3.9	Photoelectrochemical measurements.....	27
4.	Result and discussion .....	28
4.1	Wild type apo-Mb purification.....	28
4.2	UV-Vis and fluorescence analysis.....	30
4.2.1	UV-Vis analysis results of reconstituted MtPE1-Mbs .....	30
4.2.2	Fluorescence analysis results.....	37
4.3	Picosecond fluorescence decays.....	41
4.4	Cyclic voltammetry measurement.....	45
4.4.1	Analyzed with cyclic and differential pulse voltammetry (CV and DPV).....	46
4.4.2	Energy level of electron donor and acceptor.....	51
4.5	Phototriggered chemical reduction result of MtPE1 and MtPE1-Mbs.....	52
4.6	Fluorescence analysis of ZnPE1-Mb before and after irradiation.....	70
4.7	Photocurrent assay result.....	72
5.	Conclusion and future perspectives.....	77
6.	References .....	80
7.	Appendix .....	83

## Table of Figures

Figure 1-1 About half of the incoming solar energy reaches the earth's surface. <sup>1</sup> .....	2
Figure 1-2 Major techniques for converting sunlight into electricity (Source: Yole developpement) .....	2
Figure 1-3 The working principle of DSSC. Photoexcitation of the sensitizer (S) is followed by electron injection into the conduction band of an oxide semiconductor film. The redox system regenerates the dye molecules, and the dye molecules are regenerated at the counter electrode by electrons passed through the load. Potentials are referred to the normal hydrogen electrode (NHE). <sup>3</sup> .....	3
Figure 1-4 Photoexcited electron transfer in the bacterial photosynthetic unit. LH-II contains two types of BChls: B800 (dark blue) and B850 (green), which absorb at 800 nm and 850 nm. BChls in LH-I absorb at 875 nm and labeled B875 (green). P <sub>A</sub> and P <sub>B</sub> refer to the RC special pair, and B <sub>A</sub> , B <sub>B</sub> refer to the accessory BChls in the RC. The figure demonstrates the coplanar arrangement of the B850 BChl ring in LH-II, the B875 BChl ring of LH-I, and the RC BChls P <sub>A</sub> , P <sub>B</sub> , B <sub>A</sub> , B <sub>B</sub> . <sup>4</sup> .....	5
Figure 1-5 (A) Three-dimensional structure of RC from <i>Rhodobacter sphaeroides</i> ( <i>Rb. S</i> ). The L, M and H subunits are shown as orange, green and blue ribbons. (B) Schematic of the cofactors arrangement and the photo-induced ET present in RC. <sup>5</sup> .....	6
Figure 1-6 Light-dependent reactions of photosynthesis at the thylakoid membrane.....	8
Figure 1-7 Schematic working principle of the RC based bio-photoelectric cell. The photoanode is ITO/WO <sub>3</sub> -TiO <sub>2</sub> /RC film and Pt as the counter-electrode. The electrolyte is pH 8.0 Tris-HCl buffer containing 8 mM sodium dithionite. a1: Vb of WO <sub>3</sub> , a2: Cb of WO <sub>3</sub> , b1: Vb of TiO <sub>2</sub> , b2: Cb of TiO <sub>2</sub> , c1: PBPheQ <sub>A</sub> Fe <sup>2+</sup> Q <sub>B</sub> , c2: P <sup>*</sup> BPheQ <sub>A</sub> Fe <sup>2+</sup> Q <sub>B</sub> , c3: P <sup>+</sup> BPhe <sup>-</sup> Q <sub>A</sub> Fe <sup>2+</sup> Q <sub>B</sub> , c4: P <sup>+</sup> BPheQ <sub>A</sub> <sup>-</sup> Fe <sup>2+</sup> Q <sub>B</sub> , c5: P <sup>+</sup> BPheQ <sub>A</sub> Fe <sup>2+</sup> Q <sub>B</sub> <sup>-</sup> . <sup>13</sup> .....	10
Figure 1-8 Illustration of the Phe-RC/WO <sub>3</sub> -TiO <sub>2</sub> PE and photo-induced ET. Cb, conduction band; Vb, valence band; P, BChl dimmer; BPhe, bacteriopheophytin; Phe, pheophytin; Q <sub>A</sub> , the primary quinone; Q <sub>B</sub> , the secondary quinone. <sup>13</sup> .....	10



Figure 1-9 Crystal structure of myoglobin and the prosthetic group, heme. ....	11
Figure 1-10 Schematic representation of myoglobin modifications. An artificial prosthetic group inserted into apomyoglobin.....	12
Figure 1-11 Structural diagram of PE1 porphyrins.....	13
Figure 1-12 Chemical structure of (1) $(\text{Fe}^{\text{III}}\text{OH}_2)\text{-Ru}^{2+}\text{-BXV}^{4+}$ and (2) $(\text{Zn})\text{-Ru}^{2+}\text{-BXV}^{4+}$ . The structure was composed by donor (metalo-proporphyrin)-sensitizer( $\text{Ru}(\text{bpy})_3$ )-acceptor(cyclobis(paraquat- <i>p</i> -phenylene) $\text{BXV}^{4+}$ ). <sup>24</sup> .....	14
Figure 1-13 Schematic illustration of the reconstitution of 1 and 2 with apo-Mb to afford the myoglobin-based triads, $\text{Mb}(\text{Fe}^{\text{III}}\text{OH}_2)\text{-Ru}^{2+}\text{-BXV}^{4+}$ and $\text{Mb}(\text{Zn})\text{-Ru}^{2+}\text{-BXV}^{4+}$ . <sup>24</sup> .....	15
Figure 1-14 (a) Energetics and selected pathways for $\text{Mb}(\text{Fe}^{\text{III}}\text{OH}_2)\text{-Ru}^{2+}\text{-BXV}^{4+}$ in buffer solution after excitation to the $\text{Ru}(\text{bpy})_3$ excited state. The energy of the excited $\text{Ru}(\text{bpy})_3$ component was calculated from the absorption and emission spectra of catenane 5. The energies of the various charge-separated states were estimated from the corresponding redox potentials of models for the components of $\text{Mb}(\text{Fe}^{\text{III}}\text{OH}_2)\text{-Ru}^{2+}\text{-BXV}^{4+}$ . The energy levels are not corrected for any Coulombic stabilization of the intermediates. (b) Energy levels of the locally excited state of the $\text{Ru}^{2+}(\text{bpy})_3$ moiety and the hypothetical ion-pair states of $\text{Mb}(\text{Zn})\text{-Ru}^{2+}\text{-BXV}^{4+}$ and the pathways available for their interconversion. For comparison purpose, the excited states of ZnPP are not present. <sup>24</sup> .....	16
Figure 1-15 UV–visible spectral change for 10 mM of Zn–Mb, 1 M of TEA, and 1 mM of $\text{NADP}^+$ in 10mM of phosphate buffer (pH 9.0). (a) Before irradiation. (b) After 3.5 h of irradiation with visible light ( $\lambda > 390$ nm) at an intensity of 2.8 mW. Following the irradiation, spectra were measured after 1 (c), 2 (d), 3 (e), 6 (f), and 9 (g) days in the dark under an atmosphere of $\text{N}_2$ .....	18
Figure 2-1 A typical current-voltage curve. This maximum current is called the short circuit current, abbreviated $I_{\text{sc}}$ . When the module is shorted, the voltage in the circuit is zero. Conversely, the maximum voltage is produced when there is a break in the circuit. This is called the open circuit voltage, abbreviated $V_{\text{oc}}$ . Under this condition the resistance is infinitely high and there is no current, since the circuit is incomplete.	

These two extremes in load resistance, and the whole range of conditions in between them, are depicted on a graph called a I-V (current-voltage) curve. Current, expressed in amps, is on the vertical Y-axis. Voltage, in volts, is on the horizontal X-axis ..... 21

Figure 4-1 UV-Vis results : To confirm that heme has been removed by MEK method..... 29

Figure 4-2 SDS-PAGE result: To confirm apo-Mb in each steps (a) Lane 1: Apo-Mb (b) Lane 2: commercial myoglobin (c) Lane 3: Apo-Mb before dialysis (d) Lane 4: Apo-Mb after dialysis..... 29

Figure 4-3 Absorption spectra of ZnPE1-Mb in KPi solution with B (Soret) and Q bands. .... 30

Figure 4-4 Normalized steady-state absorption spectra of H<sub>2</sub>PE1 in THF, KPi buffer and reconstituted with apo-Mb in KPi. .... 32

Figure 4-5 Normalized steady-state absorption spectra of CoPE1 in THF, KPi buffer and reconstituted with apo-Mb in KPi. .... 32

Figure 4-6 Normalized steady-state absorption spectra of NiPE1 in THF, KPi buffer and reconstituted with apo-Mb in KPi. .... 33

Figure 4-7 Normalized steady-state absorption spectra of CuPE1 in THF, KPi buffer and reconstituted with apo-Mb in KPi. .... 33

Figure 4-8 Normalized steady-state absorption spectra of ZnPE1 in THF, KPi buffer and reconstituted with apo-Mb in KPi. .... 34

Figure 4-9 The emission spectra of H<sub>2</sub>PE1 and MtPE1 (Co, Ni, Cu, Zn) in THF..... 37

Figure 4-10 The steady-state emission fluorescence spectra of MtPE1 by exciting at 435 nm. (a) H<sub>2</sub>PE1 (b) CoPE1 (c) NiPE1 (d) CuPE1 (e) ZnPE1 ..... 38

Figure 4-11 The emission spectra of 2.5 μM MtPE1-Mb in 100 mM Kpi. .... 39

Figure 4-12 The steady-state emission fluorescence spectra of MtPE1-Mb by exciting at 435 nm. (a)H<sub>2</sub>PE1-Mb (b)CoPE1-Mb (c)NiPE1-Mb (d)CuPE1-Mb (e)ZnPE1-Mb ..... 40

Figure 4-13 The relationship between protein concentration and fluorescence intensity in 100 mM KPi buffer.

Obtain fluorescence intensity at  $\lambda_{em}=630nm$  (Co, Ni, Cu, Zn) and  $\lambda_{em}=668 nm$  (H<sub>2</sub>) with excitation at  $\lambda_{ex}=435$

nm.....	42
Figure 4-14 Picosecond fluorescence transients of reconstituted MtPE1-Mb in buffer solution with $\lambda_{ex} = 435$ nm at $\lambda_{em} = 630$ nm (Co, Ni, Cu, Zn) and $\lambda_{em} = 668$ nm ( $H_2$ ).....	43
Figure 4-15 Chemical structure of DDAB .....	45
Figure 4-16 Cyclic and differential pulse voltammetry (CV and DPV) analysis for wild type Myoglobin .....	47
Figure 4-17 C-V and differential pulse for $H_2$ PE1-Mb .....	48
Figure 4-18 C-V and differential pulse for CoPE1-Mb .....	48
Figure 4-19 C-V and differential pulse for NiPE1-Mb .....	49
Figure 4-20 C-V and differential pulse for CuPE1-Mb .....	49
Figure 4-21 C-V and differential pulse for ZnPE1-Mb .....	50
Figure 4-22 CV analysis of (A) 2.5 mM $NADP^+$ in 10 mM KPi (B) 1 M TEA in 10mM KPi.....	51
Figure 4-23 The energy diagram of TEA, $NADP^+$ , $H_2$ PE1-Mb, NiPE1-Mb, CuPE1-Mb, ZnPE1-Mb.....	52
Figure 4-24 Absorbance change in the solution containing 10 $\mu$ M (A) $H_2$ PE1-Mb (B) CoPE1-Mb (C) NiPE1-Mb (D) CuPE1-Mb (E) ZnPE1-Mb, 1 M TEA , and 5 mM $NADP^+$ in 100 mM KPi buffer after 5 hours irradiation. ....	55
Figure 4-25 Absorbance change in the solution containing (A)10 $\mu$ M apo-Mb (B) no photosensitizer, 1 M TEA , and 5 mM $NADP^+$ in 100 mM KPi buffer after 5 hours irradiation.....	56
Figure 4-26 Absorbance change for three kinds of condition: MtPE1-Mb/TEA/ $NADP^+$ , MtPE1-Mb/TEA/ $NADP^+$ without irradiation and kept in the dark for 5 days, MtPE1-Mb/TEA/ $NADP^+$ irradiated 5 h and kept in the dark for 5 days.....	57
Figure 4-27 Absorbance change at 340 nm in the solution containing 10 $\mu$ M of (a) $H_2$ PE1-Mb (b) CoPE1-Mb (c) NiPE1-Mb (d) CuPE1-Mb (e) ZnPE1-Mb, 1 M TEA and 5 mM $NADP^+$ after 5 h irradiation. ....	58
Figure 4-28 Four kinds of reaction conditions. (A) $NADP^+$ was mixed with ZnPE1-Mb in photoirradiated process without TEA and then TEA was added in the dark reaction, (B) ZnPE1-Mb was photoirradiated without TEA and $NADP^+$ , and then TEA and $NADP^+$ were added in the dark reaction, (C) TEA was mixed with ZnPE1-Mb in photoirradiated process and then $NADP^+$ was added in the dark reaction, and (D) ZnPE1-Mb,	

TEA and NADP<sup>+</sup> were mixed and photoirradiated simultaneously. The experiment was carried out at with 10 μM of ZnPE1-Mb, 1 M of TEA, and 5 mM of NADP<sup>+</sup> in a 100 mM phosphate buffer (pH 9.2)..... 59

Figure 4-29 (A)Comparing the peak shift of ZnPE1-Mb after 12 h irradiation in different conditions, including ZnPE1-Mb only, ZnPE1-Mb/TEA, ZnPE1-Mb/NADP<sup>+</sup>, and ZnPE1-Mb/TEA/NADP<sup>+</sup>. (B) Magnify of Soret band..... 60

Figure 4-30 UV-Visible spectral change for 10 μM MtPE1-Mb, 1 M of TEA, and 5 mM of NADP<sup>+</sup> in 100 mM phosphate buffer (pH 9.2) upon continuous photoirradiation. (A) ZnPE1-Mb, (B) H<sub>2</sub>PE1-Mb, (C) CoPE1-Mb, (D) NiPE1-Mb, and (E) CuPE1-Mb..... 62

Figure 4-31 Absorbance change at 340 nm of the solution containing 10 μM (a) H<sub>2</sub>PE1-Mb, (b) CoPE1-Mb, (c) NiPE1-Mb, (d) CuPE1-Mb, and (e) ZnPE1-Mb, 1 M of TEA, 5 mM of NADP<sup>+</sup> upon continuous photoirradiation. .... 62

Figure 4-32 UV-Visible spectral change of (A) H<sub>2</sub>PE1-Mb, (B) ZnPE1-Mb, (C) CoPE1-Mb, (D) NiPE1-Mb, and (E) CuPE1-Mb and TEA were photoirradiated for 5 h then added NADP<sup>+</sup> to keep in the dark for 5 days..... 63

Figure 4-33 Absorbance change at 340 nm, (A) H<sub>2</sub>PE1-Mb, (B) ZnPE1-Mb, (C) CoPE1-Mb, (D) NiPE1-Mb, and (E) CuPE1-Mb and TEA were photoirradiated for 5 h then added NADP<sup>+</sup> to keep in the dark for 5 days.... 64

Figure 4-34 UV-Visible spectral change for 10 μM MtPE1, 1 M of TEA, and 5 mM of NADP<sup>+</sup> in 100 mM phosphate buffer (pH 9.2) upon 5 h photoirradiation. (A) H<sub>2</sub>PE1, (B) CoPE1, (C) NiPE1, (D) CuPE1 and (E) ZnPE1..... 65

Figure 4-35 Absorbance change at 340 nm contains 10 μM MtPE1, 1 M of TEA, and 5 mM of NADP<sup>+</sup> in 100 mM phosphate buffer (pH 9.2) upon 5h photoirradiation. (A) H<sub>2</sub>PE1, (B) CoPE1, (C) NiPE1, (D) CuPE1, and (E) ZnPE1..... 66

Figure 4-36 Absorbance change in the solution containing 0.625, 2, 5, and 10 μM of ZnPE1-Mb, 1M of TEA, and 5mM of NADP<sup>+</sup> in 100mM phosphate buffer (pH 9.2) upon 5 h photoirradiation. (Appendix 1)..... 67

Figure 4-37 Test of TEA effect. (A) Similar experiment as Fig.4-24, but changed the concentration of TEA. (B) Combined overall efficiency after 5 days of different concentration TEA. (Appendix 2)..... 68

**Figure 4-38** The difference of fluorescence emission spectra for ZnPE1-Mb in variety condition: before (A) and after (B) photoirradiated with  $\lambda_{ex} = 340$  nm..... 70

**Figure 4-39** Fluorescence emission comparison of variety condition, including 100 mM KPi, 1M TEA, 2.5 mM NADP<sup>+</sup>, 2.5 mM NADPH, NADP<sup>+</sup>+TEA. .... 71

**Figure 4-40** The emission intensity of different concentration NADPH..... 71

**Figure 4-41** UV-vis absorption spectra of MtPE1-Mbs on TiO<sub>2</sub> film ..... 72

**Figure 4-42** The photovoltaic characteristics of (A)H<sub>2</sub>PE1-Mb, (B)CoPE1-Mb, (C)NiPE1-Mb, (D)CuPE1-Mb, and (E)ZnPE1-Mb –sensitized solar cells. All measurements were performed under AM1.5 illumination (100 mW cm<sup>-2</sup>). For comparison, the individual blank TiO<sub>2</sub> films before sensitization are shown as red curves... 75



# 1. Introduction

## 1.1 The global energy crisis

Abundant energy is indispensable for modern civilizations. But the energy crisis has become the most important issue in nowadays. Some investigations point out that the supply of oil and natural gas will be unable to keep up for demand, and the production of oil and natural gas would be shortage at 2015. We need alternative energy urgently. Alternative energy we need is not based on the burning of fossil fuels or the splitting of atoms which will cause undesirable effects of pollution, such as greenhouse effect and nuclear waste, etc. Fortunately there are many means of harnessing energy which have less damaging impacts on our environment.

The sun supply Earth with a steady stream of energy. The total solar energy absorbed by Earth's atmosphere, oceans and land masses is approximately 3,850,000 exajoules (EJ) per year.(Fig.1-1)<sup>1</sup> The amount of solar energy reaching the surface of the planet is so vast that in one year it is about twice as much as will ever be obtained from all of the Earth's non-renewable resources of coal, oil, natural gas, and mined uranium combined. No other energy supply could conceivably be as plentiful as the 120,000 terawatts the sun provides ceaselessly and unbidden. <sup>2</sup>

If we could convert sun energy into useful forms, the reliance on fossil fuels and nuclear power don't be needed. And the production of climate-change agents and hazardous waste materials could be substantially reduced. The question is how can all of this freely available solar energy be captured and transformed into useful energy forms?

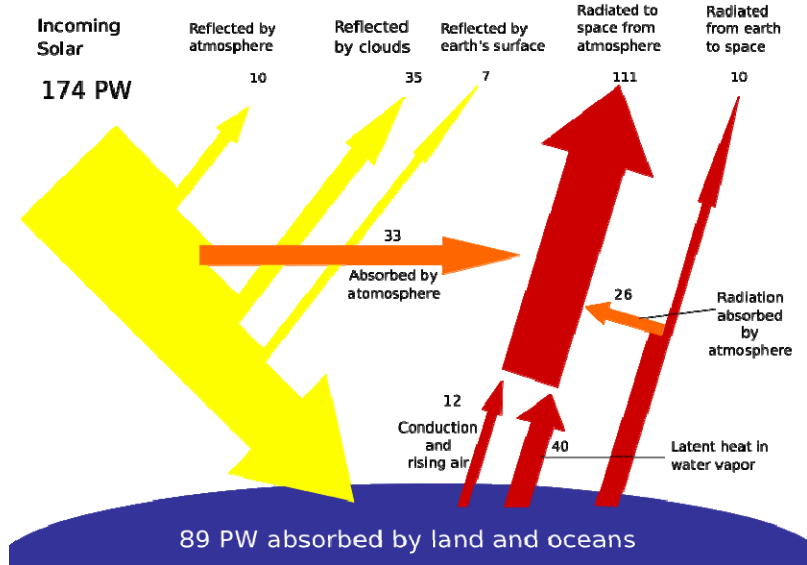


Figure 1-1 About half of the incoming solar energy reaches the earth's surface.<sup>1</sup>

## 1.2 Techniques for converting sunlight into electricity

Solar photovoltaic cells capture the light energy and convert it into electric power, are one of the most promising devices for sustainable and renewable sources of clean energy. Now, solar cells are classified into three developing directions: (1) silicon based, (2) chemical based, and (3) new materials in the field of solar cell research. (Fig.1-2)

	2008	2010 status	2015 status
Si Wafer based (Mono and Polycrystalline)	Mass production		
Amorphous (a-Si)	Mass production		
Tandem a-Si / Si Crystalline	Mass production		
Thin film Si Crystalline	Industrial research	Mass production	
CIS / CIGS	Mass production		
CdTe	Mass production		
III V	Industrial research on concentrator; Mass production for cells	Mass production	
Dye Sensitized	Industrial research and pilot plant	Mass production	
Full Organic	Experimental research	Industrial research and pilot plant	Mass production
Hybrid	Experimental research	Industrial research and pilot plant	Mass production

Figure 1-2 Major techniques for converting sunlight into electricity (Source: Yole development)

Among them, the operational principle of dye sensitized solar cell (DSSC) is given in fig. 1-3.<sup>3</sup> The DSSC consists of photoactivated-dye, mesoscopic oxide semiconductor ( $\text{TiO}_2$ ,  $\text{ZnO}$ ,  $\text{Nb}_2\text{O}_5$ ), redox electrolyte or an organic hole conductor (usually  $\text{I}^-/\text{I}_3^-$  in acetonitrile), conducting glass (usually ITO, FTO) and cathode (Pt). Monolayer photo-sensitized dye is absorbed on the surface of the nanocrystalline film and immersed in a redox mediator. When the dye is excited by incoming light to become excited state (electron + hole); the electron is injected into the conduction band of the semiconductor, while the hole remains on the dye, which gets into an oxidized state (missing an electron). The redox electrolyte provides electron to the dye, and gets oxidized in turn. The electron in the semiconductor is injected into the anode. And electrolyte regenerate at the counter electrode by electrons passed through the load.

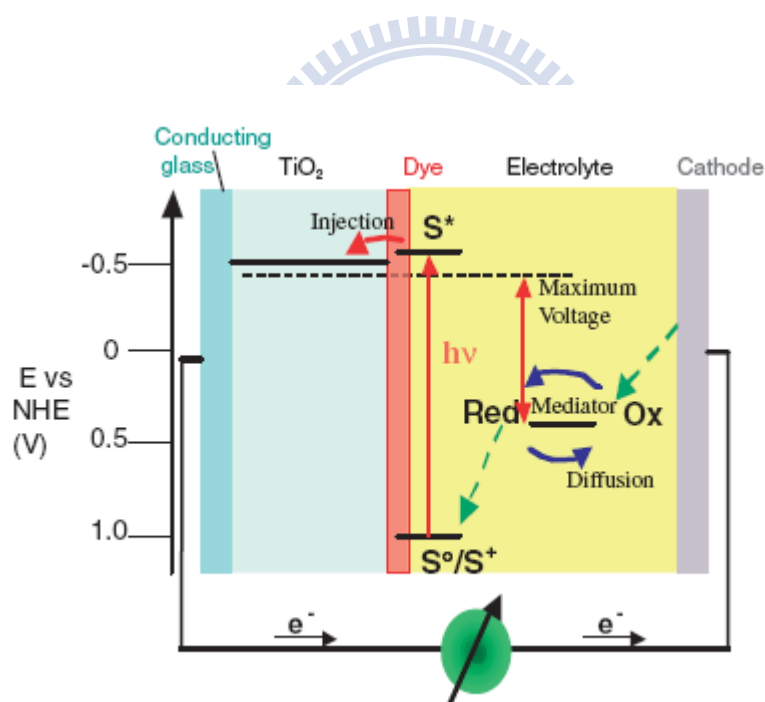


**Figure 1-3 The working principle of DSSC. Photoexcitation of the sensitizer (S) is followed by electron injection into the conduction band of an oxide semiconductor film. The redox system regenerates the dye molecules, and the dye molecules are regenerated at the counter electrode by electrons passed through the load. Potentials are referred to the normal hydrogen electrode**



(NHE).<sup>3</sup>

### 1.3 Natural photosynthesis mechanisms

Extremely fine craftsmanship of nature is the ultimate goal for chemist. Natural photosystem plays a role of solar energy harvesting and energy conversion. The importance and complexity of photosynthesis has led many researchers to look for ways to duplicate the fundamental characteristics of these electron transfer reactions in simplified chemical systems. And it's an integrated system including light harvesting, photo-induced charge separation, and synthesis of higher-energy compounds.

Photosynthetic apparatus consists of a number of photoactive proteins, which harvest solar energy and synchronize all of their function to make photosynthesis unabridged and efficient. During photosynthesis, plants and certain bacterial systems convert light energy into electrochemical energy and eventually into chemical potential energy stored in carbohydrates and other compounds. Photosynthesis start by the absorption of a photon by light-harvesting (antenna) complexes that usually comprise a large number of pigments embedded in protein matrices. This process is followed by an efficient energy migration over many pigments within the antenna system until a reaction center is encountered.

Knowing how plants and bacteria harvest light for photosynthesis so efficiently may provide a new idea for energy requirements.

Photosynthesis, natural biosphere drives energy from sunlight energy. Photosynthetic organisms, *i.e.*, plants, algae and photosynthetic bacteria, have developed efficient systems to harvest the light of the sun and to use the light energy to drive their metabolic reactions.

#### 1.3.1 Bacterial photosynthesis -Purple bacteria

Purple bacteria are the paragon of harvesting light. Nearly all energy gained from the absorption

of a photon is transferred to the reaction center. In purple bacteria, the photosynthetic membranes contain two types of light-harvesting complexes: light harvesting complex I (LH-I) and light harvesting complex II (LH-II). The structure is showed in Fig.1-4.<sup>4</sup>

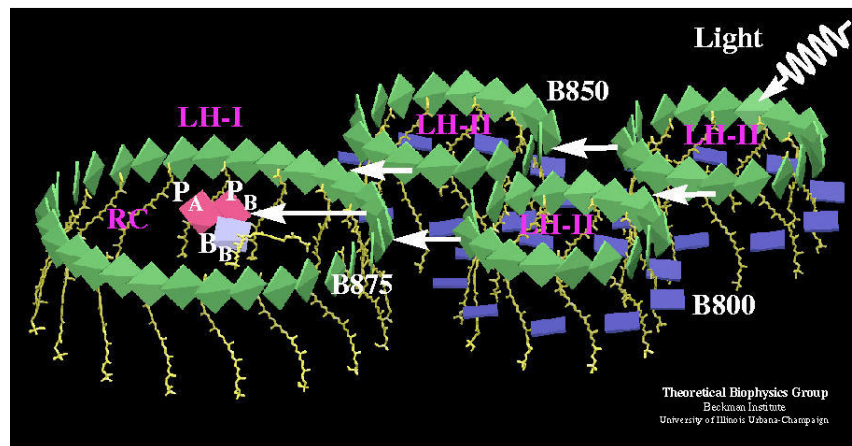


**Figure 1-4 Photoexcited electron transfer in the bacterial photosynthetic unit. LH-II contains two types of BChls: B800 (dark blue) and B850 (green), which absorb at 800 nm and 850 nm. BChls in LH-I absorb at 875 nm and labeled B875 (green).  $P_A$  and  $P_B$  refer to the RC special pair, and  $B_A$ ,  $B_B$  refer to the accessory BChls in the RC. The figure demonstrates the coplanar arrangement of the B850 BChl ring in LH-II, the B875 BChl ring of LH-I, and the RC BChls  $P_A$ ,  $P_B$ ,  $B_A$ ,  $B_B$ .<sup>4</sup>**

X-ray structure of RC (from *Rhodospseudomonas viridis*, *Rps. V*) was first published in 1985. Typically, RC (from *Rb. S*) is embedded in the bacterial cytoplasmic membrane and is composed of three subunits labeled L, M and H. The L and M subunits, each forming five transmembrane  $\alpha$ -helices, are related by an axis of approximate two-fold symmetry. The more hydrophilic subunit H is located at the cytoplasmic surface and binds to both the L and M subunits. Except the one carotenoid molecule, cofactors including a bacteriochlorophyll (BChl) dimer (termed as P) known as the primary donor, two monomer bacteriochlorophylls ( $BChl_A$  and  $BChl_B$ ), two bacteriopheophytins

(BPhe<sub>A</sub> and BPhe<sub>B</sub>), two quinones (Q<sub>A</sub> and Q<sub>B</sub>) and one non-heme iron are symmetrically arranged in the L and M subunits.<sup>5</sup>

All of the cofactors are binding to the proteins non-covalently. It is the well established photo-induced electron transfer (ET) system. Via the photoexcitation of P or received excitation energy transferring from the antenna, the excited state of P (P\*) forms and then decays in about 3–4 ps to form the charge separation state P<sup>+</sup>BPhe<sub>A</sub><sup>-</sup>. Subsequently, BPhe<sub>A</sub><sup>-</sup> transfers an electron to Q<sub>A</sub> with a constant of about 200 ps at room temperature, yielding the state P<sup>+</sup>Q<sub>A</sub><sup>-</sup>. And ET from Q<sub>A</sub><sup>-</sup> to Q<sub>B</sub> takes a few hundred μs. (Fig.1-5)<sup>5</sup>

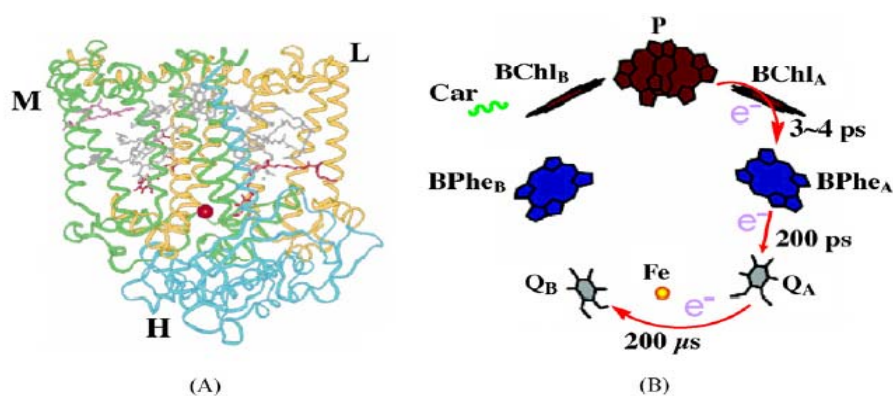
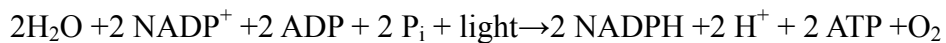


**Figure 1-5 (A) Three-dimensional structure of RC from *Rhodobacter sphaeroides* (*Rb. S*). The L, M and H subunits are shown as orange, green and blue ribbons. (B) Schematic of the cofactors arrangement and the photo-induced ET present in RC.<sup>5</sup>**

### 1.3.2 Plant photosynthesis

Light-dependent reactions take place in the thylakoid membranes of the chloroplasts in green plant. Plants synthesize ATP and NADPH by utilizing light energy. One molecule of the pigment chlorophyll absorbs one photon and drives the electron to pheophytin. And pheophytin passes the electron to a quinone molecule, starting a flow of electrons down an electron transport chain that leads to reduction of NADP<sup>+</sup> to NADPH at last. A proton gradient is created across the chloroplast

membrane. Its dissipation is used by ATP synthase for the concomitant synthesis of ATP. The chlorophyll molecule regains the lost electron from a H<sub>2</sub>O molecule and releases a dioxygen (O<sub>2</sub>) molecule. The overall reaction for the light-dependent reactions under the conditions of non-cyclic electron flow in green plants is:



Some specific wavelengths of light can support photosynthesis. It depends on the type of accessory pigments present. There are two forms of light-dependent reaction: non-cyclic and cyclic reaction. In the non-cyclic reaction, the photons are captured in the light-harvesting antenna complexes of photosystem II by chlorophyll and other accessory pigments. When a chlorophyll molecule of the photosystem II reaction center obtains sufficient excitation energy from the adjacent antenna pigments, an electron is transferred to the primary electron-acceptor molecule, pheophytin. This process called photo-induced charge separation. These electrons are transported through an electron transport chain, called *Z-scheme*, that generates a chemiosmotic potential across the membrane. In *Z-scheme*, electrons are excited due to the light absorbed by the photosystem I. A second electron carrier accepts electrons, which again is passed down lowering energies of electron acceptors. The energy created by the electron acceptors is used to move hydrogen ions across the thylakoid membrane into the lumen. Electrons are used to reduce the co-enzyme NADP<sup>+</sup>, which has functions in the light-independent a reaction. An ATP synthase enzyme uses the chemiosmotic potential to make ATP during photophosphorylation. NADPH is the terminal product of redox reaction in the *Z-scheme*. The cyclic reaction is similar to that of the non-cyclic, but differs in the form that its generates only ATP, and no NADPH is created. The cyclic reaction takes place only at photosystem I. Once the electron is displaced from the photosystem, the electron is passed down the electron acceptor molecules and returns back to photosystem I, from where it was emitted, hence the

name *cyclic reaction*.<sup>6</sup> (Fig.1-6)

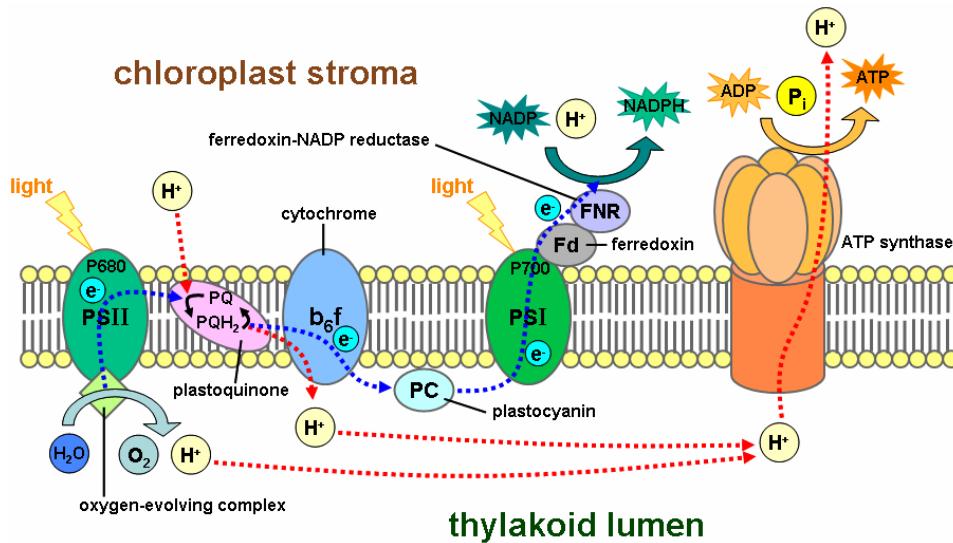


**Figure 1-6 Light-dependent reactions of photosynthesis at the thylakoid membrane.**

### 1.3.3 The importance of protein scaffold in photosystem

Photosynthetic apparatus is a typical electronic device, including molecular optical and electronic circuitry organized by a protein scaffold. It occurs with an amazingly high efficiency. Photo-induced electron transfer to yield long-lived charge-separated (CS) states is the most fundamental energy conversion process. Photosynthetic membrane proteins play a role of bio-device for solar energy harvesting and energy conversion. They can stabilize the charge-separated state and excited-state lifetimes. Protein structural deformation will induce lifetime shortening of excited state.<sup>7-10</sup>

## 1.4 Artificial photosynthesis

Artificial photosynthesis is a way to mimic the photosynthesis of plants artificially. The photosynthetic apparatus of both photosynthetic bacteria and higher plants involves a reaction center

surrounded by intricate arrays of pigments that form an energy gradient for efficient light collection. Artificial systems that can mimic this excellent natural system have attracted great interest.

## 1.5 Biosolar cell

Presently, the great part of biosolar cell applies the organisms directly from natural plant or photosynthetic bacteria to create the biophotovoltaic devices.<sup>8,9</sup> Minority are artificial materials.<sup>11,12</sup>

To convert sun energy to electric energy, utilization of novel nanoporous materials as powerful electrode surfaces for biomolecules immobilization has achieved significant progress. The advantages of these matrixes with nanoporous structure are high surface area, pore volume, ideal biocompatibility, and improved electrochemical, photoelectrochemical activity, etc. These characteristics can entrap and retain the high activity of protein and promote the direct or photo-induced ET. Increased efforts on constructing nanoporous films for biomolecules entrapments have provided great possibilities to the development of versatile biosensors and bioelectronics.<sup>12</sup>

Lu *et al.* constructed a nano-crystalline TiO<sub>2</sub> films prepared by anodic electrodeposition which was successful for RC adsorption. The porosity of the TiO<sub>2</sub> film provided a relatively high surface area for RC immobilization and retained the activity of the protein. They proved that protein was unaltered on the electrode surface. WO<sub>3</sub>-TiO<sub>2</sub> and RC had well-matched energy levels to enhance photoelectric performance of the derived bio-PEs especially in the red to NIR region as compared with that of the TiO<sub>2</sub>-RC ones.(Fig.1-7) The pigment exchanged RC (BPhe was replaced to Phe) adsorbed onto the above-mentioned nanostructured WO<sub>3</sub>-TiO<sub>2</sub> could strongly promote the photocurrent generation. (Fig. 1-8) Phe was utilized to replace BPhe in the native-RC for decreasing the ultrafast excited-state relaxation rate of RC itself. Improved photo-induced ET from RC mutant to the WO<sub>3</sub>-TiO<sub>2</sub> electrodes, which was deduced from the experimental results of femtosecond (fs) pump-probe dynamics, fluorescence (FL) emission and NIR photoelectric responses, was proved undoubtedly.<sup>13</sup>

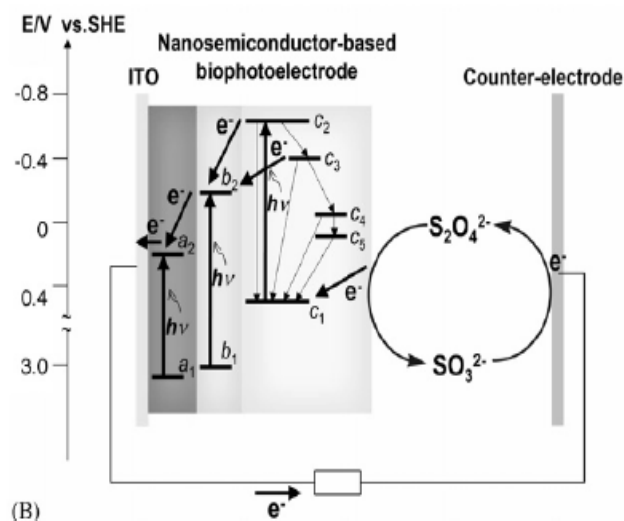


Figure 1-7 Schematic working principle of the RC based bio-photoelectric cell. The photoanode is ITO/WO<sub>3</sub>-TiO<sub>2</sub>/RC film and Pt as the counter-electrode. The electrolyte is pH 8.0 Tris-HCl buffer containing 8 mM sodium dithionite. a<sub>1</sub>: V<sub>b</sub> of WO<sub>3</sub>, a<sub>2</sub>: C<sub>b</sub> of WO<sub>3</sub>, b<sub>1</sub>: V<sub>b</sub> of TiO<sub>2</sub>, b<sub>2</sub>: C<sub>b</sub> of TiO<sub>2</sub>, c<sub>1</sub>: PBPheQ<sub>A</sub>Fe<sup>2+</sup>Q<sub>B</sub>, c<sub>2</sub>: P<sup>+</sup>BPheQ<sub>A</sub>Fe<sup>2+</sup>Q<sub>B</sub>, c<sub>3</sub>: P<sup>+</sup>BPhe-Q<sub>A</sub>Fe<sup>2+</sup>Q<sub>B</sub>, c<sub>4</sub>: P<sup>+</sup>BPheQ<sub>A</sub>-Fe<sup>2+</sup>Q<sub>B</sub>, c<sub>5</sub>: P<sup>+</sup>BPheQ<sub>A</sub>Fe<sup>2+</sup>Q<sup>B-</sup>.<sup>13</sup>

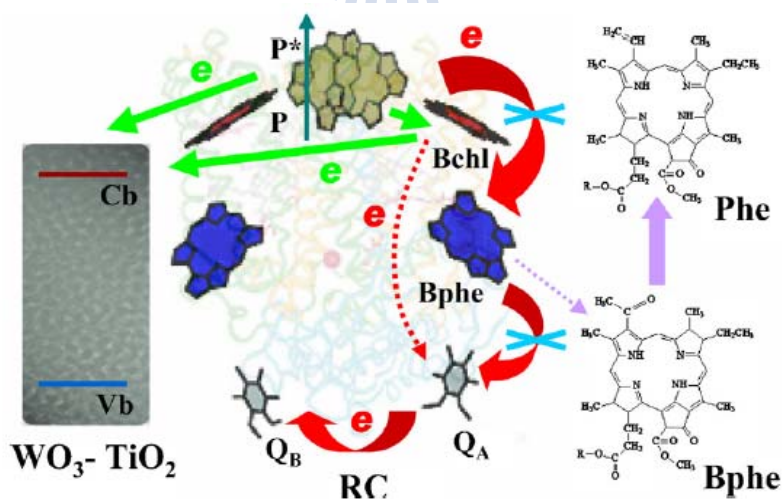


Figure 1-8 Illustration of the Phe-RC/WO<sub>3</sub>-TiO<sub>2</sub> PE and photo-induced ET. C<sub>b</sub>, conduction band; V<sub>b</sub>, valence band; P, BChl dimmer; BPhe, bacteriopheophytin; Phe, pheophytin; Q<sub>A</sub>, the

**primary quinone; Q<sub>B</sub>, the secondary quinone.**<sup>13</sup>

## **1.6 Myoglobin**

Myoglobin is a single-chain globular protein with 153 amino acids, containing a heme (iron-containing porphyrin) prosthetic group in the center around which the remaining apoprotein folds. It has eight alpha helices (named A-H) and a hydrophobic core. (Fig.1-9) It has a molecular weight of 16,700 daltons, and is the primary oxygen-carrying pigment of muscle tissues. In 1958, Kendrew *et al* first used X-ray crystallography technology to solve the structure of myoglobin, it was the first solved protein crystal structure. The X-ray structure shows the relative position of amino acid residues and prosthetic group. The hydrophobic amino acid residues are folded into Mb molecule and surround the prosthetic group; the hydrophilic amino acid residue are positioned at outer surface and provide solubility in water. On the other hand, due to its commercial availability, a single electro-active iron heme as a prosthetic group and a known structure, Mb is considered to be an ideal model protein for the study of heme proteins or enzymes.<sup>14,15</sup>

**Figure 1-9 Crystal structure of myoglobin and the prosthetic group, heme.**



The ability of Mb to bind oxygen depends on the presence of heme, when this prosthetic group is lost, Mb maintains its native solubility and conformational structural characteristics and refers as apo-Mb. Apo-Mb demonstrates various differences from its holo-form; its red color is lost and the protein has both a lower ellipticity, lower stability, and less compact.<sup>16</sup>

We are interested and focus on the electron-transfer (ET) reaction and the chemical reactivity of Mb, because the small globular Mb could be a suitable model to understand the physicochemical properties of hemo-proteins.<sup>17</sup> The heme pocket of Mb can stabilize the reduced and oxidized states of the iron complex. There are three types of methods to give Mb with new functions: (i) modification of functional group on protein surface<sup>18</sup> (ii) mutation of amino residues for Mb<sup>19</sup> (iii) reconstitution of an artificial prosthetic group with apo-Mb.<sup>18-21</sup> The reconstitution of Mb with an artificially created prosthetic group is a unique method for introducing a new chemical function into the protein. (Fig1-10)<sup>22</sup>

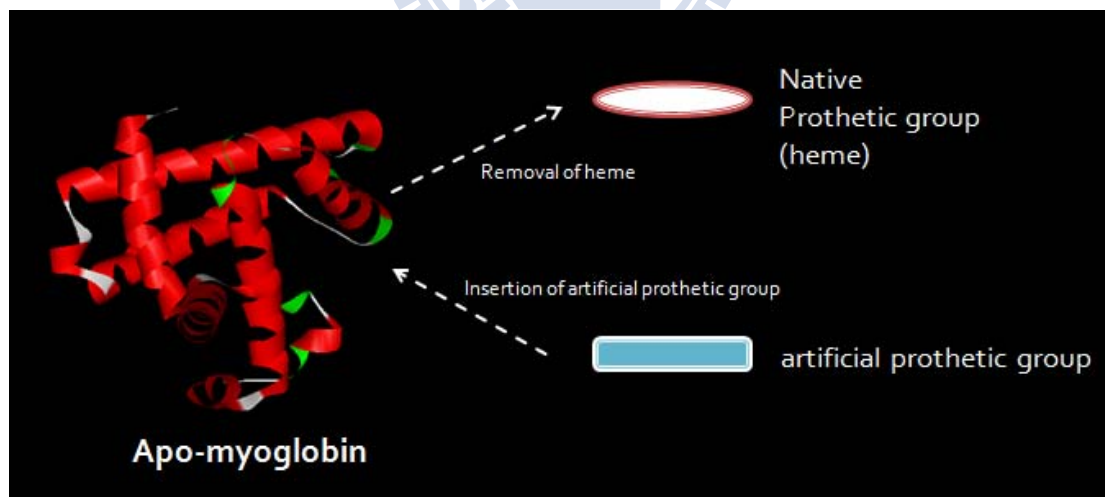


**Figure 1-10 Schematic representation of myoglobin modifications. An artificial prosthetic group inserted into apo-Mb.**

### 1.6.1 Why is myoglobin?

Prothetic group heme is non-covalently bound in the cavity of myoglobin. Artificial prothetic group (photosensitizer) can easily be replaced into protein cage. Native heme is the analog of porphyrin. Different metals integrated with porphyrins the function and the property will be variable. And it can be modified with chromophores to enhance the ability of photosensitization. In homologous protein (cytochrome c), the prothetic group is covalently bound in the cavity. The process of removing the prothetic group, the destructive HF is necessary. So we chose myoglobin as our protein model.

### 1.6.2 Pigment (MtPE1)

Metallo-5-(4-carboxy-phenylethynyl)-10, 20-biphenylporphines (MtPE1) were denoted as H<sub>2</sub>PE1, CoPE1, NiPE1, CuPE1, and ZnPE1. The structure of MtPE1 system is comprised by three parts : (i) metallo biphenylporphyrin (MtBPP) unit serves as light-harvesting center to provide photo-induced electrons, (ii) the PE group is connected to the meso position of the porphyrin to transfer the electrons efficiently, and (iii) the carboxylic acid (CA) attached to the end of the spacer serves as an anchoring group to bond tightly onto the surface of TiO<sub>2</sub> nanoparticles.(Fig1-11).<sup>23</sup>

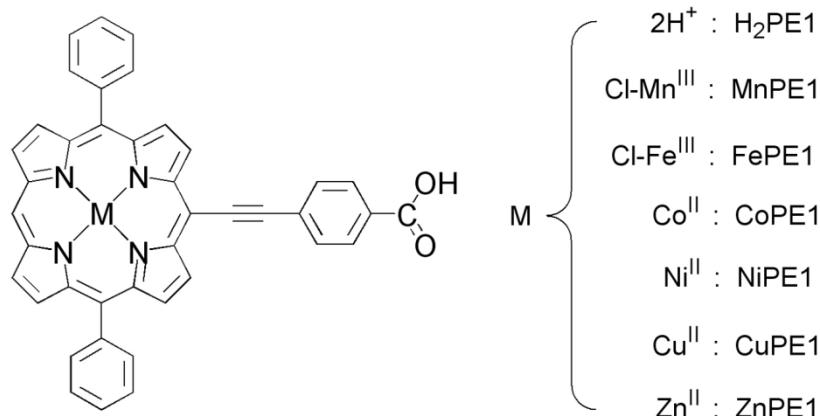


**Figure 1-11 Structural diagram of PE1 porphyrins**

## 1.7 The application of myoglobin in electron transfer study.

### 1.7.1 Myoglobin based triads

Hu *et al.* created a protein-based semi-synthetic photoreaction center which used Mb as a model protein to study photo-induced electron transfer processes (ET).<sup>24</sup> To mimic the function of photosynthetic organisms that converted light energy to chemical potential in the form of long-lived charge-separated states, the system was constructed in a protein by cofactor reconstitution. Two factors ( $\text{Fe}^{\text{III}}\text{OH}_2$ )- $\text{Ru}^{2+}$ - $\text{BXV}^{4+}$  (1) and (Zn)- $\text{Ru}^{2+}$ - $\text{BXV}^{4+}$  (2) (Fig1-12) were reconstituted with the acceptor (cyclobis(paraquat-*p*-phenylene)  $\text{BXV}^{4+}$ ) and the sensitizer ( $\text{Ru}(\text{bpy})_3$ ) are noncovalently linked in a catenane type, and the sensitizer is covalently linked with the donor (metallo-protoporphyrin) located in the myoglobin pocket.(Fig1-13)

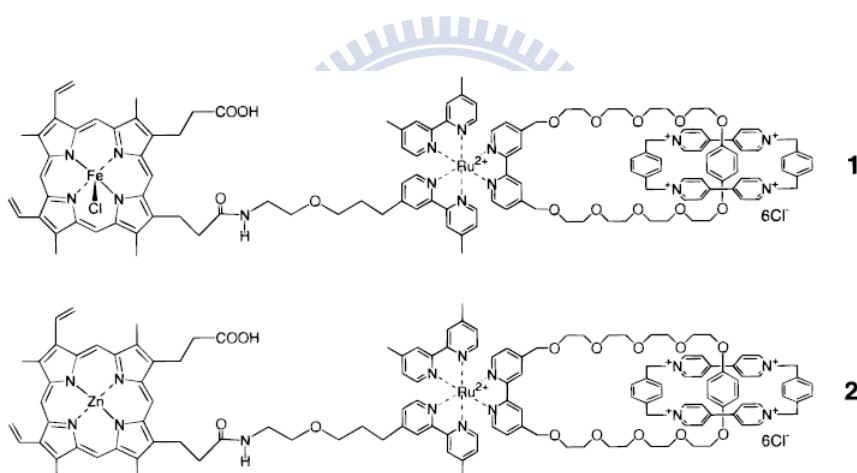


**Figure 1-12 Chemical structure of (1) ( $\text{Fe}^{\text{III}}\text{OH}_2$ )- $\text{Ru}^{2+}$ - $\text{BXV}^{4+}$  and (2) (Zn)- $\text{Ru}^{2+}$ - $\text{BXV}^{4+}$ . The structure was composed by donor (metallo-protoporphyrin)-sensitizer( $\text{Ru}(\text{bpy})_3$ )-acceptor(cyclobis(paraquat-*p*-phenylene)  $\text{BXV}^{4+}$ ).**<sup>24</sup>

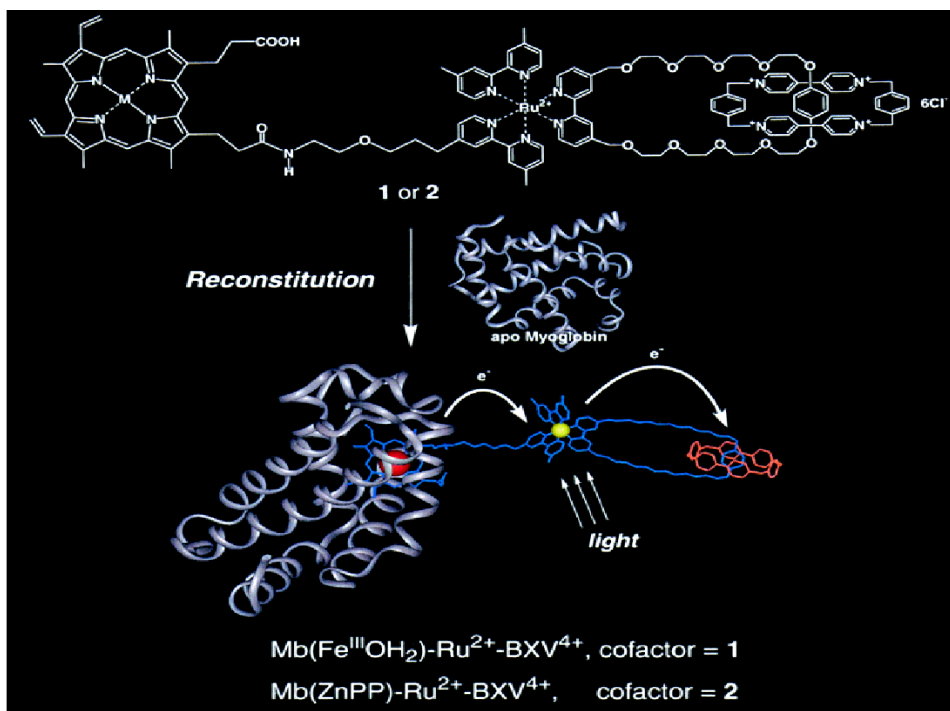
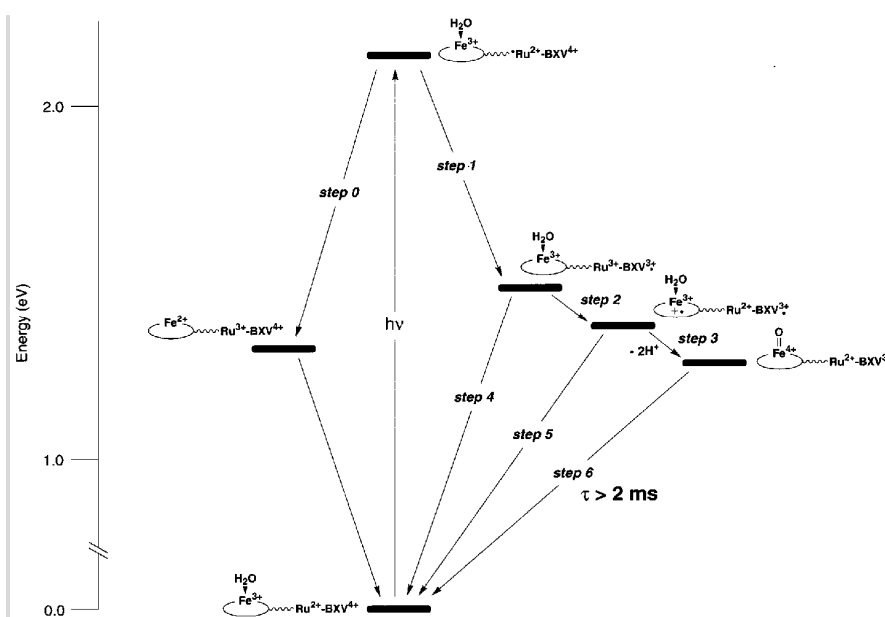


**Figure 1-13 Schematic illustration of the reconstitution of 1 and 2 with apo-Mb to afford the myoglobin-based triads, Mb(Fe<sup>III</sup>(OH<sub>2</sub>))-Ru<sup>2+</sup>-BXV<sup>4+</sup> and Mb(Zn)-Ru<sup>2+</sup>-BXV<sup>4+</sup>.<sup>24</sup>**

The resulting electron transfer processes of reconstituted Mb(Fe<sup>III</sup>(OH<sub>2</sub>))-Ru<sup>2+</sup>-BXV<sup>4+</sup> and Mb(Zn)-Ru<sup>2+</sup>-BXV<sup>4+</sup> were analyzed by steady-state absorption, fluorescence and transient absorption. In summary, their study clearly demonstrated that Mb plays a critical role in biological electron transfer, including (1) isolation of the redox partners in a multicomponent assembly to prevent their stacking in the ground state, (2) fixation of the conformation of a chromophore and the protein surface, (3) regulation of the ET pathway among singlet ET, triplet ET, a short-cut process and stepwise process, and (4) control of the lifetime of a resultant charge-separated state. (Fig1-14)

(a)



(b)

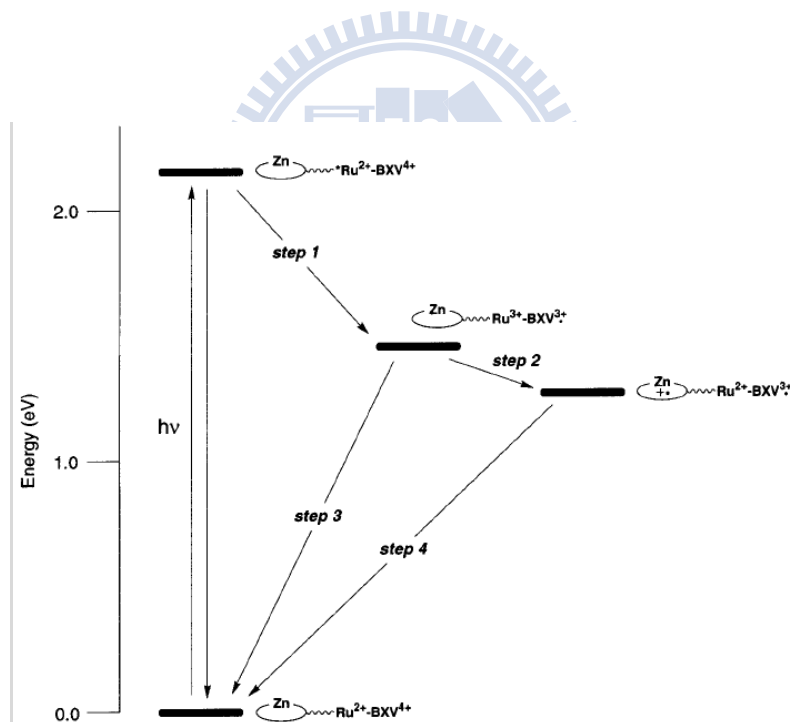


Figure 1-14 (a) Energetics and selected pathways for Mb(Fe<sup>III</sup>OH<sub>2</sub>)-Ru<sup>2+</sup>-BXV<sup>4+</sup> in buffer solution after excitation to the Ru(bpy)<sub>3</sub> excited state. The energy of the excited Ru(bpy)<sub>3</sub> component was calculated from the absorption and emission spectra of catenane 5. The energies of the various charge-separated states were estimated from the corresponding redox

potentials of models for the components of  $\text{Mb}(\text{Fe}^{\text{III}}\text{OH}_2)\text{-Ru}^{2+}\text{-BXV}^{4+}$ . The energy levels are not corrected for any Coulombic stabilization of the intermediates. (b) Energy levels of the locally excited state of the  $\text{Ru}^{2+}(\text{bpy})_3$  moiety and the hypothetical ion-pair states of  $\text{Mb}(\text{Zn})\text{-Ru}^{2+}\text{-BXV}^{4+}$  and the pathways available for their interconversion. For comparison purpose, the excited states of ZnPP are not present.<sup>24</sup>



### 1.7.2 Photochemical reduction of $\text{NADP}^+$ by Zn-Mb as simple model of photosystem I

Nishiyama *et al.* reported a simple model of photosystem I by forming NADPH. Zinc protoporphyrin (Zn-PP) reconstituted myoglobin (ZnMb) as a photo-sensitized enzyme, triethanolamine (TEA) as a sacrificial donor, and  $\text{NADP}^+$  as an electron acceptor. Upon irradiation, the absorbance increase at 340nm which is attributed to NADPH formation. (Fig1-15) When Zn-PP used as a photo-sensitizer instead of Zn-Mb, the NADPH absorbance is not apparent. The difference of the efficiency may be caused by the lifetime of excited triplet. When Zn-PP reconstituted with apo-Mb, excited triplet lifetime increase apparently and cause the high efficiency of NADPH formation.<sup>25,26</sup>

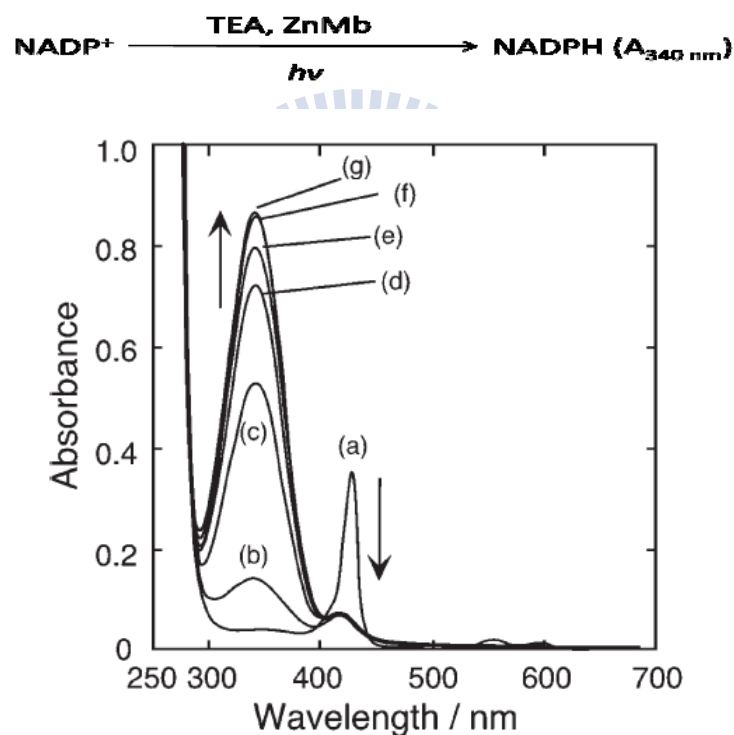


**Figure 1-15 UV-visible spectral change for 10 mM of Zn-Mb, 1 M of TEA, and 1 mM of  $\text{NADP}^+$  in 10 mM of phosphate buffer (pH 9.0). (a) Before irradiation. (b) After 3.5 h of irradiation with visible light ( $\lambda > 390 \text{ nm}$ ) at an intensity of 2.8 mW. Following the irradiation, spectra were measured after 1 (c), 2 (d), 3 (e), 6 (f), and 9 (g) days in the dark under an atmosphere of  $\text{N}_2$ .**

## 2. Specific aims

Biosolar cell is our ultimate aim. First, we need to construct a simple artificial photosynthetic apparatus. MtPE1 are series of photo-sensitizers. Due to the MtPE1 are easy to self-aggregation and self-quenched, we reconstituted MtPE1 with apo-Mb to let them as a monomer inside the protein and attempt to stabilize excited lifetime.

Some basic studies help us to understand the properties of MtPE1-Mb. UV-Vis, fluorescence, TCSPC help us to recognize whether MtPE1s are inside the protein or not. To compare the photo-induced  $\text{NADP}^+$  conversion efficiency of MtPE1-Mb which is photo-sensitized enzyme, triethanolamine (TEA) was used as a sacrificial donor and  $\text{NADP}^+$  was used as an electron acceptor. CV analysis helps us to infer whether is the well-matched energy level of electron donor and acceptor from HOMO and LUMO.

### 2.1 Reconstitution of MtPE1 with wild-type apo-Mb

We reconstitute dye with apo-Mb to prevent prosthetic groups aggregation and to extend the lifetime of charge-separation state. The MtPE1 dyes trend to self-aggregate and the photo-induce excited state lifetime will be self-quenched. The situation of self-quench will decrease the conversion efficiencies ( $\eta$ ). So we reconstitute MtPE1 with apo-Mb to avoid the aggregation. First, we need to purify the wild-type apo-Mb by ethyl methyl ketone method.<sup>27</sup> After we get apo-Mb, reconstitution of various MtPE1 with apo-Mb is the critical step in our project. Base on the principle of changing pH to induce apo-Mb unfolding and refolding, various prosthetic groups can be reconstituted with apo-Mb. This procedure can keep prosthetic group monomer inside the apo-Mb, and this method is convenient for us to further proceed in our experiments.



## **2.2 Optic assay of reconstituted MtPE1-Mb (UV-Vis, fluorescent and TCSPC)**

In order to create a biosolar cell system, the basic knowledge of optic and electrochemistry is prerequisite. We detect UV-Vis spectra to confirm the light absorption range of these proteins and compare the peak shift in different condition. The detection of fluorescent emission spectra which is excited at Soret band will be analyzed and getting preliminary information of photo-induce electron transfer process. Time-correlated single-photon-counting system (TCSPC) and fluorescence optically gated (up-conversion) system (FOG) are two critical technologies for us to distinguish photo-induced charge-separated state and to understand the details of the photo-induced electron transfer mechanism. In our proposal, these detections are essential for us to research basic optic information of these reconstituted MtPE1-Mbs and apply it in biosolar cell study.

## **2.3 Electrochemistry assay of reconstituted MtPE1-Mb (CV)**

Directionality of electron transfer is a basic feature of many biological processes, (e.g., photosynthesis). We can use the reduction potential, oxidation potential and cooperate with UV-Vis analysis to calculate the LUMO, HOMO and band gap. Studies with protein solution often are confronted with such challenges as the difficulty to achieve the direct electrochemistry of protein on some bare electrodes as well as the poor reversibility of the direct heterogeneous electron transfer reactions between electrode and protein .When electrode surface modified with detergent (didodecyldimethylammonium bromide, DDAB) can get reversible electron transfer between protein and electrode. DDAB films would provide a biomembrane-like microenvironment for incorporated proteins.

## **2.4 Photoirradiation assay of reconstituted MtPE1-Mb**

About converting light energy to chemical energy, well-matched energy level electron donor and acceptor are needed. Triethanolamine (TEA) is used as a sacrificial donor,  $\text{NADP}^+$  is used as an

electron acceptor and MtPE1-Mb is photo-sensitized enzyme. Based on this simple system, we compared the photo-induced  $\text{NADP}^+$  conversion efficiency of free base and MtPE1-Mb.

## 2.5 Photoelectronics assay of reconstituted MtPE1-Mb (IV)

For biosolar cell study, current/voltage measurement (IV curve) is essential indexes to judge the photovoltaic performances of the solar cell. The IV curve shows a graphical presentation of the current versus the voltage from a photovoltaic cell as the load is increased from the short circuit (no load) condition to the open circuit (maximum voltage) condition. The shape of the curve characterizes cell performance. (Fig. 2-1)

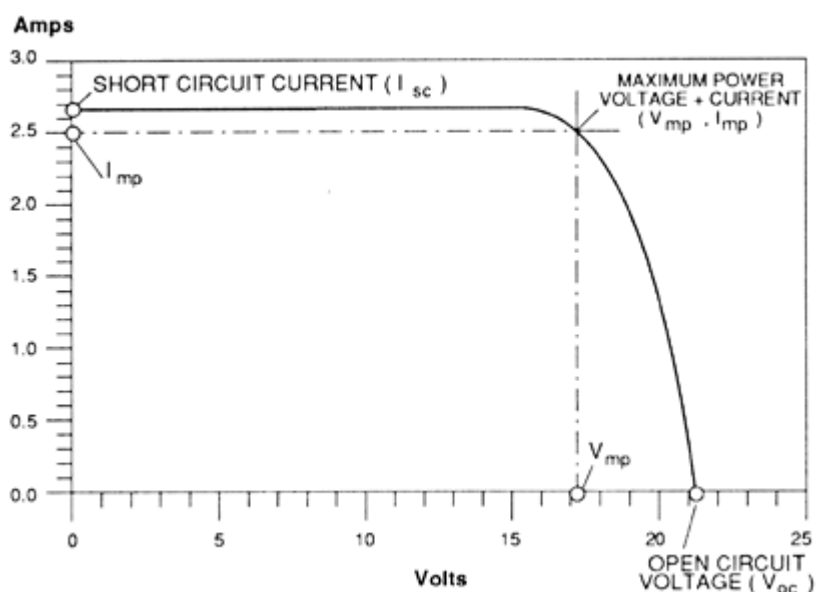


**Figure 2-1 A typical current-voltage curve. This maximum current is called the short circuit current, abbreviated  $I_{sc}$ . When the module is shorted, the voltage in the circuit is zero. Conversely, the maximum voltage is produced when there is a break in the circuit. This is called the open circuit voltage, abbreviated  $V_{oc}$ . Under this condition the resistance is infinitely high and there is no current, since the circuit is incomplete. These two extremes in load resistance, and the whole range of conditions in between them, are depicted on a graph**

called an I-V (current-voltage) curve. Current, expressed in amps, is on the vertical Y-axis.  
Voltage, in volts, is on the horizontal X-axis



### 3. Experimental materials and procedures

#### 3.1 Experimental materials

Acetic acid (Merck)

30% Acrylamide (GE Healthcare)

APS (GE Healthcare)

2,2'-azino-bis(3-ethylbenzothiazoline 6-sulfonic acid)(ABTS)(Sigma)

Amicon ultrafiltration membrane (Millipore)

Ammonium sulfate (Merck)

Coomassie® Brilliant blue R 250 (Merck)

DEAE Sephacel (Amersham Pharmacia Biotech)

Dialysis membrane (Cellu®Sep T<sub>1</sub>)

Didodecyldimethylammonium bromide (DDAB) (Aldrich)

Dimethyl sulfoxide (MP Biomedicals)

Ethyl methyl ketone (Merck)

Glycerol (Merck)

Hydrogen chloride (Merck)

LMW-SDS Marker Kit (Amersham Pharmacia Biotech)

Methanol (Merck)

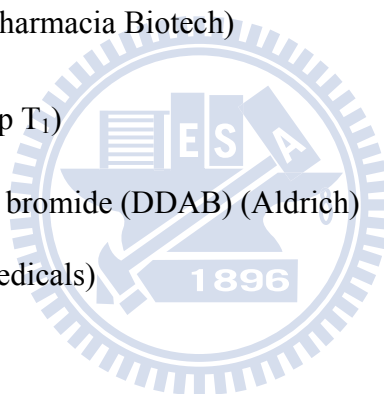
2-mercaptoethanol (Merck)

Metallo-5-(4-carboxy-phenylethynyl)-10,20-biphenylporphines (C.-Y. Lin Lab)

Myoglobin (Sigma-Aldrich)

Nicotinamide adenine dinucleotide phosphate (NADP<sup>+</sup>) (Fluka)

Potassium chloride (Merck)



Potassium diphosphate (Merck)

Potassium phosphate (Merck)

Sephadex G-25 (GE Healthcare)

Sodium acetate (Merck)

Sodium bromide (Merck)

Sodium chloride (AMRESCO)

Sodium hydroxide (Merck)

TEMED (GE Healthcare)

Tris base (USB)

Triethanolamine (TEA) (Merck)

TiO<sub>2</sub> film (Eric W.-G. Diau Lab)

### **3.2 Experimental apparatus**

Allegra™ 21R Centrifuge (Beckman Coulter)

8453 UV-Visible Spectrophotometer (Agilent Technologies)

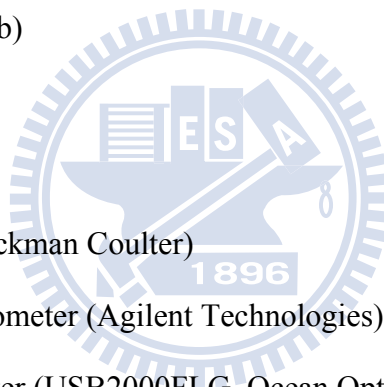
Fluorescence Spectrophotometer (USB2000FLG, Ocean Optics)

Time-correlated single-photon-counting system (TCSPC, FluoTime 200, PicoQuant)

CHI electrochemical analyzer (CH Instruments)

Photochemical reactor PR-2000 (Panchum)

AM1.5 solar simulator XES-502S (SAN-EI ELETRIC)



### 3.3 Obtain wild type apo-Mb from myoglobin by Methyl ethyl ketone method

Methyl ethyl ketone method was used to extract the heme from the Mb protein matrix.<sup>27</sup> Briefly, 100 mg of Mb (Sigma-Aldrich) that was without additional purification was dissolved in 30 ml of ice-cold, salt-free PBS. The pH was adjusted to 2.0 by adding 0.1 N HCl dropwise while stirring in order to denature the protein and let the heme prosthetic group to be extracted easily. Equivalent of ice-cold methyl ethyl ketone (30 mL) was mixed with the acid denatured Mb solution and shook in a separating funnel for a short time. After extraction, a hazy pale yellow aqueous layer (bottom) which contained the protein (apo-Mb) was separated from the dark brown methyl ethyl ketone layer which contained heme. The aqueous (apo-Mb) layer was shook with a 30 ml of ice-cold methyl ethyl ketone again in order to separate apo-Mb and heme thoroughly. The apo-Mb solution was transferred to a dialysis belt which had been prepared according to a standard procedure. The solution was then dialyzed against ddH<sub>2</sub>O for 2 to 3 hours to remove methyl ethyl ketone. The procedure was repeated for two times with renewed ddH<sub>2</sub>O and finally the solution was dialyzed in salt-free PBS buffer overnight. After dialysis, the pH of protein solution was adjusted to 7.0 to enhance the yield of apo-Mb and preserved at -20 degree.

### 3.4 Reconstitution of apo-Mb with MtPE1

Reconstitution of metallo--5-(4-carboxy-phenylethynyl)-10,20-biphenylporphines (MtPE1) into apo-Mb followed the modified method of Axup *et al.*<sup>28</sup> Briefly, a 1.5-fold excess of metallo-protoporphyrins in dimethyl sulfoxide (DMSO) solution was added dropwise to a 10 mM KPi/DMSO (4/1) buffer pH 12 containing apo-Mb and cooled in an ice bath. After incubation for 15 min, the solution was adjusted to pH 6.8 and was allowed to stir for 6h at 4 °C. The solution was transferred into a dialysis membrane against ddH<sub>2</sub>O, with two changes of ddH<sub>2</sub>O to remove DMSO, followed by additional dialysis against 10 mM KPi buffer pH 6.8 for overnight. The solution was then filtrated with 0.45 µm cellulose membrane before applied to a Sephadex G-25 column,

equilibrated with 100 mM KPi buffer pH 6.8, and eluted with the same buffer at 4 °C. The protein band was collected and stored at -20 °C for later experiments.

### **3.5 Steady-state spectral measurements**

UV-visible spectra of MtPE1 and reconstituted MtPE1-Mbs were recorded with 8453 UV-Visible Spectrophotometer (Agilent Technologies). Emission spectra were measured with a composite CCD spectrometer (USB2000FLG, Ocean Optics). The excitation source contains a pulsed diode-laser head (LDH-P-C-400, PicoQuant) coupled with a laser-diode driver (PDL-800B, PicQuant) that produces excitation pulses at 435 nm with an average power  $\sim 700 \mu\text{W}$ .

### **3.6 Picosecond fluorescence decays**

Picoseconds lifetime was measured by time-correlated single-photon-counting system (TCSPC, FluoTime 200, PicoQuant). The excitation source came from either a femtosecond laser system (Verdi-10 and Mira 900D, Coherent) at 435 nm (double from an 860-nm, PicoQuant) at 435 nm; the instrument response is  $\sim 30$  ps using the fs laser system while it increases to  $\sim 80$  ps using the ps laser system. The temperature of fluorescence decay experiments was kept at 10 °C.

### **3.7 CV analysis and differential pulse voltammetry (DPV)**

A CHI electrochemical analyzer (CH Instruments) was used for cyclic and differential pulse voltammetry. In electrochemical measurement, experiments employed a three-electrode cell with Ag/AgCl reference electrode, a platinum wire auxiliary electrode and a glassy carbon electrode (GCE) as working electrode. Before each experiment, the glassy carbon electrode was published with powered alumina and rinsed with distilled water as a pretreatment. 10 mM DDAB suspensions were dissolved in water and ultrasonicated for several hours to produce clear vesicle dispersions. Clear vesicle dispersions of 10 mM DDAB containing 0.25 mM protein was used to make films.

Equal volume of protein and dispersion were spread on a GCE and dried overnight. Cyclic voltammetry at DDAB-protein film was performed in 50 mM acetate buffer pH 7. Prior to measurements, buffer solution was purged with nitrogen gas at least 15 min, and then stopped apply nitrogen gas during the experiment.<sup>29-31</sup>

### 3.8 Photoirradiation experiment

The reduction efficiency of MtPE1-Mbs were recorded with photochemical reactor PR-2000 (Panchum). Photoirradiation was carried out under room temperature using 16 W Xe lamp. The light intensity at the cell was 6 mW / cm<sup>2</sup>.

### 3.9 Photoelectrochemical measurements

The photovoltaic property of MtPE1 and reconstituted MtPE1-Mbs adsorbing on nanocrystalline TiO<sub>2</sub> films were analyzed by I-V measurements, a 300-W xenon light source of solar simulator (SAN-EI ELECTRIC) was used as the irradiation source. The spectral output of the lamp matched the AM 1.5 (100 mW/cm<sup>2</sup>) solar spectrum. Incident light intensities were adjusted with neutral wire mesh attenuators. The current-voltage characteristics were determined by applying an external potential bias to the cell and measuring the photocurrent using a Keithley model 2400 digital source meter. The overall conversion efficiency  $\eta$  of the photovoltaic cell is calculated from the integral photocurrent density ( $J_{sc}$ ), the open-circuit photovoltage ( $V_{oc}$ ), the fill factor of the cell (ff), and the intensity of the incident light ( $I_{ph}$ ).

$$\eta = J_{sc} V_{oc} ff / I_{ph}$$



## 4. Result and discussion

### 4.1 Wild type apo-Mb purification

The acid–acetone method was usually used to extract heme from hemeproteins in previous study. In this method, protein is precipitated as solid phase and can be collected by filtration and centrifugation. However, high concentration of acetone was used to ensure the protein was completely precipitated, but protein denatured usually occurs. And it makes the method difficult to apply quantitatively. Methyl-ethyl ketone (MEK) substitution for acetone can avoid to exposure the protein to high concentration of acetone and the bothersome step of re-dissolving the precipitation. It attributes to MEK is just partially miscible with water, enable heme and protein to be rapid and completely separated to organic layer and liquid layer.

The result of apo-Mb purification by MEK method is shown in figure 4-1. The absorption spectrum of Mb<sup>WT</sup> showed absorption protein peak at 280 nm and Soret band at 410 nm in buffer solution. The absorption spectrum of heme showed absorption maximum of Soret band at 383nm in MEK and THF. Apo-Mb extracted from Mb by MEK method gave only one signal at 280nm, and no Soret band. It proved that heme group was removed from Mb and gained apo-Mb. And figure 4-2 showed the SDS-PAGE result of purification by MEK method.

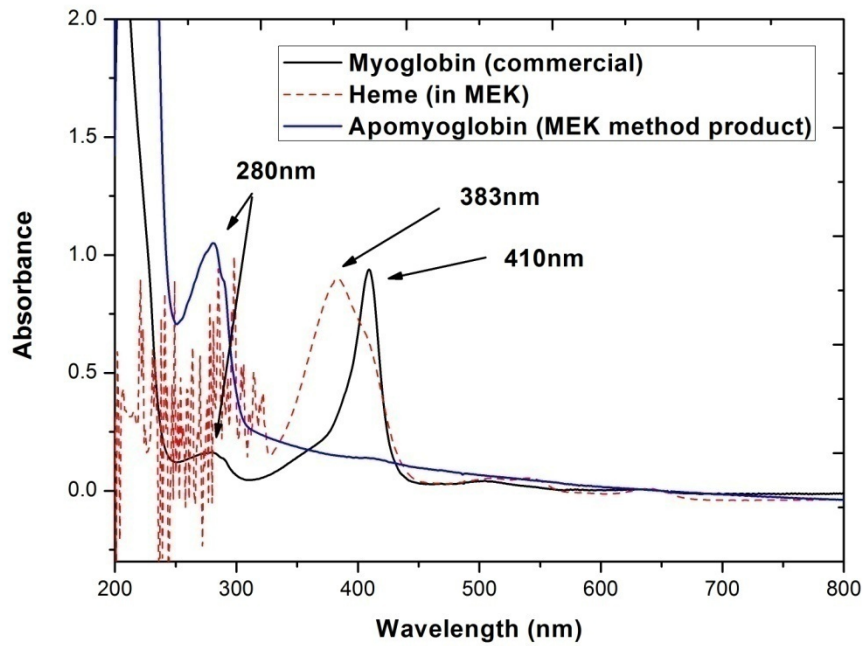


Figure 4-1 UV-Vis results : To confirm that heme has been removed by MEK method.

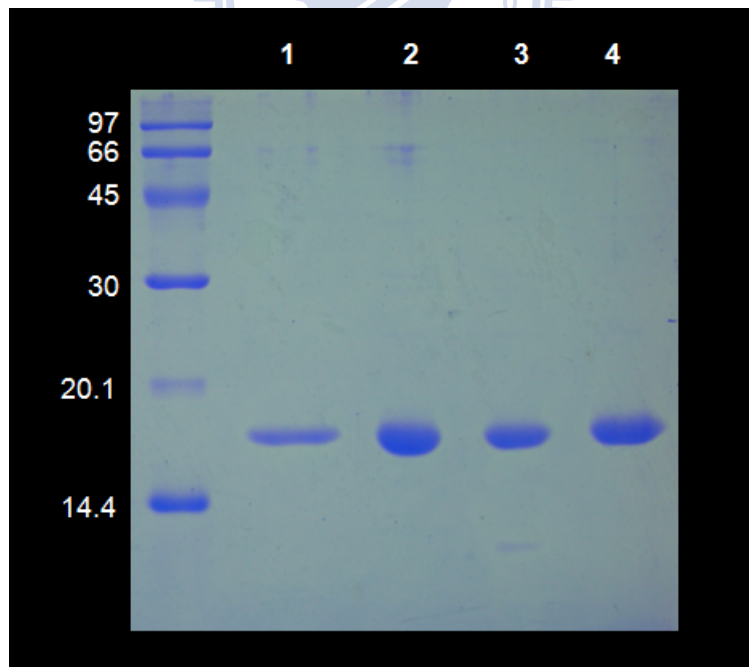
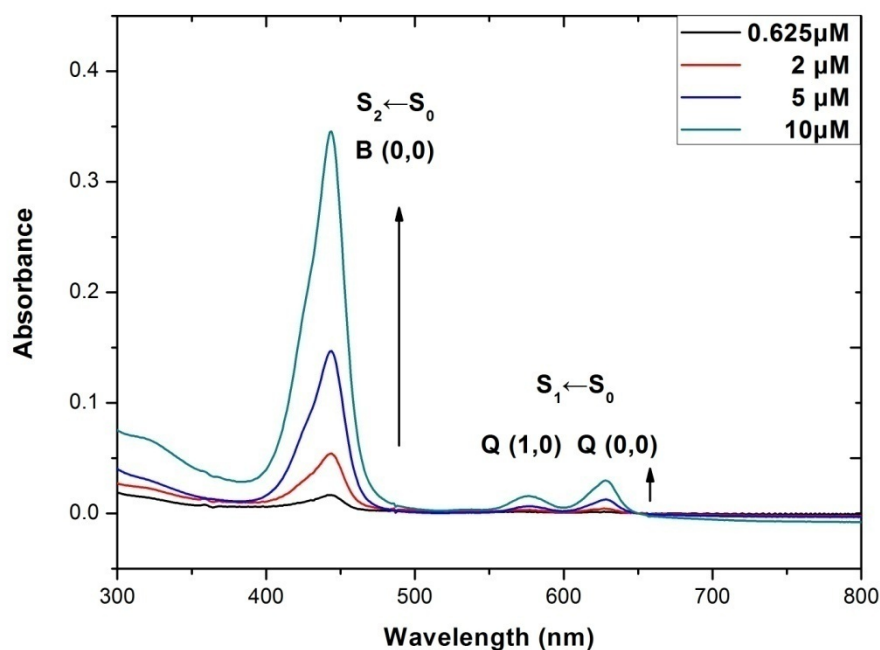


Figure 4-2 SDS-PAGE result: To confirm apo-Mb in each steps (a) Lane 1: Apo-Mb (b) Lane 2: commercial myoglobin (c) Lane 3: Apo-Mb before dialysis (d) Lane 4: Apo-Mb after dialysis.

## 4.2 UV-Vis and fluorescence analysis

### 4.2.1 UV-Vis analysis results of reconstituted MtPE1-Mbs

The absorption spectra of MtPE1-Mbs all consist of two branches, the Soret (or B) band in the higher energy region and weak Q bands in lower energy region, traditionally identified as the  $S_0 \rightarrow S_2$  ( $n \rightarrow \pi^*$ ) and  $S_0 \rightarrow S_1$  ( $\pi \rightarrow \pi^*$ ) transitions, respectively. (Fig4-3)



**Figure 4-3 Absorption spectra of ZnPE1-Mb in KPi solution with B (Soret) and Q bands.**

We have successfully reconstituted five MtPE1 (H<sub>2</sub>PE1, CoPE1, NiPE1, CuPE1 and ZnPE1) with apo-Mb. Figure 4-4 to 4-8 showed the UV-Vis spectrum comparison of reconstituted MtPE1-Mbs in KPi buffer, MtPE1 in KPi buffer, and MtPE1 in tetrahydrofuran (THF). UV-Vis spectrum could be used to ascertain if MtPE1 were successfully reconstituted with apo-Mb. MtPE1 almost could not dissolve in phosphate buffer, so there was no absorption in UV-Vis spectrum. Reconstituted MtPE1 with apo-Mb could enhance the solubility in KPi buffer. Comparing with

MtPE1 dissolved in THF, the UV-Vis spectra of reconstituted MtPE1-Mbs were shifted in both Soret and Q band. The spectral shift was related to the polarity of surrounding environment for MtPE1. The absorption spectrum of MtPE1 in KPi buffer were red shift for the Q bands by comparing with MtPE1 in THF. In theory, increasing the polarity of environment leads to decreasing energy of a typical  $\pi \rightarrow \pi^*$  state and red shift of absorption peak in porphyrins. So the energy gap of  $S_0 \rightarrow S_1$  transition of MtPE1-Mb was smaller than that of MtPE1 in THF, which was consistent with the red shift spectral feature of Q bands. However, the broad and red shifted spectral features of MtPE1 in 100mM Kpi buffer pH 7 were generally attributed to the formation of MtPE1 aggregation. MtPE1 might change the structure via the same procedure of MtPE1-Mb reconstitution, but without apo-Mb. (Maybe different solvent and pH value cause the different form of aggregation for MtPE1 and result in various shift of absorption peaks) (Fig. 4-4 to Fig. 4-8 blue line) A conjecture was apo-Mb could protect MtPE1 against the excessive pH change in the process of reconstitution. When MtPE1 were reconstituted with apo-Mb to form MtPE1 complex in buffer solution, the Soret band of the complex became sharp and blue shift.

Table 4-1 listed the absorption maxima and extinction coefficients of MtPE1. The extinction coefficients decreased from Zn, H<sub>2</sub>, Cu, Co to NiPE1. Q bands of H<sub>2</sub>PE1 were divided into four groups due to its lower symmetry. Table 4-2 listed the absorption maxima of MtPE1-Mbs.

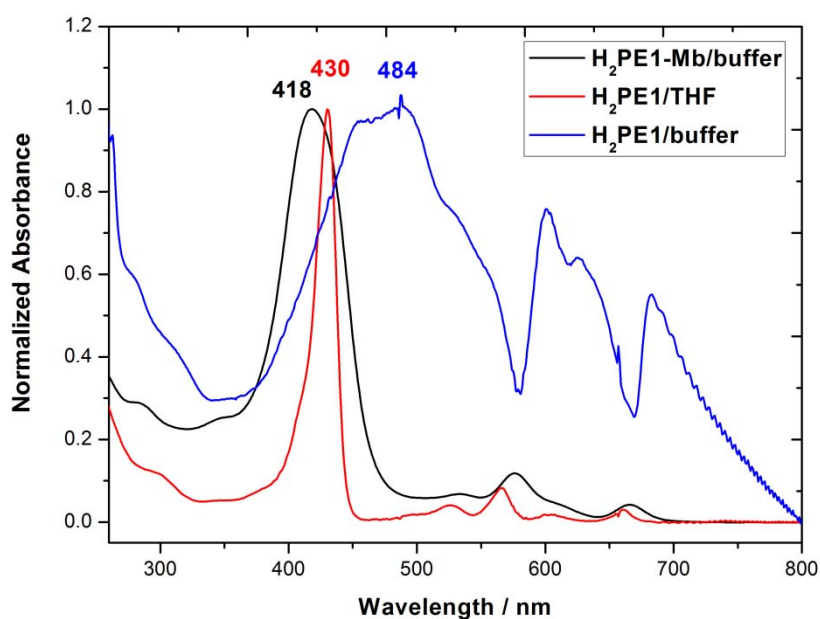


Figure 4-4 Normalized steady-state absorption spectra of H<sub>2</sub>PE1 in THF, 100mM KPi buffer and reconstituted with apo-Mb in 100mM KPi.

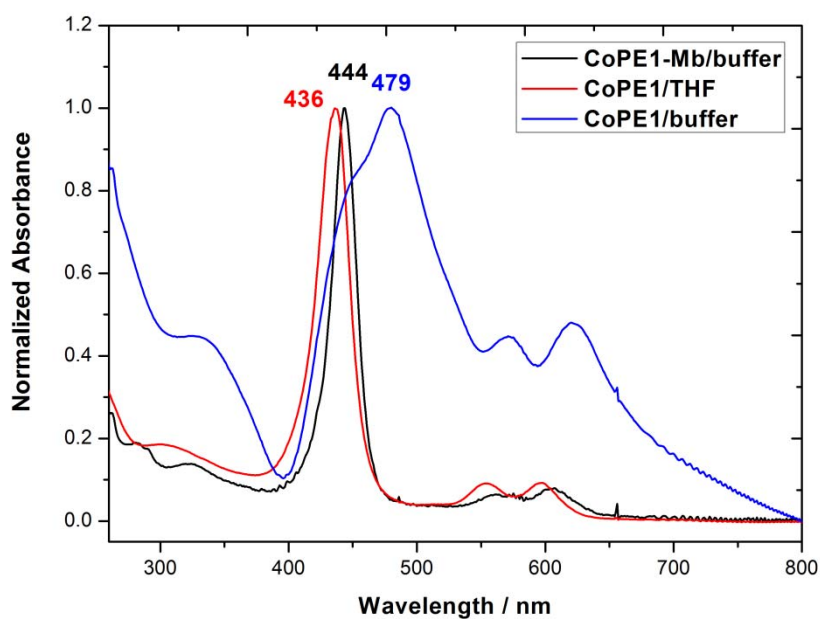
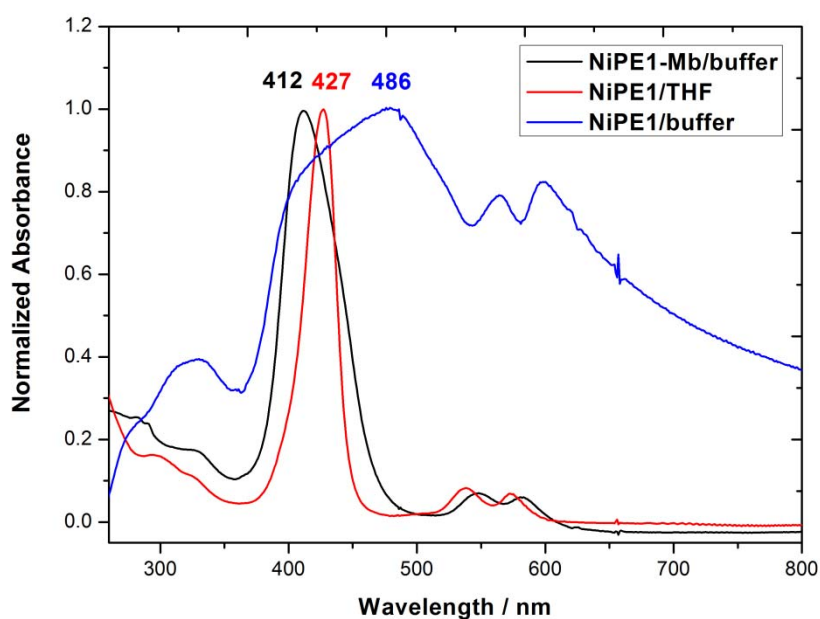
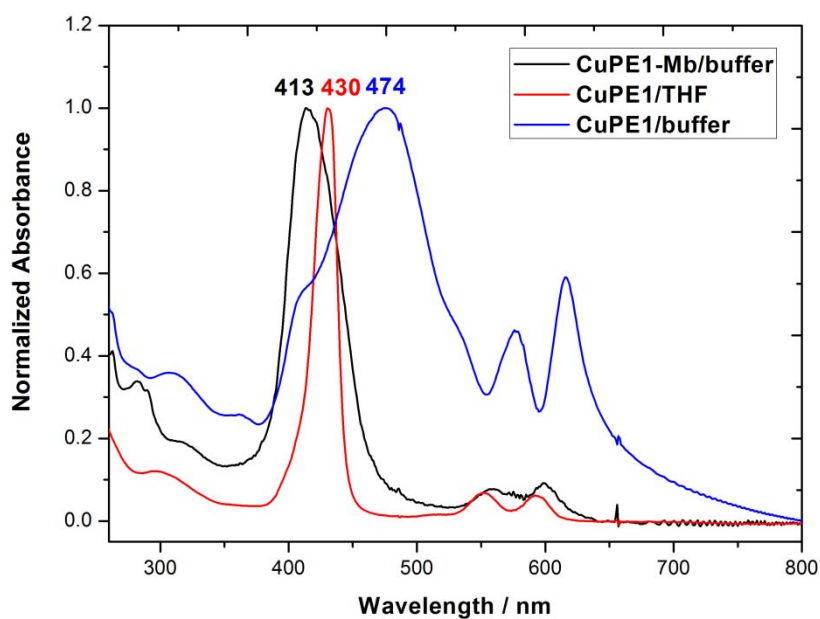


Figure 4-5 Normalized steady-state absorption spectra of CoPE1 in THF, 100mM KPi buffer and reconstituted with apo-Mb in 100mM KPi.



**Figure 4-6** Normalized steady-state absorption spectra of NiPE1 in THF, 100mM KPi buffer and reconstituted with apo-Mb in 100mM KPi.



**Figure 4-7** Normalized steady-state absorption spectra of CuPE1 in THF, 100mM KPi buffer and reconstituted with apo-Mb in 100mM KPi.

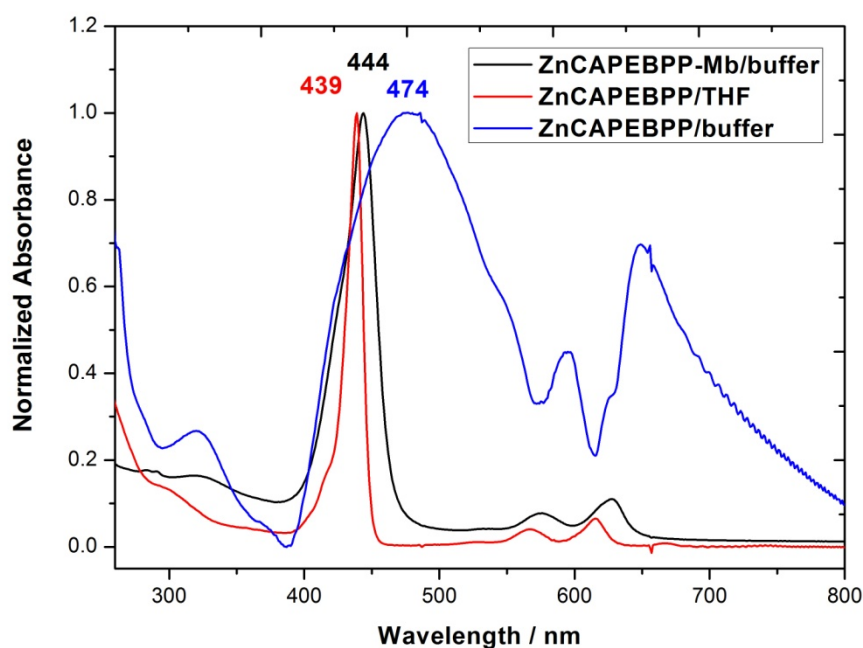


Figure 4-8 Normalized steady-state absorption spectra of ZnPE1 in THF, 100mM KPi buffer and reconstituted with apo-Mb in 100mM KPi.

Table 4-1 Absorption maxima (nm) and the extinction coefficients ( $\text{cm}^{-1}\text{M}^{-1}$ ) of MtPE1

Entry <sup>a</sup>	Soret ( $\log \epsilon$ )	Q ( $\log \epsilon$ )
H <sub>2</sub> PE1	430 (5.54)	526 (4.12), 566 (4.37) 604 (3.77), 661 (3.96)
CoPE1	430 (5.40)	541 (4.15), 577 (4.09)
NiPE1	427 (5.36)	538 (4.23), 573 (4.14)
CuPE1	431 (5.50)	552 (4.24), 594 (4.20)
ZnPE1	439 (5.65)	568 (4.23), 616 (4.44)

<sup>a</sup> This work was measured in THF

**Table 4-2 Absorption maxima (in nm)of MtPE1-Mbs**

<b>Entry<sup>a</sup></b>	<b>Soret band</b>	<b>Q band</b>
<b>H<sub>2</sub>PE1-Mb</b>	<b>418</b>	<b>534, 576 615, 666</b>
<b>CoPE1-Mb</b>	<b>444</b>	<b>558, 607</b>
<b>NiPE1-Mb</b>	<b>412</b>	<b>548, 581</b>
<b>CuPE1-Mb</b>	<b>413</b>	<b>557, 599</b>
<b>ZnPE1-Mb</b>	<b>444</b>	<b>576, 628</b>

<sup>a</sup> This work was measured in 100mM KPi buffer

The Soret band of ZnPE1 in KPi buffer became much broader than that of ZnPE1-Mb in Kpi buffer and Zn-PP in THF, whereas red-shift was observed for the Soret and Q bands. The broad and red-shifted spectral features of ZnPE1 in KPi buffer are generally attributed to a side-by-side aggregation (J type aggregation) of ZnPE1 aggregates in aqueous solution. Ribo *et al.* discussed in detail the formation of H- and J-aggregates, which are characterized by face-to-face and side-by-side arrangements of the porphyrins, respectively.<sup>32</sup> In the case of J-aggregates, a red shift of the Soret band is expected.<sup>32</sup> The putative red-shifted Q-band absorption peaks signify that the assembly consists of head-to-tail aggregates (J-aggregates).<sup>33,34</sup> A red-shift was observed for both the Soret and the Q bands of ZnPE1-Mb in KPi buffer solution. Because the energy of a typical  $\pi$ - $\pi^*$  state in



porphyrins decreases with increasing solvent polarity, the energy gap of the  $S_0 \rightarrow S_1$  transition for ZnPE1-Mb in KPi buffer is smaller than that of Zn-PP in THF, which is consistent with the red shifted spectral feature of the Q band of the former with respect to the latter. The same is true for the  $S_0 \rightarrow S_2$  transition of ZnPE1-Mb in KPi buffer for which a 5 nm red-shift of Soret band was observed by comparing with ZnPE1 in THF.



## 4.2.2 Fluorescence analysis results

### 4.2.2.1 MtPE1

The Emission spectra of H<sub>2</sub>PE1 and MtPE1 (Co, Ni, Cu, Zn) in THF excited at 435nm were shown in figure 4-9. The emission spectrum of H<sub>2</sub>PE1 showed emission maxima at 621, 663 and 723 nm, and MtPE1 (Co, Ni, Cu, Zn) at 621 and 670 nm. The emission fluorescence spectra of MtPE1 showed a mirror image of the Q band. By comparing with ZnPE1, the fluorescence intensity of MtPE1 (Co, Ni, Cu) was relatively weak. The loss of fluorescence might be quenched by the metal in the center of H<sub>2</sub>PE1 with unfilled d orbital. The fluorescence spectrum in THF shows S<sub>1</sub>→ S<sub>0</sub> emission with corresponding maxima located at 621 and 663 nm, respectively.

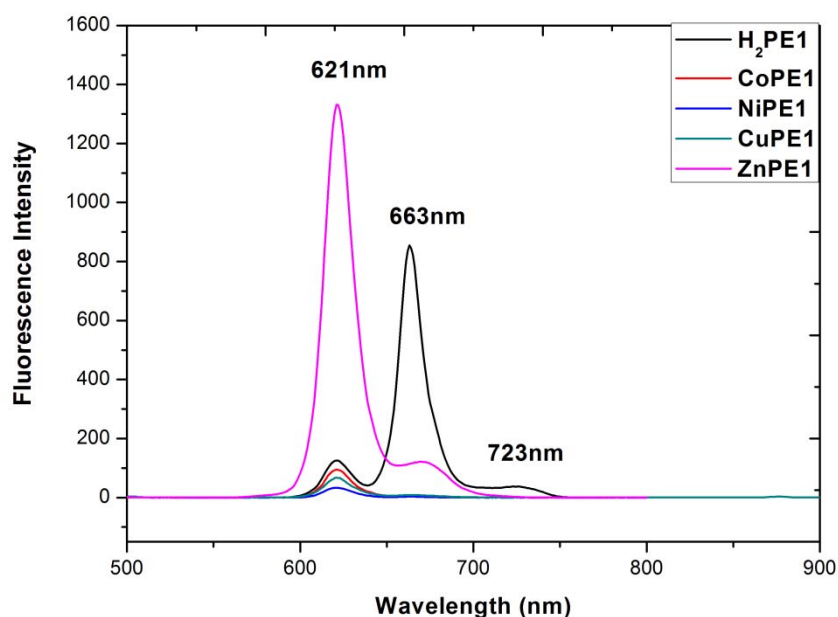


**Figure 4-9** The emission spectra of H<sub>2</sub>PE1 and MtPE1 (Co, Ni, Cu, Zn) in THF.

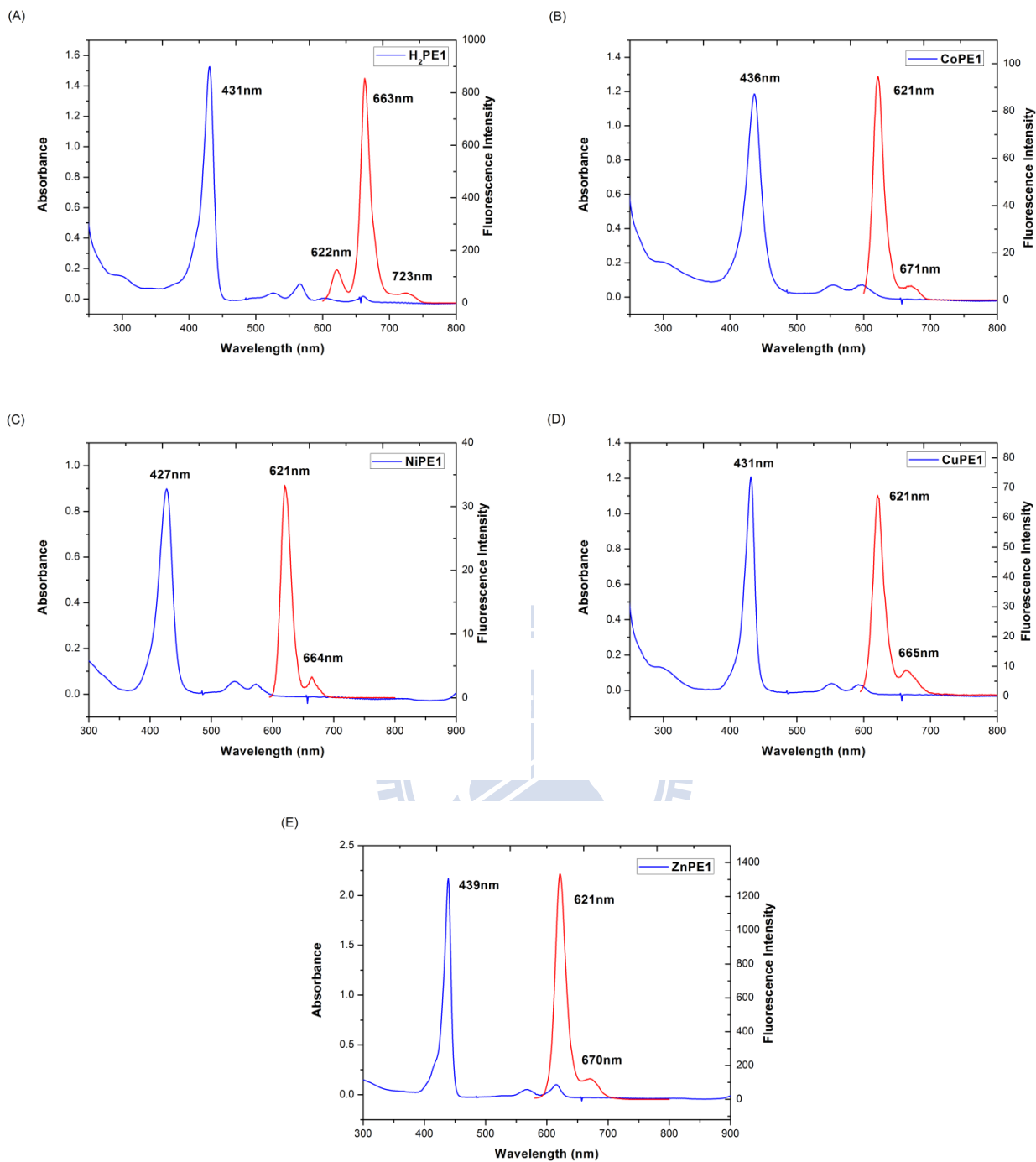


**Figure 4-10 The steady-state emission fluorescence spectra of MtPE1 by exciting at 435nm. (a) H<sub>2</sub>PE1 (b) CoPE1 (c) NiPE1 (d) CuPE1 (e) ZnPE1**

#### 4.2.2.2 MtPE1-Mbs

The emission spectra of H<sub>2</sub>PE1-Mb and MtPE1-Mbs (Co, Ni, Cu, Zn) in 100 mM KPi excited at 435nm were shown in figure 4-11. The emission spectrum of H<sub>2</sub>PE1-Mb showed emission maxima at 630, 668 and 730 nm, and MtPE1-Mbs (Co, Ni, Cu, Zn) at 621 and 670 nm. The emission fluorescence spectra of MtPE1-Mbs showed a mirror image of the Q band. By Comparing with ZnPE1-Mb, the fluorescence intensity of other MtPE1-Mbs (Co, Ni, Cu) was relatively weak. Like the conjecture of MtPE1 in THF previously, the lost of fluorescence might be quenched by the metal in the center of H<sub>2</sub>PE1 with unfilled *d* orbital. The fluorescence spectrum in THF showed S<sub>1</sub>→ S<sub>0</sub> emission with corresponding maxima located at 630 and 668nm, respectively.

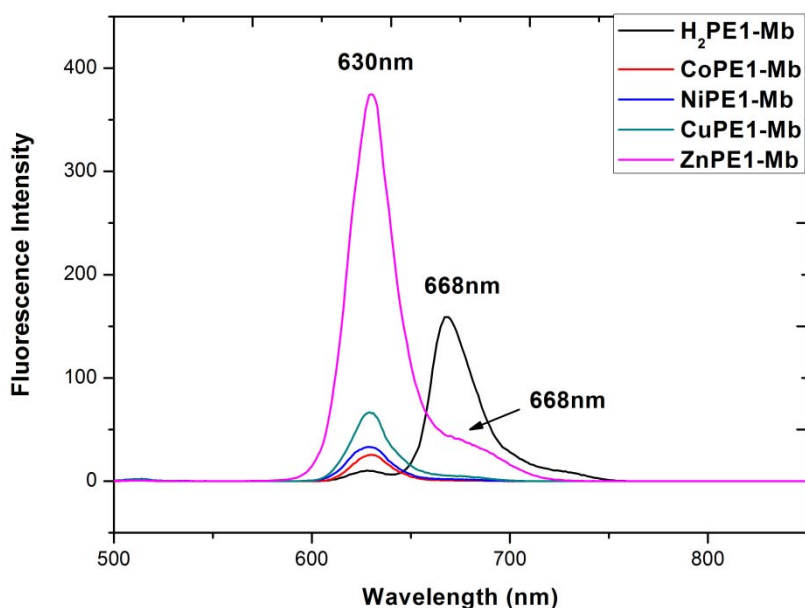


**Figure 4-11** The emission spectra of 2.5 $\mu$ M MtPE1-Mb in 100 mM Kpi.

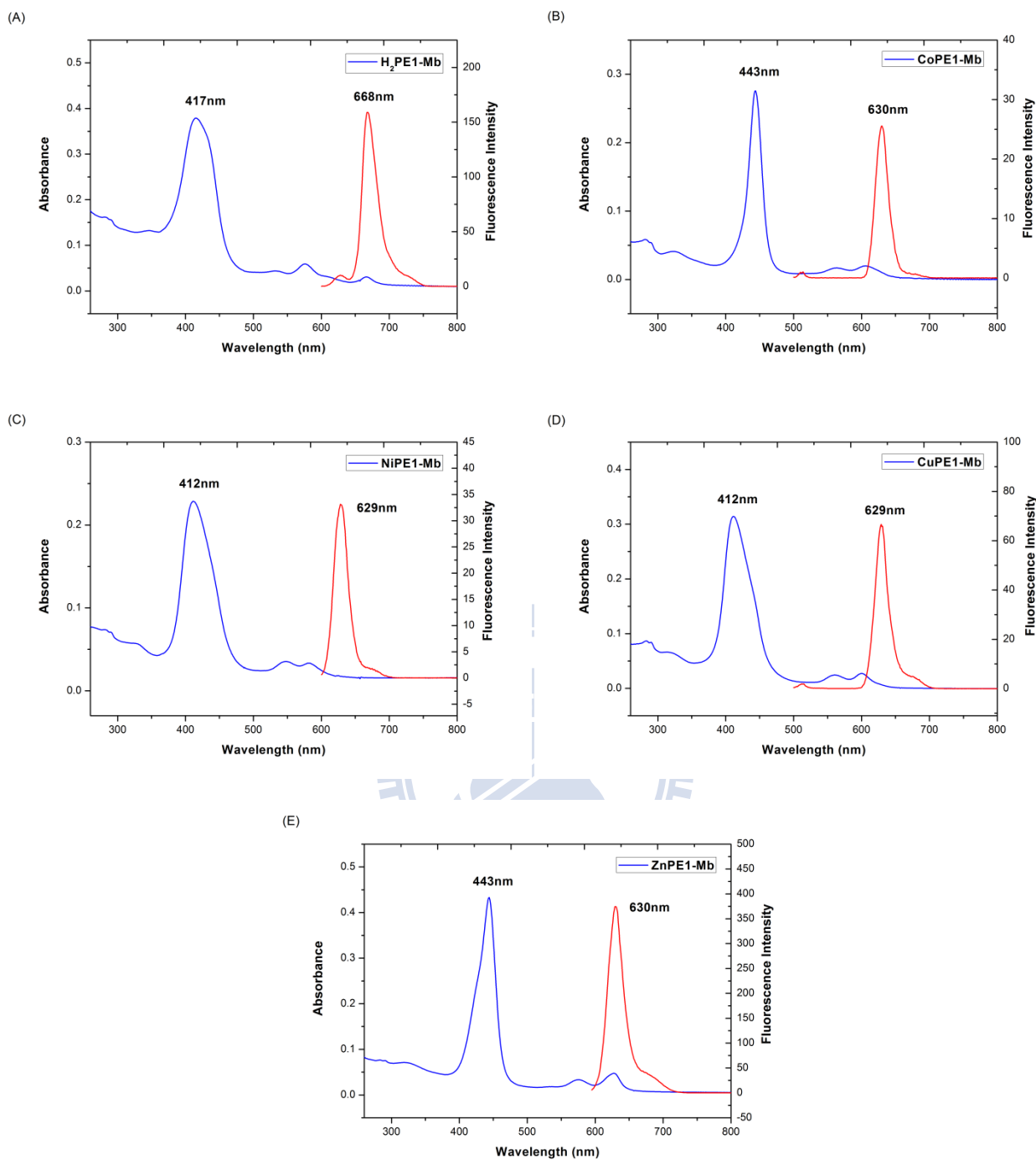
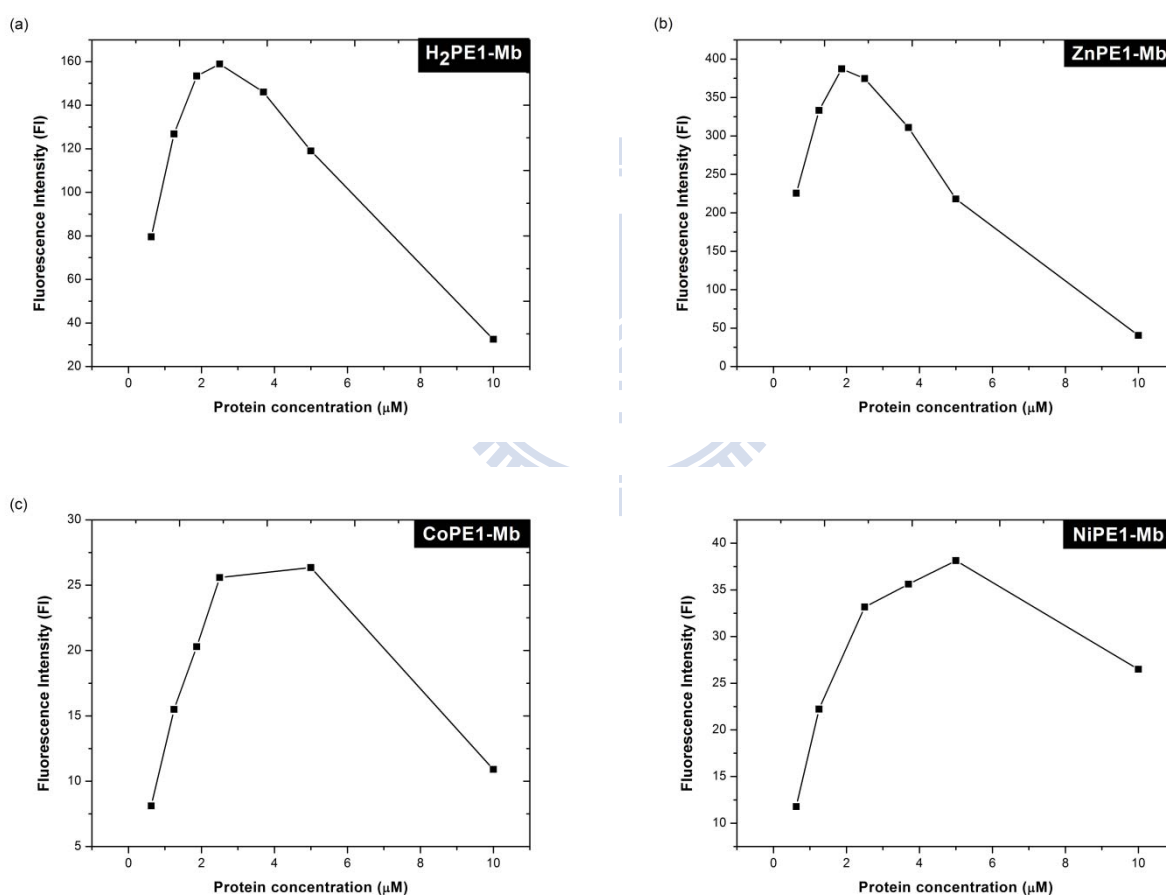


**Figure 4-12** The steady-state emission fluorescence spectra of MtPE1-Mb by exciting at 435 nm.

(a) H<sub>2</sub>PE1-Mb (b) CoPE1-Mb (c) NiPE1-Mb (d) CuPE1-Mb (e) ZnPE1-Mb

### 4.3 Picosecond fluorescence decays

The relationship between protein concentration and fluorescence intensity were showed in figure 4-13. Based on the results, we could know that when the protein concentration was higher than  $\sim 2.5$   $\mu\text{M}$ , the fluorescence intensity was decreased by high concentration effect. To avoid self-quenching attributed to high concentration effect, adjustment of protein concentration was needed to keep off interaction between fluorescence molecules. In addition to retain high fluorescence intensity concurrently, the protein concentration for picosecond time-resolved fluorescence measurement is  $2\sim 2.5$   $\mu\text{M}$ .



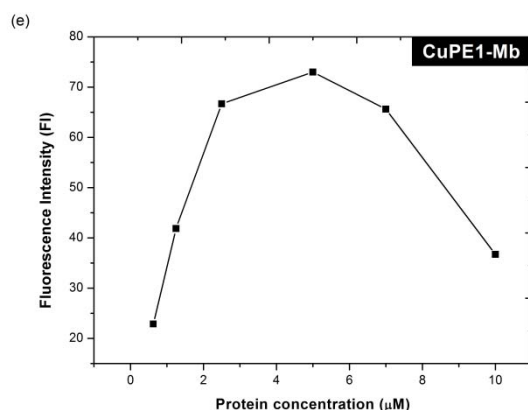


**Figure 4-13 The relationship between protein concentration and fluorescence intensity in 100mM KPi buffer. Obtain fluorescence intensity at  $\lambda_{\text{em}}=630\text{nm}$  (Co, Ni, Cu, Zn) and  $\lambda_{\text{em}}=668\text{nm}$  ( $\text{H}_2$ ) with excitation at  $\lambda_{\text{ex}}=435\text{nm}$ .**

According to Ching-Yao *et. al.* femtosecond investigation, the transients reflect the behavior occurring in electronic states  $S_2$  and  $S_1$  of ZnPE1 in THF, and discuss the internal conversion (IC)  $S_2 \rightarrow S_1$  and  $S_1 \rightarrow T_1$  intersystem crossing (ISC).

Our relaxation dynamic studies were analyzed by picosecond measurement, and emphasized that  $S_1 \rightarrow T_1$  intersystem crossing. The transients observed at  $\lambda_{\text{em}} = 620 \text{ nm}$  (Co, Ni, Cu, Zn) and  $\lambda_{\text{em}} = 663 \text{ nm}$  ( $\text{H}_2$ ) reflected the dynamical behavior occurring in electronic state  $S_1$  of MtPE1 in THF. And the transients observed at  $\lambda_{\text{em}} = 630 \text{ nm}$  (Co, Ni, Cu, Zn) and  $\lambda_{\text{em}} = 668 \text{ nm}$  ( $\text{H}_2$ ) reflected the relaxation dynamics in electronic state  $S_1$  of MtPE1-Mb in 100 mM KPi buffer. Figure 4-14 shows the results of fluorescent decays. Comparing with the lifetime  $\tau_1 = 2.338 \text{ ns}$  of a monomeric ZnPE1 in THF, the  $\tau_2 = 2.4716 \text{ ns}$  of ZnPE1-Mb in 100mM KPi was the  $S_1 \rightarrow T_1$  intersystem crossing (ISC) of the monomeric ZnPE1 inside the heme pocket of apo-Mb. The  $\tau_1$  with short lifetime was contributed by free ZnPE1 molecules out of the Mb in the form of ZnPE1 aggregates in KPi buffer. Except the lifetime of  $\text{H}_2\text{PE1}$  and  $\text{H}_2\text{PE1-Mb}$  were 8.827 ns and 10.062 ns, respectively, the lifetime of others (Co, Ni, Cu, Zn) were about  $\sim 2 \text{ ns}$ .

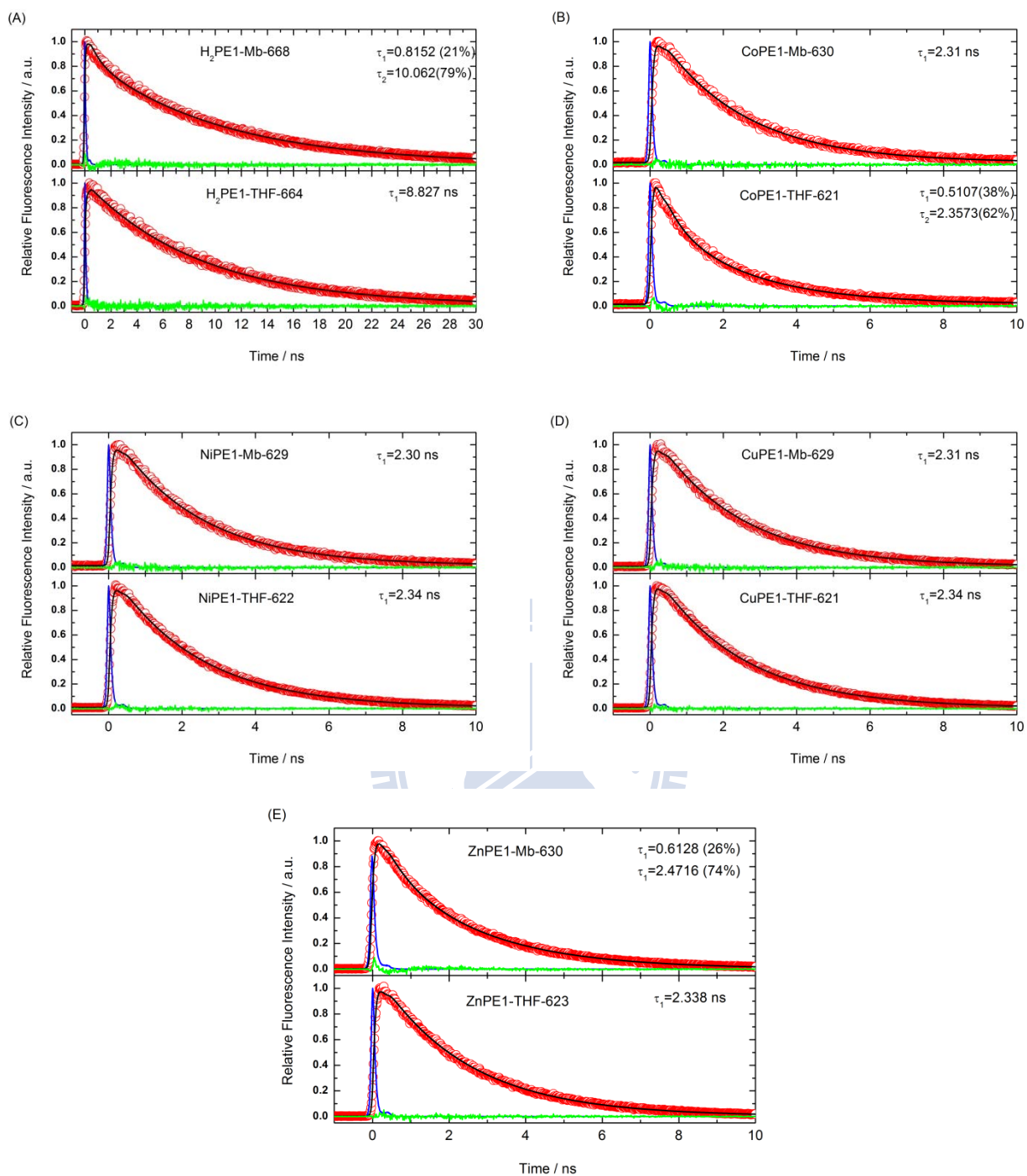


**Figure 4-14 Picosecond fluorescence transients of reconstituted MtPE1-Mb in buffer solution with  $\lambda_{\text{ex}} = 435 \text{ nm}$  at  $\lambda_{\text{em}} = 630 \text{ nm}$  (Co, Ni, Cu, Zn) and  $\lambda_{\text{em}} = 668 \text{ nm}$  ( $\text{H}_2$ ).**

The fluorescence lifetime results of MtPE1 and MtPE1-Mb were summarized at Table 4-3 and Table 4-4.



**Table 4-3 Fluorescence lifetime<sup>a</sup> of the excited state of MtPE1 in THF**

Entry	emission /nm	$\tau_{S1}/ns$
H <sub>2</sub> PE1	622, 664, 723	$\tau_1=8.827$ ns
CoPE1	621, 671	$\tau_1=0.65$ (36%) $\tau_2=2.371$ (64%)
NiPE1	620, 664	$\tau_1=2.34$
CuPE1	621, 665	$\tau_1=2.34$
ZnPE1	621, 670	$\tau_1=2.338$

<sup>a</sup> S<sub>1</sub> lifetimes were monitored at 620nm or 664nm

**Table 4-4 Fluorescence lifetime<sup>a</sup> of the excited state of MtPE1-Mb in 100mM KPi buffer**

Entry	emission /nm	$\tau_{S1}/ns$
H <sub>2</sub> PE1-Mb	668	$\tau_1=0.8152$ (21%) $\tau_2=10.062$ (79%)
CoPE1-Mb	630	$\tau_1=2.317$
NiPE1-Mb	629	$\tau_1=2.30$
CuPE1-Mb	629	$\tau_1=2.31$
ZnPE1-Mb	630	$\tau_1=0.6128$ (26%) $\tau_2=2.4716$ (74%)

<sup>a</sup> S<sub>1</sub> lifetimes were monitored at 630nm or 668nm

#### 4.4 Cyclic voltammetry measurement

Direct electron transfer between proteins and the electrode can be a model system to aid the understanding of electron transfer mechanisms in biological system. Studies with protein solution may be often confronted with challenges such as the difficulty to achieve the direct electrochemistry of protein on some bare electrodes and the poor reversibility of the direct heterogeneous electron transfer reactions between electrodes and biological molecules. The reasons that inhibit the direct electron transfer between electrodes and proteins may be mainly attributed to i) electroactive prosthetic groups deep within the protein structure , ii) adsorption denaturation of protein onto electrodes, iii) unsymmetric distribution of surface charges on protein molecules and iv) low rate of mass transfer process of proteins.<sup>35</sup> It was found that electrode modified with surfactant (dodecyldimethylammonium bromide, DDAB) providing bio-membrane-like microenvironment was useful for the study of protein redox chemistry.<sup>30</sup>

Didodecyldimethylammonium bromide (DDAB) is one kind of cationic surfactant, the structure contain one positively charged head group and two hydrocarbon tails. (Fig. 4-15)



**Figure 4-15 Chemical structure of dodecyldimethylammonium bromide (DDAB)**

Under suitable concentration and temperature, DDAB molecules can be self-assembled into a double-layer structure either as vesicles in the dispersion or as an ordered multilayer film on solid surfaces. The critical value ( $T_c$ ) of DDAB is at about 16 °C. As the temperature below  $T_c$ , the bilayer structure exists in a highly ordered tail-to-tail form with all hydrocarbon chain in a trans configuration. The all-trans configuration characterizes a solid-like phase called the “gel” state. As

temperature increases to above  $T_c$ , the increase in energy may lead to kinks of the hydrocarbon chains and an increase in fluidity of the bilayers. The “chain melting” at above  $T_c$  results in a liquid crystal phase, so the DDAB double-layer structure takes the liquid crystal state at room temperature. The ordered structure of DDAB bilayers is very similar to biomembrane, in which the constituent lipids are arranged in a double-layer structure with the tail-to-tail configuration, and proteins are adsorbed onto the surface or imbedded into the bilayers.

We can use the reduction potential, oxidation potential and cooperate with UV-Vis analysis to calculate the LUMO, HOMO and band gap. To ascertain if MtPE1-Mbs have well-matched energy levels to apply in energy conversion study. All complex are analyzed with cyclic and differential pulse voltammetry.

#### **4.4.1 Analyzed with cyclic and differential pulse voltammetry (CV and DPV)**

CV for Mb-DDAB films at  $0.1 \text{ V}^{-1}\text{s}^{-1}$  in pH 7 acetate buffer containing no Mb show two pairs of cathodic-anodic peaks. The first pair of peaks centered  $-0.17 \text{ V}$  vs. Ag/AgCl represented the  $\text{MbFe}^{\text{III}}/\text{Fe}^{\text{II}}$  couple. The second pair of peaks centered at about  $-1.02\text{V}$  vs. Ag/AgCl represented the  $\text{MbFe}^{\text{II}}/\text{Fe}^{\text{I}}$  couple.(Fig 4-16 (A)) By using DPV, the results of CV could be confirmed more clearly. (Fig 4-16 (B))

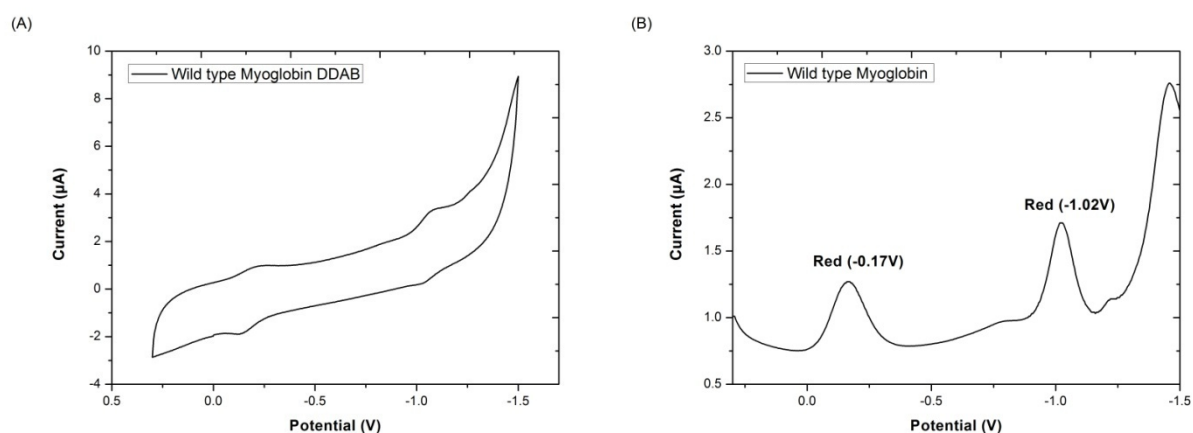


**Figure 4-16 Cyclic and differential pulse voltammetry (CV and DPV) analysis for wild type Myoglobin**

Peak separations of the redox couples for the  $\text{MbFe}^{\text{III}}/\text{Fe}^{\text{II}}$  and  $\text{MbFe}^{\text{II}}/\text{Fe}^{\text{I}}$  in native Mb at  $100 \text{ mVs}^{-1}$  were  $40 \text{ mV}$  and  $35 \text{ mV}$ , respectively, which are smaller than  $58 \text{ mV}$ , suggesting that the redox current at the electrode is from the surface-confined species of Mb in DDAB film.

The first one electron transfer reaction which was porphyrin-ring reduction of  $\text{H}_2$ , Ni, Cu, and ZnPE1-Mbs, were observed at  $-0.97 \text{ V}$ ,  $-1.04 \text{ V}$ ,  $-1.15 \text{ V}$  and  $-1.14 \text{ V}$ , respectively. (Fig. 4-17 to Fig. 4-21) In addition, metal-center reactions were observed at  $-0.632 \text{ V}$  for Co(II/I)PE1-Mb. The reduction reactions of PE1 substituent were observed at  $-0.8 \text{ V}$ ,  $-1.04 \text{ V}$ ,  $-0.964 \text{ V}$ ,  $-1.028 \text{ V}$  for  $\text{H}_2$ , Ni, Cu, and ZnPE1. The overall results are shown in Table 4-5 and Table 4-6. The maximal change with MtPE1-THF was the shift of PE1 substituent reduction potential. Maybe the shift of PE1 substituent reduction potential could be attributed to the interaction between MtPE1, apo-Mb and DDAB.

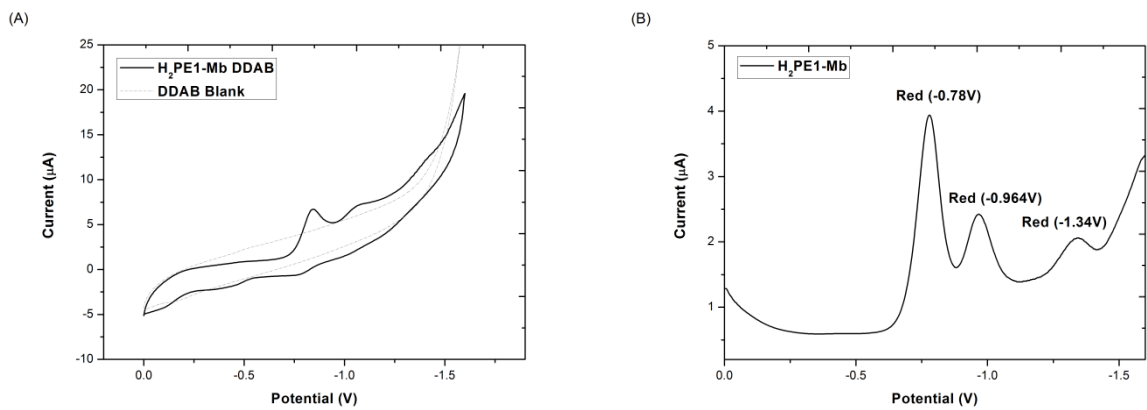


**Figure 4-17 C-V and differential pulse for  $\text{H}_2\text{PE1-Mb}$**

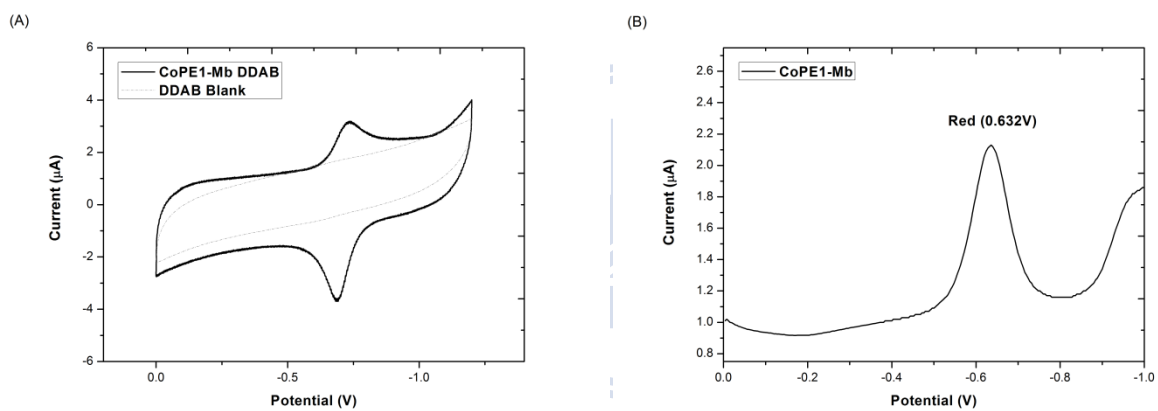


**Figure 4-18 C-V and differential pulse for  $\text{CoPE1-Mb}$**

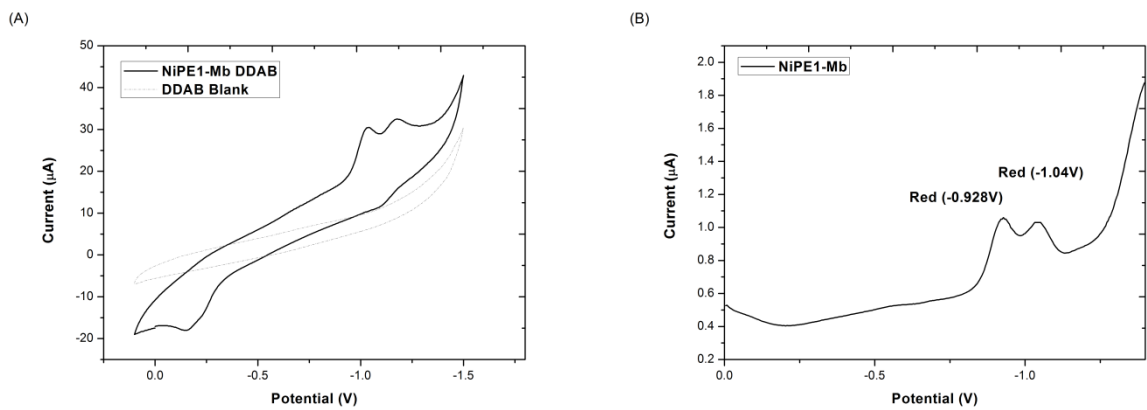


**Figure 4-19 C-V and differential pulse for NiPE1-Mb**

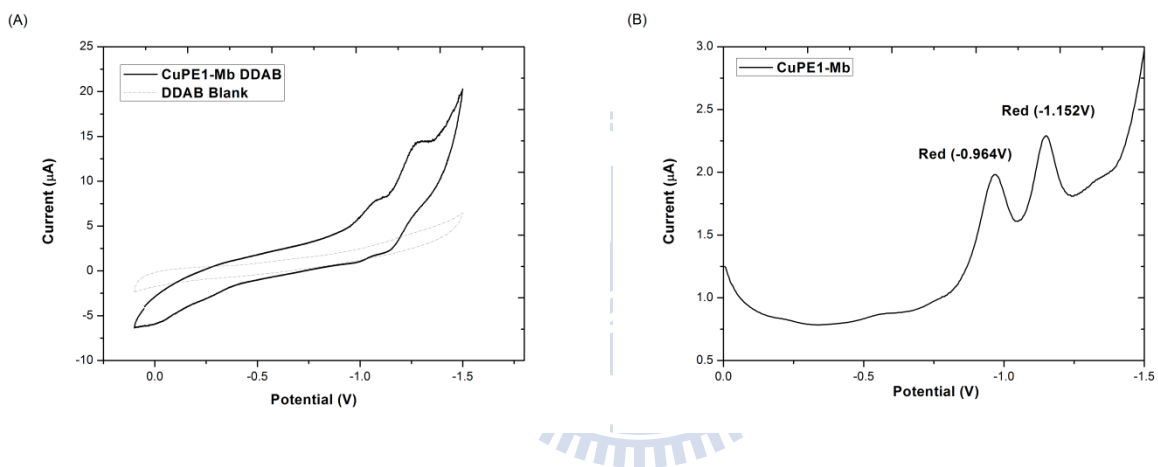


**Figure 4-20 C-V and differential pulse for CuPE1-Mb**

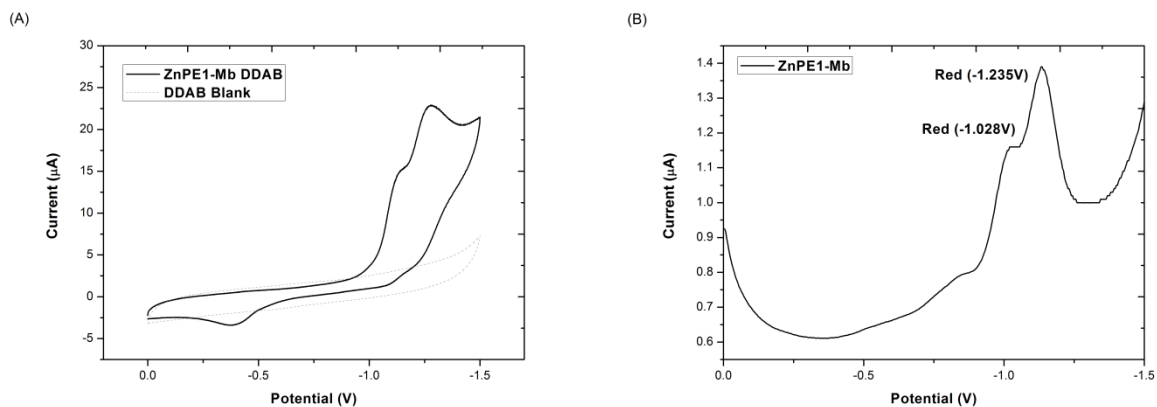


Figure 4-21 C-V and differential pulse for ZnPE1-Mb

Table 4-5 Redox potentials of MtPE1

Entry <sup>a</sup>	PE substituent reduction	Metal-centered reactions	Porphyrin ring reduction 1	Porphyrin ring reduction 2
H <sub>2</sub> PE1	-0.90(E <sub>pc</sub> )		-1.02	-1.47
CoPE1	overlapped	Co <sup>III/I</sup> =-0.86		
NiPE1	-0.95(E <sub>pc</sub> )		-1.10	
CuPE1	-0.80(E <sub>pc</sub> )		-1.14	
ZnPE1	-0.81		-1.24	

<sup>a</sup> This work. (THF/0.1M TBAP/SCE)

**Table 4-6 Redox potentials of MtPE1-Mbs-DDAB**

Entry <sup>a</sup>	PE substituent reduction	Metal-centered reactions	Porphyrin ring reduction 1	Porphyrin ring reduction 2
H <sub>2</sub> PE1-Mb	-0.8		-0.964	-1.34
CoPE1-Mb		Co <sup>III/I</sup> =-0.632		
NiPE1-Mb	-1.04		-1.04	
CuPE1-Mb	-0.964		-1.13	
ZnPE1-Mb	-1.028		-1.235	

<sup>a</sup> This work. (Acetate buffer/Ag/AgCl)

#### 4.4.2 Energy level of electron donor and acceptor

According to investigation, the redox potential of TEA and NADP<sup>+</sup> at pH 8.0 is 0.7 V and -0.35 V, respectively. Our CV results of TEA and NADP<sup>+</sup> are shown in figure 4-22.

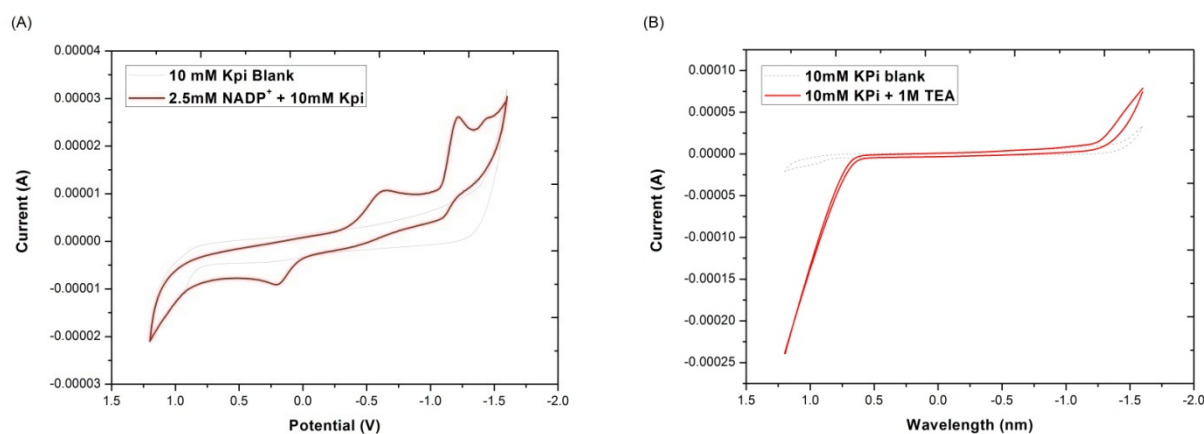


**Figure 4-22 CV analysis of (A) 2.5 mM NADP<sup>+</sup> in 10 mM KPi (B) 1 M TEA in 10mM KPi**



Based on the CV result of MtPE1-Mbs, we utilized the reduction potential of porphyrin ring to estimate the LUMO. Cooperating with  $\lambda_{\text{Knee section}}$  from UV-Vis spectra, the formula energy gap =  $1240/\lambda_{\text{Knee section}}$  and  $\text{LUMO} = \text{HOMO} - \text{Energy gap}$  help us to estimate the HOMO. Including MtPE1, TEA and  $\text{NADP}^+$ , the overall electron flow are illustrated in figure 4-23. We can assume that the electron transfer from TEA and  $\text{MtPE1-Mb}^*$  to  $\text{NADP}^+$  successfully, except CoPE1-Mb. The CV data of CoPE1-Mb doesn't show the reduction potential of porphyrin ring.

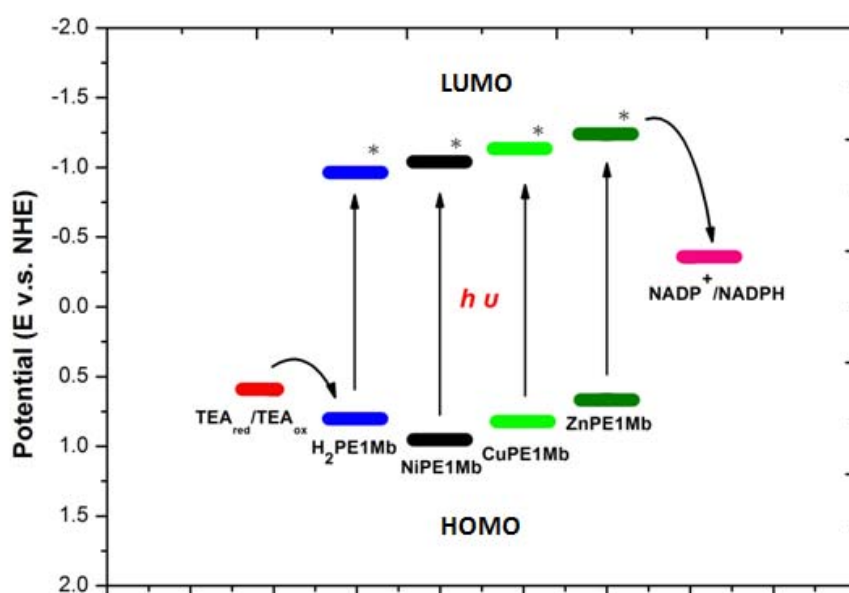


**Figure 4-23** The energy diagram of TEA,  $\text{NADP}^+$ ,  $\text{H}_2\text{PE1-Mb}$ ,  $\text{NiPE1-Mb}$ ,  $\text{CuPE1-Mb}$ ,  $\text{ZnPE1-Mb}$ .

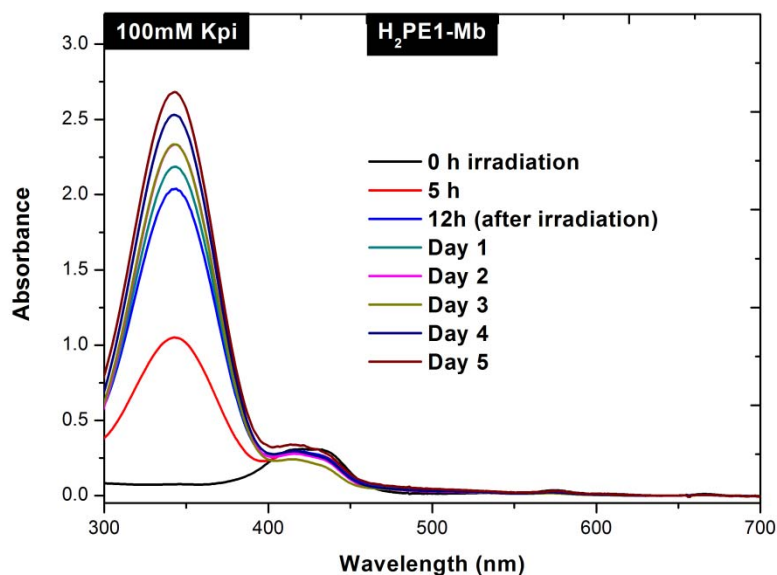
#### 4.5 Phototriggered chemical reduction result of MtPE1 and MtPE1-Mbs

Photochemical reduction of nicotinamide adenine dinucleotide phosphate ( $\text{NADP}^+$ ) using MtPE1 reconstituted myoglobin (MtPE1-Mb) functions as a photosensitizer, with triethanolamine (TEA) as a sacrificial donor. This simple model can let us compare the conversion efficiency with MtPE1 and MtPE1-Mbs. The experiment was carried out with  $10 \mu\text{M}$  MtPE1-Mbs,  $1 \text{ M}$  TEA, and  $5$

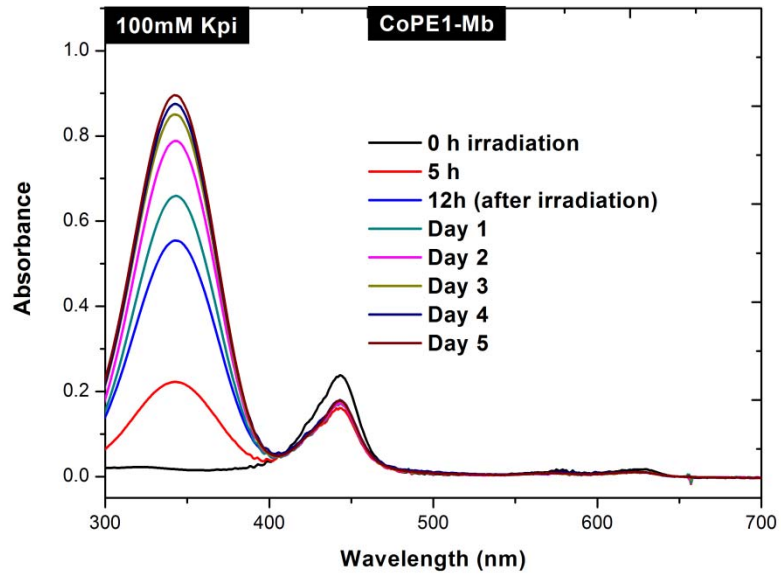
mM NADP<sup>+</sup> in 100 mM phosphate buffer on photoirradiation. By photoirradiated with single wavelength light at 419 nm, the increase of the absorbance at 340nm was attributed to NADPH formation. Figure 4-24 showed the visible spectral change of a 100 mM phosphate buffer solution (pH 9.2) containing 1 M of TEA, 10 μM of MtPE1-Mb, and 5 mM of NADP<sup>+</sup> for 5 hours photoirradiation then kept in the dark for 5 days.

And we also followed the same experimental conditions by using apo-Mb and no photosensitizer to do the negative control measurement. (Fig. 4-25)

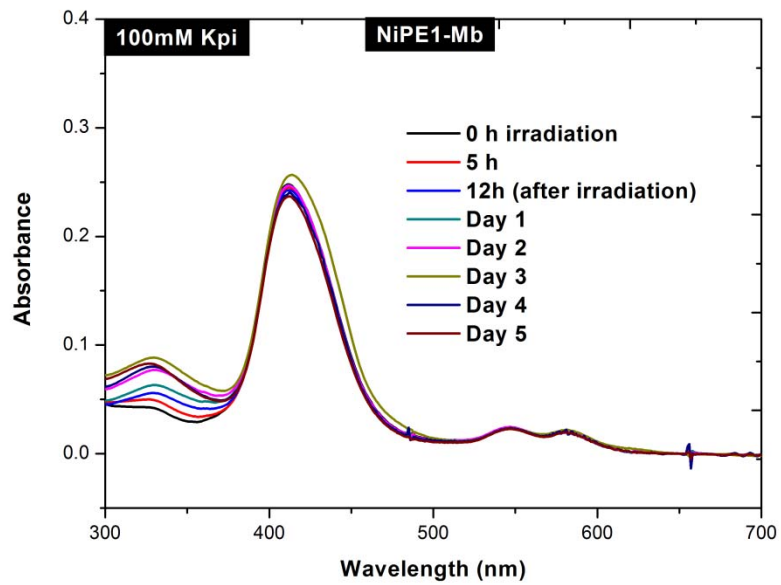
(A)



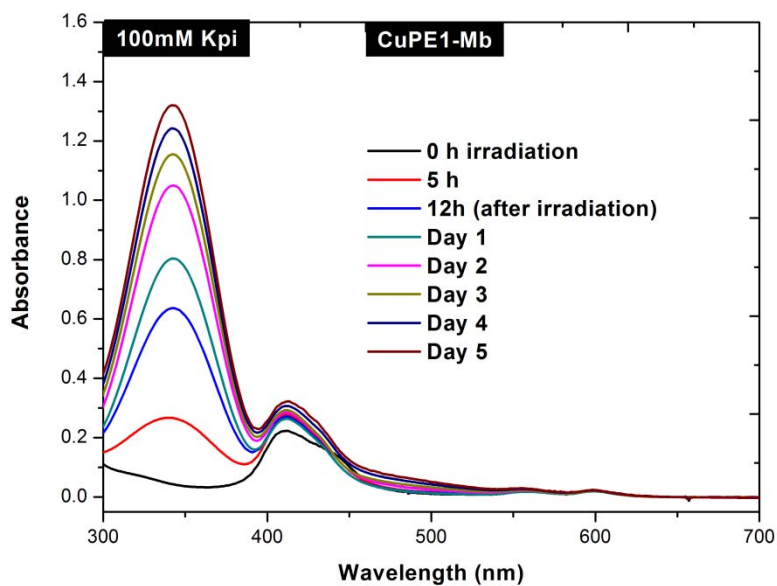
(B)



(C)



(D)



(E)

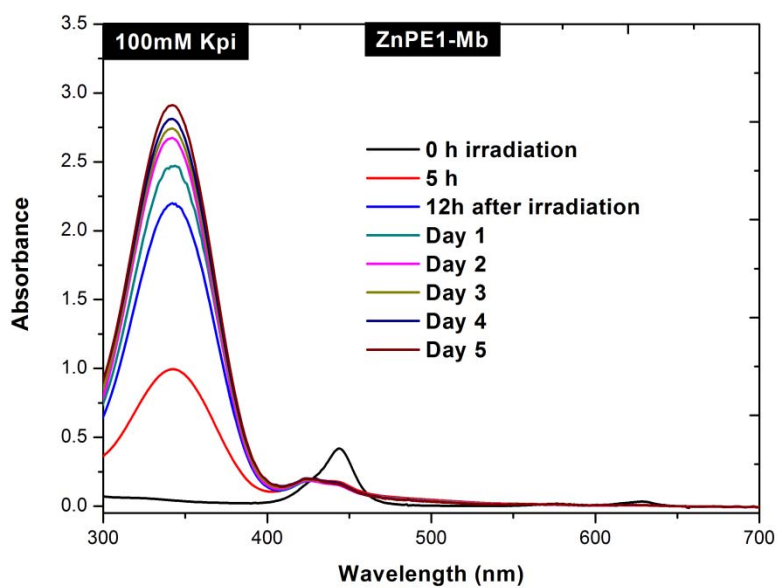


**Figure 4-24 Absorbance change in the solution containing 10 $\mu$ M (A) H<sub>2</sub>PE1-Mb (B) CoPE1-Mb (C) NiPE1-Mb (D) CuPE1-Mb (E) ZnPE1-Mb, 1 M TEA , and 5 mM NADP<sup>+</sup> in 100 mM KPi buffer after 5 hours irradiation.**

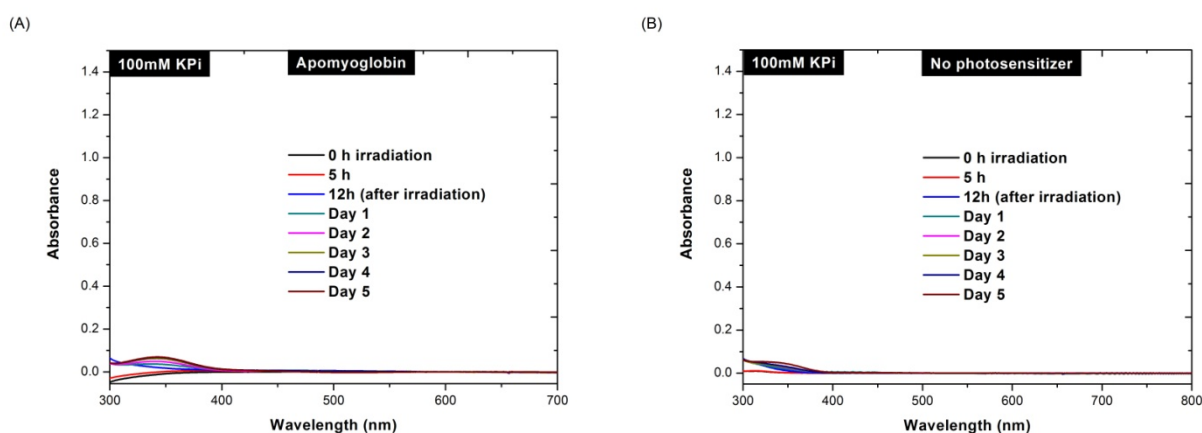


**Figure 4-25 Absorbance change in the solution containing (A)10 $\mu$ M apo-Mb (B) no photosensitizer, 1 M TEA , and 5 mM NADP<sup>+</sup> in 100 mM KPi buffer after 5 hours irradiation.**

And we performed similar experiment as in figure 4-24 but without photoirradiation, the results are showed in figure 4-26. The results display three kinds of conditions: MtPE1-Mb/TEA/NADP<sup>+</sup>, MtPE1-Mb/TEA/NADP<sup>+</sup> without irradiation and kept in the dark for 5 days, MtPE1-Mb/TEA/NADP<sup>+</sup> irradiated for 5 h then kept in the dark for 5 days-Without irradiation, very few NADP<sup>+</sup> was reduced.

After 5 days, approximately 4.5 mM of NADP<sup>+</sup> was converted to NADPH by ZnPE1-Mb. The conversion efficiency of MtPE1-Mbs is exhibited below. (Fig. 4-27) The absorbance at 340 nm increased gradually and reached the steady-state.

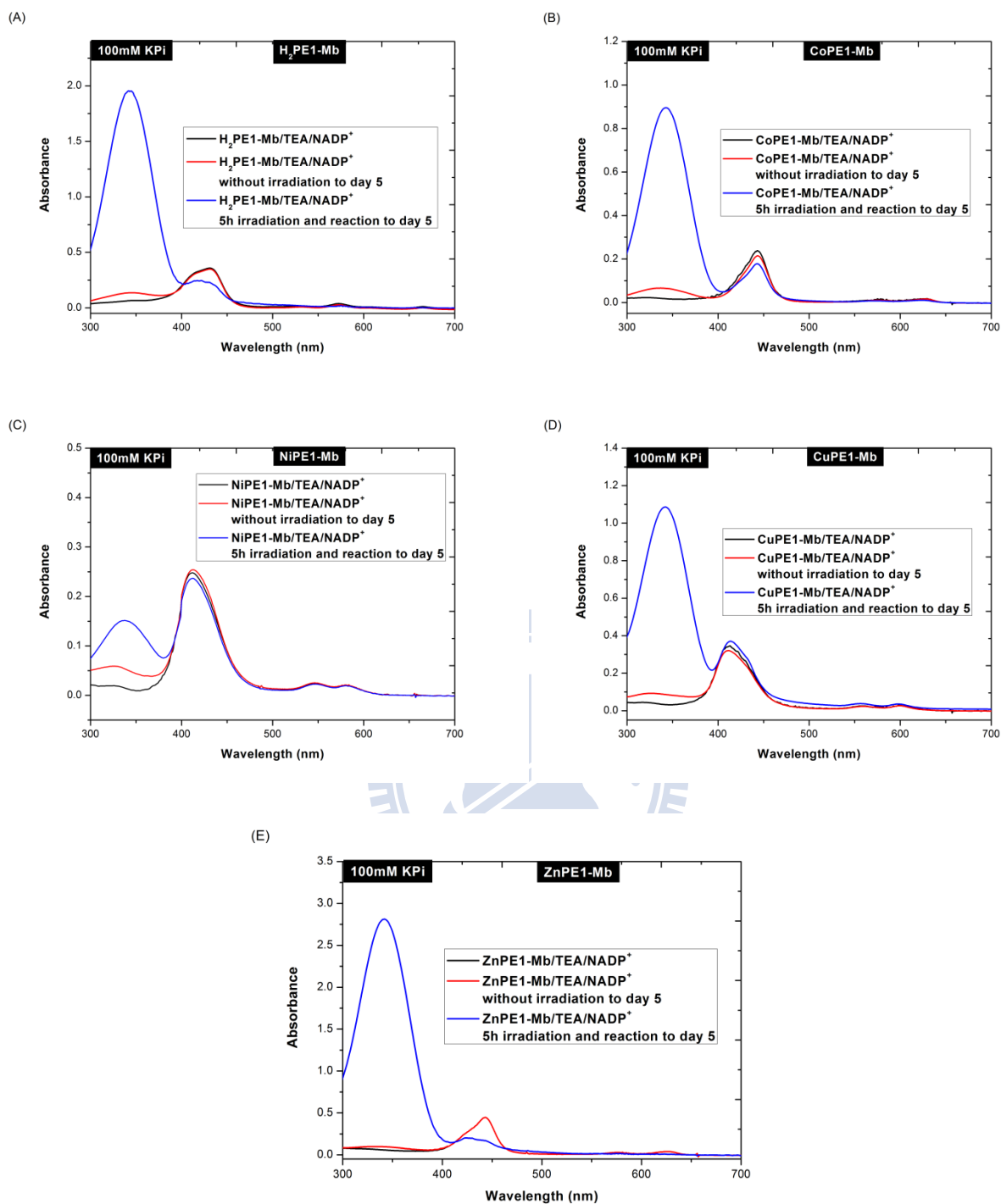


**Figure 4-26 Absorbance change for three kinds of condition:  $\text{MtPE1-Mb/TEA/NADP}^+$ ,  $\text{MtPE1-Mb/TEA/NADP}^+$  without irradiation and kept in the dark for 5 days,  $\text{MtPE1-Mb/TEA/NADP}^+$  irradiated 5 h and kept in the dark for 5 days.**

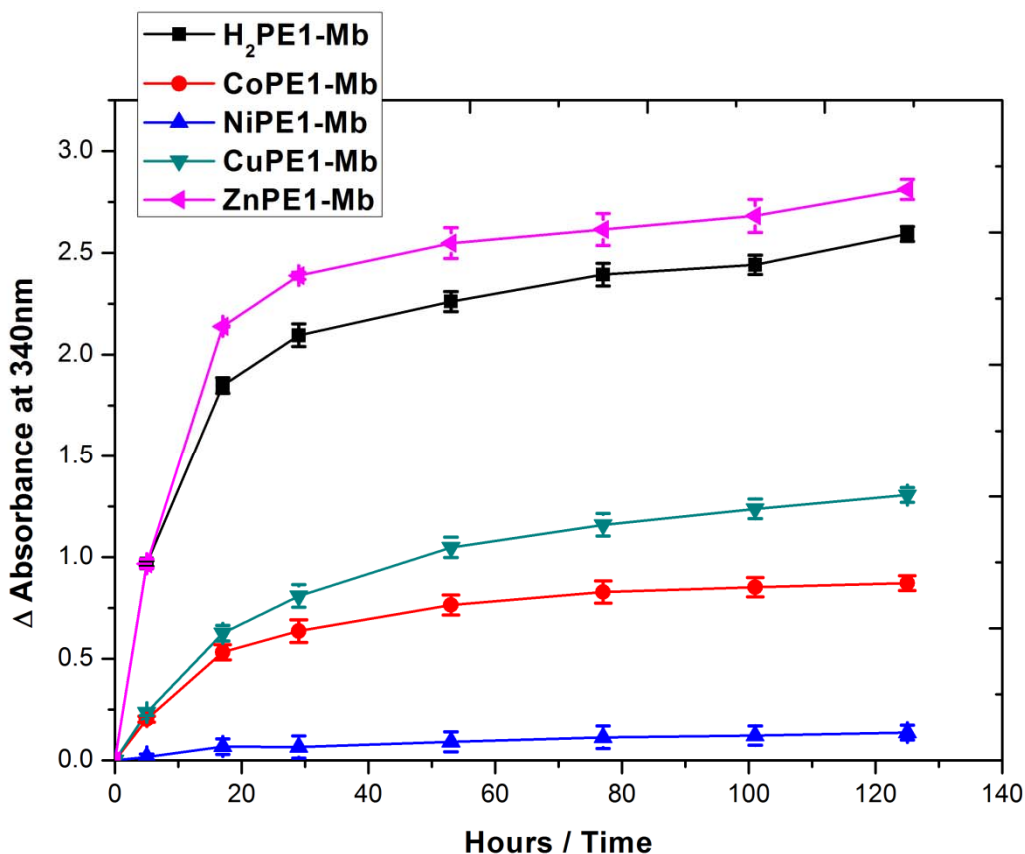


**Figure 4-27 Absorbance change at 340 nm in the solution containing 10  $\mu$ M of (a) H<sub>2</sub>PE1-Mb (b) CoPE1-Mb (c) NiPE1-Mb (d) CuPE1-Mb (e) ZnPE1-Mb, 1 M TEA and 5 mM NADP<sup>+</sup> after 5h irradiation.**

Interestingly, when irradiation was stopped, the absorbance at 340 nm still increased with time in the dark. We inferred that photosensitizer integrated with TEA to form a catalyst, which could catalyze NADP<sup>+</sup> to NADPH continually at least 5 days. The prerequisite of NADPH formation was both photosensitizer and TEA existed simultaneously in photoirradiated process. To test and verify this hypothesis, we examined several kinds of reaction conditions. (1) NADP<sup>+</sup> was mixed with ZnPE1-Mb in photoirradiated process without TEA and then TEA was added in the dark reaction, (2) ZnPE1-Mb was photoirradiated without TEA and NADP<sup>+</sup>, and then TEA and NADP<sup>+</sup> were added in

the dark reaction, (3) TEA was mixed with ZnPE1-Mb in photoirradiated process and then  $\text{NADP}^+$  was added in the dark reaction, and (4) ZnPE1-Mb, TEA and  $\text{NADP}^+$  were mixed and photoirradiated simultaneously. (Fig. 4-28)

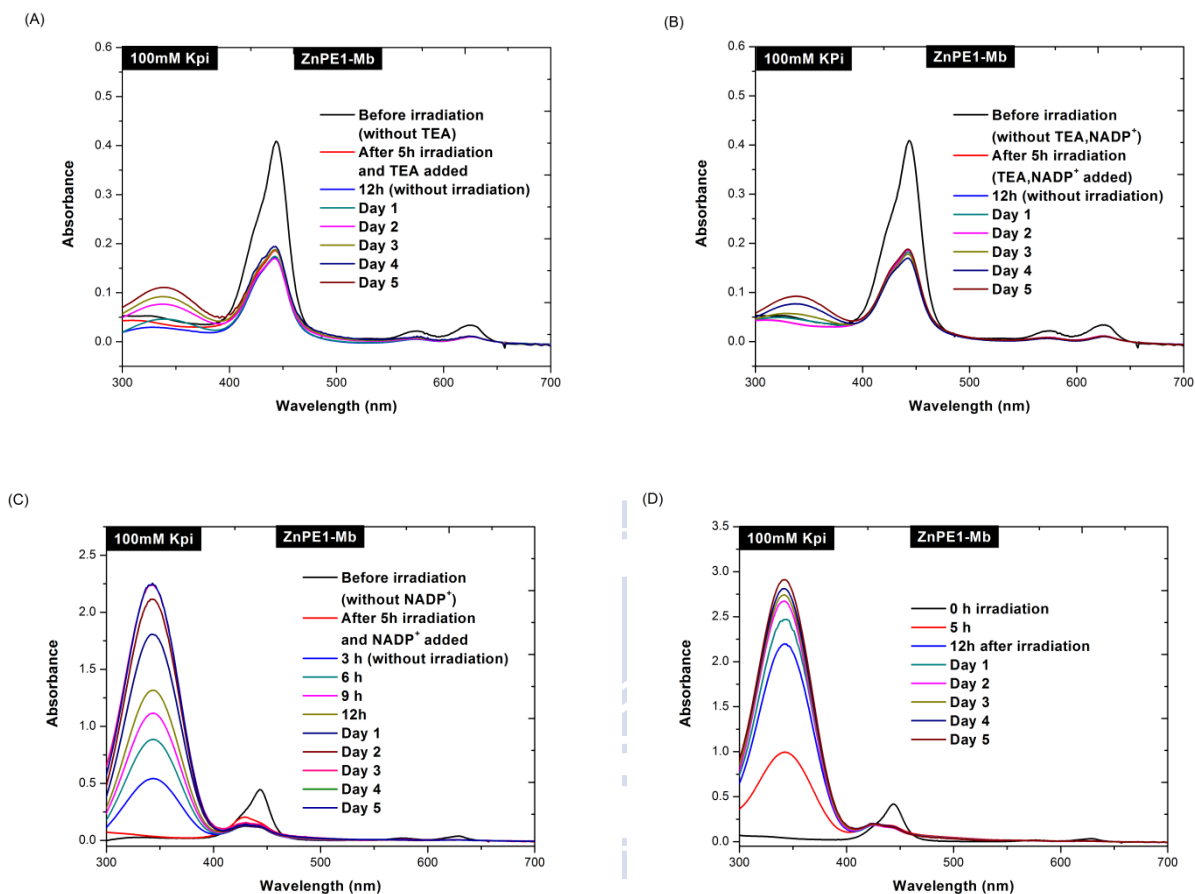
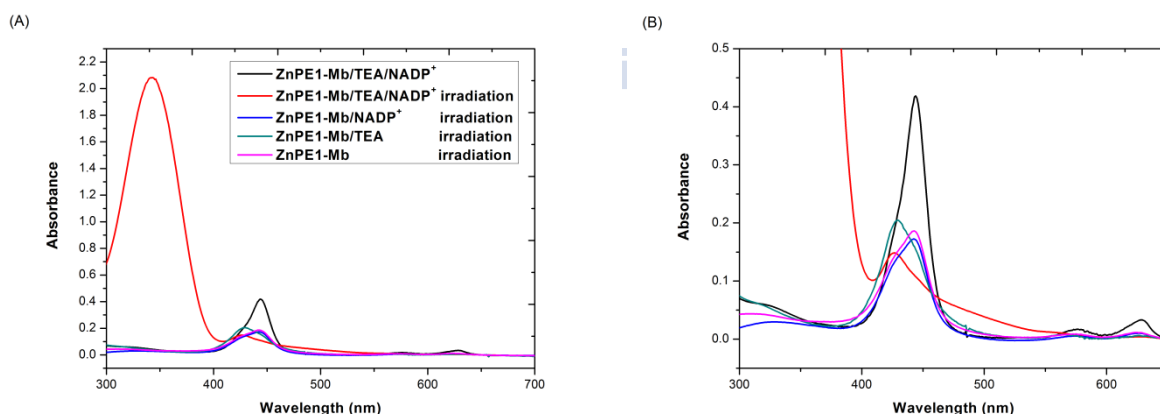


**Figure 4-28** Four kinds of reaction conditions (A)  $\text{NADP}^+$  was mixed with ZnPE1-Mb in photoirradiated process without TEA and then TEA was added in the dark reaction, (B) ZnPE1-Mb was photoirradiated without TEA and  $\text{NADP}^+$ , and then TEA and  $\text{NADP}^+$  were added in the dark reaction, (C) TEA was mixed with ZnPE1-Mb in photoirradiated process and then  $\text{NADP}^+$  was added in the dark reaction, and (D) ZnPE1-Mb, TEA and  $\text{NADP}^+$  were mixed and photoirradiated simultaneously. The experiment was carried out at with  $10\ \mu\text{M}$  of ZnPE1-Mb,  $1\ \text{M}$  of TEA, and  $5\ \text{mM}$  of  $\text{NADP}^+$  in a  $100\ \text{mM}$  phosphate buffer (pH 9.2).



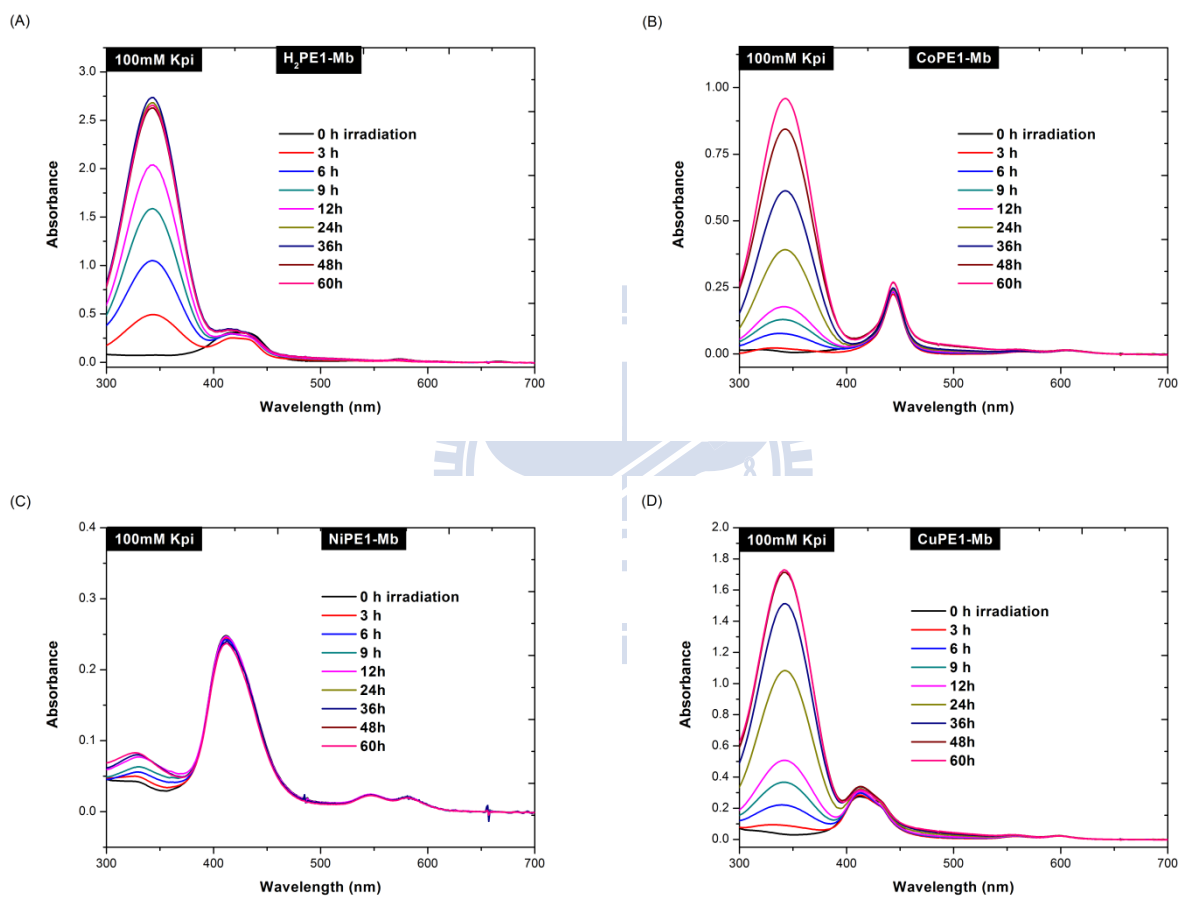
When TEA was added to the photoirradiated solution containing ZnPE1-Mb and NADP<sup>+</sup> in the dark reaction, very few NADPH was produced. Similar result was observed when both TEA and NADP<sup>+</sup> were added to the photoirradiated ZnPE1-Mb solution in the dark reaction. But when NADP<sup>+</sup> was added to the photoirradiated solution containing ZnPE1-Mb and TEA, NADPH formation occurred with the appropriate conversion efficiency as the reaction of ZnPE1-Mb, TEA and NADP<sup>+</sup> mixed and photoirradiated simultaneously. By inference, TEA might play an important role in this photochemical reduction system.

When ZnPE1-Mb/TEA existed simultaneously and be irradiated, the wavelength of Soret band was shifted to approximately 427 nm. Without TEA, the Soret band of ZnPE1-Mb just decayed and no peak shifted. (Fig. 4-29) We conjectured that photoirradiation might induce structural change in ZnPE1-Mb, and the peak shift might be attributed to the interaction of ZnPE1-Mb and TEA or the oxidation form of ZnPE1-Mb after irradiation. We will further try to separate and analyze this unknown complex.



**Figure 4-29 (A) Comparing the peak shift of ZnPE1-Mb after 12 h irradiation in different conditions, including ZnPE1-Mb only, ZnPE1-Mb/TEA, ZnPE1-Mb/NADP<sup>+</sup>, and ZnPE1-Mb/TEA/NADP<sup>+</sup>. (B) Magnify of Soret band**

Subsequently, we examined several kinds of irradiation conditions to analyze the conversion efficiency of different MtPE1-Mbs and MtPE1. These conditions include (a) MtPE1-Mbs/TEA/NADP<sup>+</sup> by continuous irradiation for 60 h (Fig. 4-30), (b) MtPE1-Mbs and TEA were photoirradiated for 5 h then added NADP<sup>+</sup> to keep in the dark for 5 days (Fig. 4-32), and MtPE1/TEA/NADP<sup>+</sup> were photoirradiated for 5 h and kept in the dark for 5 days. (Fig. 4-24)



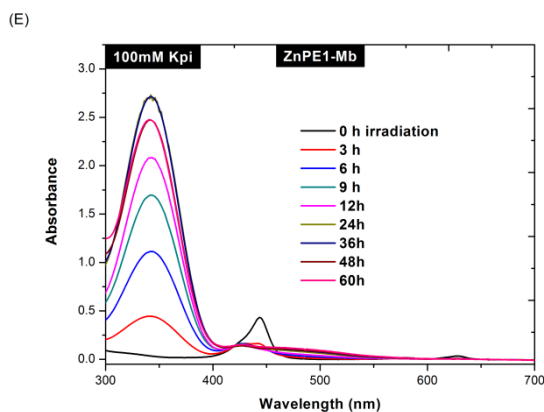


Figure 4-30 UV-Visible spectral change for 10 $\mu$ M MtPE1-Mb, 1M of TEA, and 5 mM of NADP<sup>+</sup> in 100 mM phosphate buffer (pH 9.2) upon continuous photoirradiation. (A) ZnPE1-Mb, (B) H<sub>2</sub>PE1-Mb, (C) CoPE1-Mb, (D) NiPE1-Mb, and (E) CuPE1-Mb.

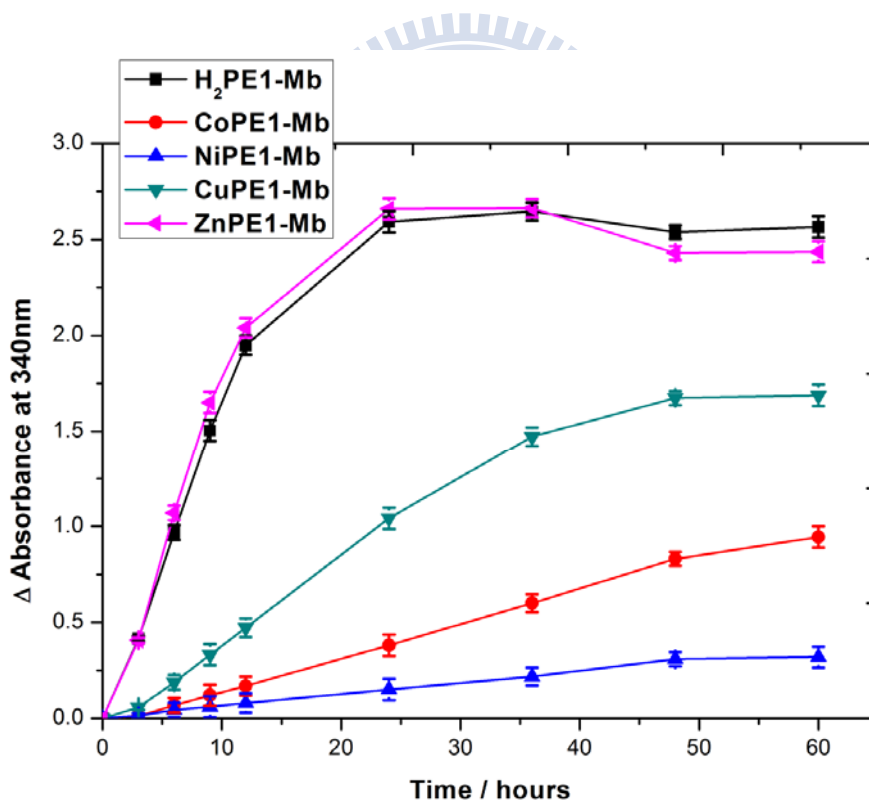


Figure 4-31 Absorbance change at 340 nm of the solution containing 10  $\mu$ M (a) H<sub>2</sub>PE1-Mb, (b) CoPE1-Mb, (c) NiPE1-Mb, (d) CuPE1-Mb, and (e) ZnPE1-Mb, 1 M of TEA, 5 mM of NADP<sup>+</sup> upon continuous photoirradiation.

According to the result showed in figure 4-31, continuous photoirradiation spend 4~10 folds of irradiation time to reach the same efficiency of 5 h irradiation. This result indicated that dark reaction is necessary.

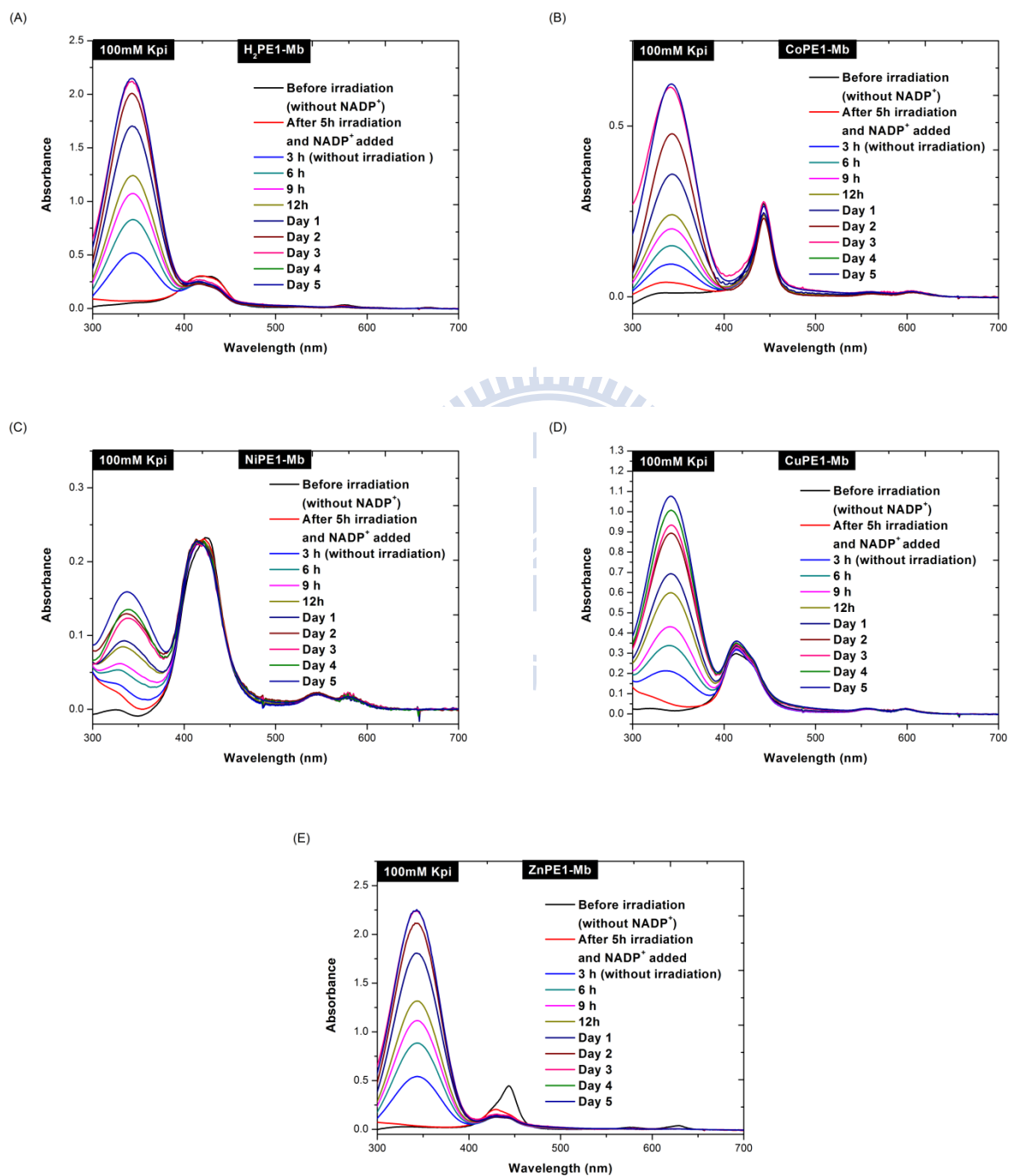


Figure 4-32 UV-Visible spectral change of (A) H<sub>2</sub>PE1-Mb, (B) ZnPE1-Mb, (C) CoPE1-Mb, (D)

NiPE1-Mb, and (E) CuPE1-Mb and TEA were photoirradiated for 5 h then added NADP<sup>+</sup> to keep in the dark for 5 days.

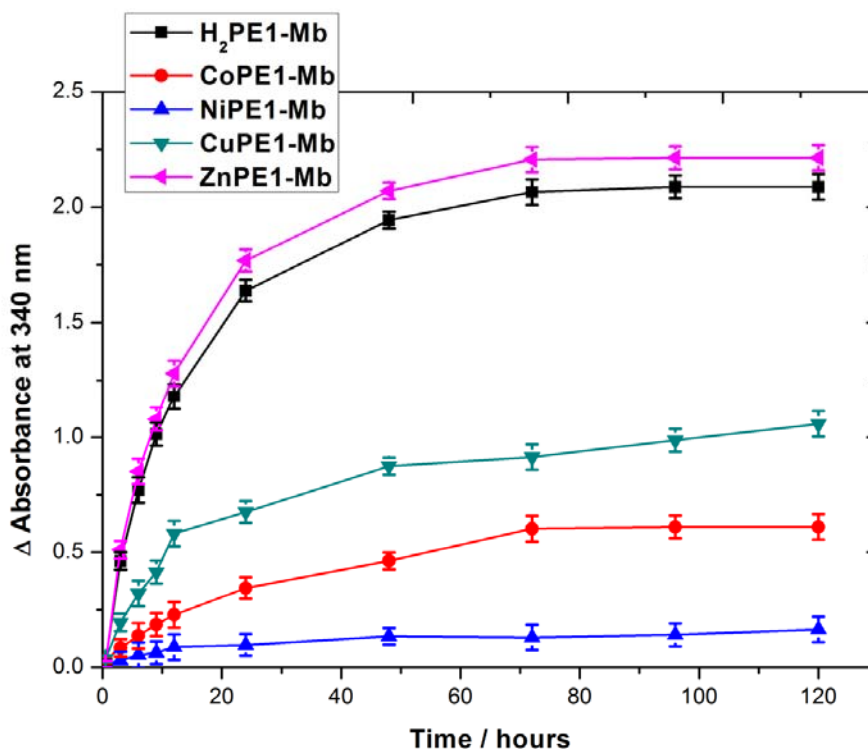
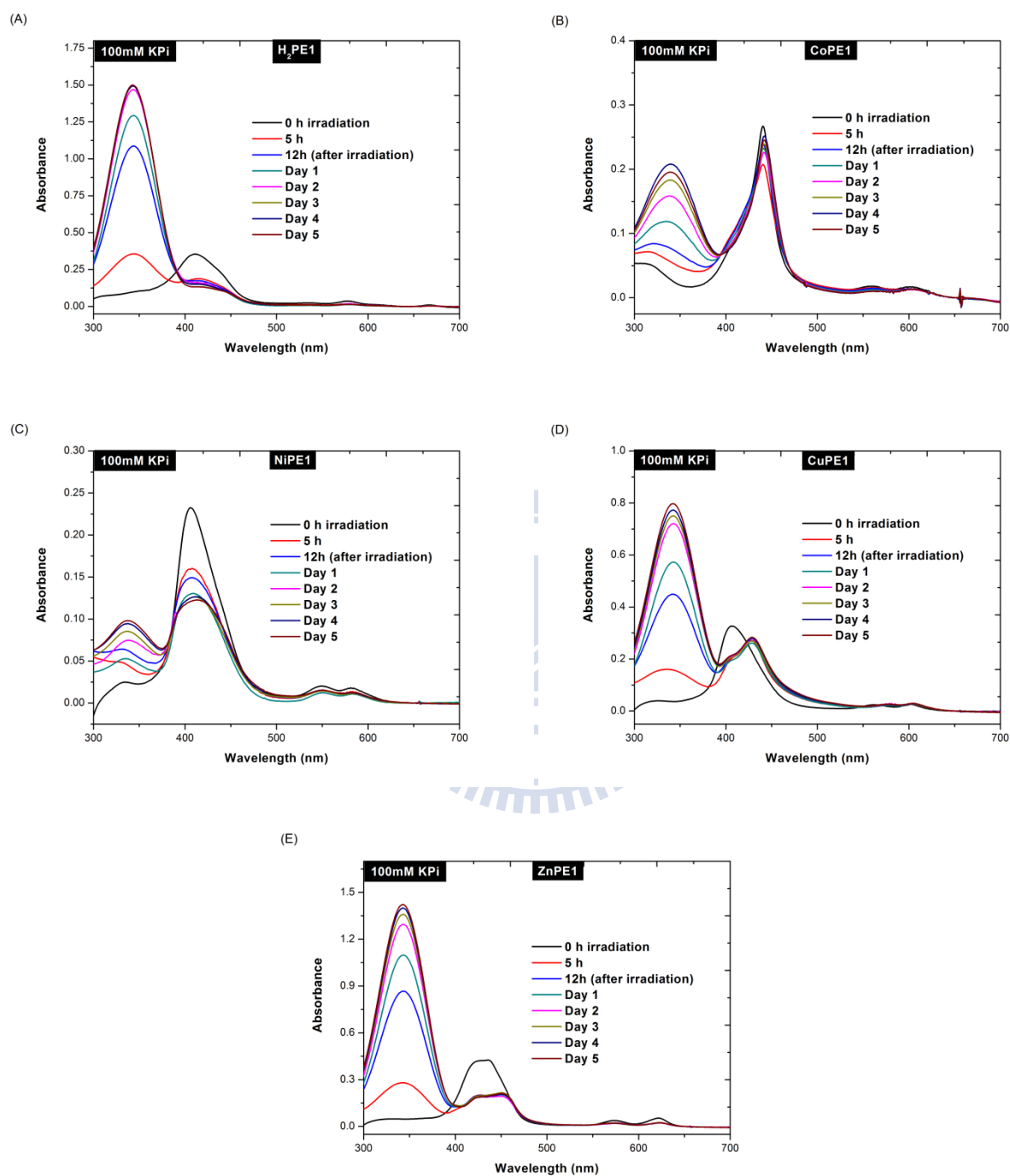


Figure 4-33 Absorbance change at 340 nm, (A) H<sub>2</sub>PE1-Mb, (B) ZnPE1-Mb, (C) CoPE1-Mb, (D) NiPE1-Mb, and (E) CuPE1-Mb and TEA were photoirradiated for 5 h then added NADP<sup>+</sup> to keep in the dark for 5 days.

MtPE1-Mbs and TEA were photoirradiated for 5 h then added NADP<sup>+</sup> to keep in the dark for 5 days, the conversion efficiency of it was approximate to that of MtPE1-Mb/TEA/NADP<sup>+</sup> photoirradiated for 5 h then kept in the dark for 5 days. We compared the results of different conditions, and found that the photoirradiation of MtPE1-Mb and TEA played an important role in the reaction. TEA was necessary to coexist with sensitizer (MtPE1-Mbs) to be excited. We supposed that high energy complex MtPE1-Mb<sup>\*</sup>/TEA is formed after irradiation. MtPE1-Mb<sup>\*</sup>/TEA existed at

least 2~3 days, and converted  $\text{NADP}^+$  to  $\text{NADPH}$  continuously.



**Figure 4-34 UV-Visible spectral change for 10 μM MtPE1, 1 M of TEA, and 5 mM of NADP<sup>+</sup> in 100 mM phosphate buffer (pH 9.2) upon 5 h photoirradiation. (A) H<sub>2</sub>PE1, (B) CoPE1, (C) NiPE1, (D) CuPE1 and (E) ZnPE1.**

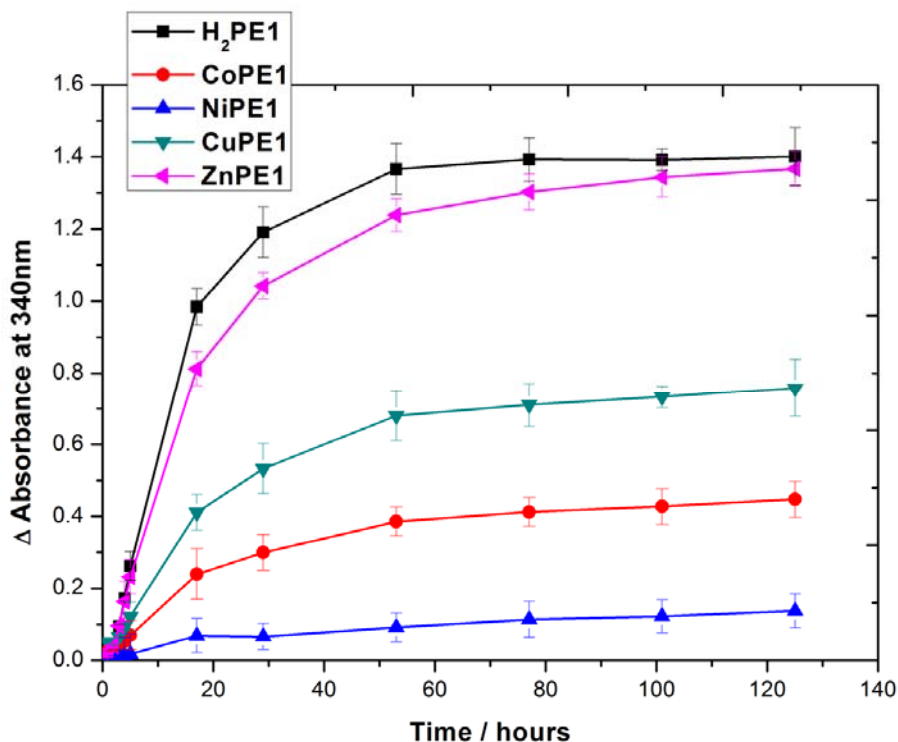


**Figure 4-35 Absorbance change at 340nm contains 10 $\mu$ M MtPE1, 1 M of TEA, and 5 mM of NADP<sup>+</sup> in 100 mM phosphate buffer (pH 9.2) upon 5h photoirradiation. (A) H<sub>2</sub>PE1, (B) CoPE1, (C) NiPE1, (D) CuPE1, and (E) ZnPE1.**

Comparing the result of MtPE1, ZnPE1 and H<sub>2</sub>PE1 had almost 100% conversion efficiency. The trend of conversion performance was similar with MtPE1-Mbs, but about 2-folds less than MtPE1-Mbs.

The conversion efficiency depended on the concentration of TEA, NADP<sup>+</sup>, sensitizer, pH, light intensity...etc. The pH is a factor to control the electrostatic interaction between MtPE1-Mb and NADP<sup>+</sup>. Mb has negative charge at pH 9.2, and more easily fascinate NADP<sup>+</sup> for NADPH formation. The concentration of photosensitizers also affected the conversion efficiency. (Fig. 4-36)

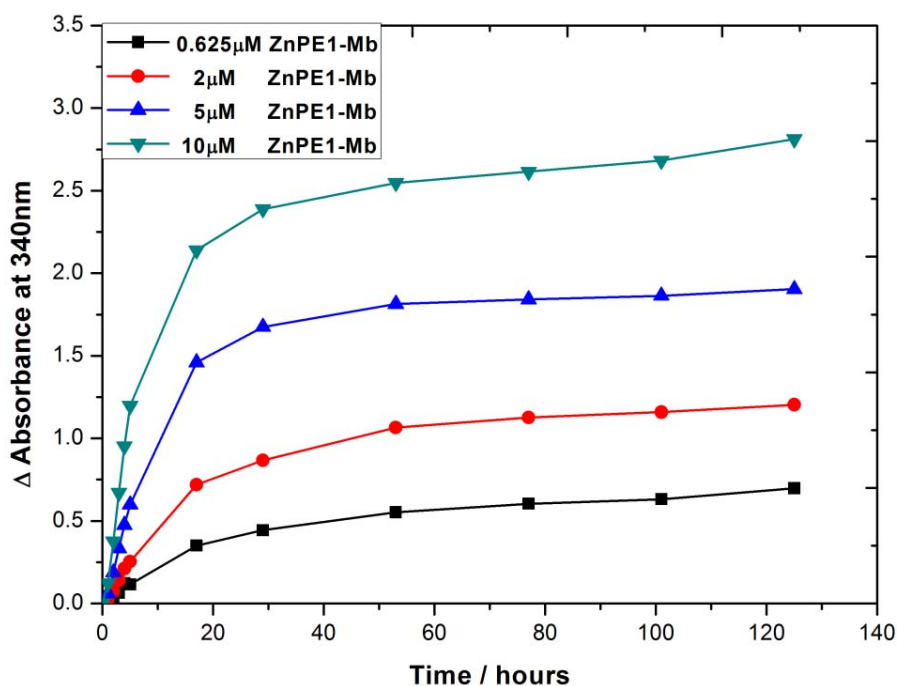


**Figure 4-36 Absorbance change in the solution containing 0.625, 2, 5, and 10  $\mu\text{M}$  of ZnPE1-Mb, 1M of TEA, and 5mM of  $\text{NADP}^+$  in 100mM phosphate buffer (pH 9.2) upon 5 h photoirradiation. (Appendix 1)**

The conversion efficiency also depended on the concentration of the sacrificial donor TEA. To determine the effect of the TEA, we performed the similar experiments as in figure 4-24 but changed the concentration of TEA. Figure 4-37 (A) showed the absorbance change at 340 nm with time. When the concentration of TEA was increased from 0 M to 1 M, the conversion efficiency was also increased. Figure 4-37 (B) showed the absorbance change at 340 nm vs. different concentration of TEA. The result showed when the concentration increased to 0.5 M; the formation of NADPH was conspicuous. 1 M of TEA could provide best conversion efficiency.



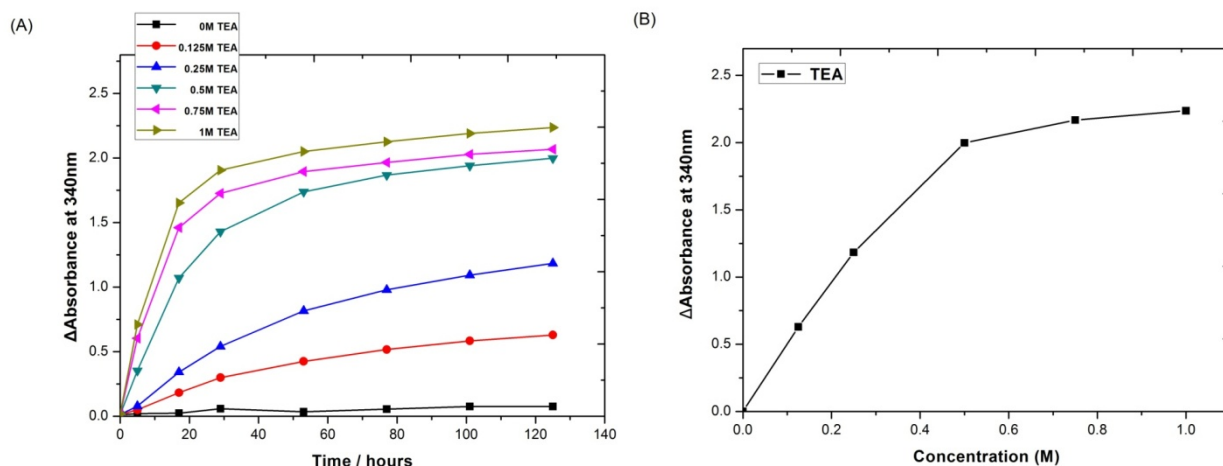


Figure 4-37 Test of TEA effect. (A) Similar experiment as Fig.4-24, but changed the concentration of TEA. (B) Combined overall efficiency after 5 days of different concentration TEA. (Appendix 2)

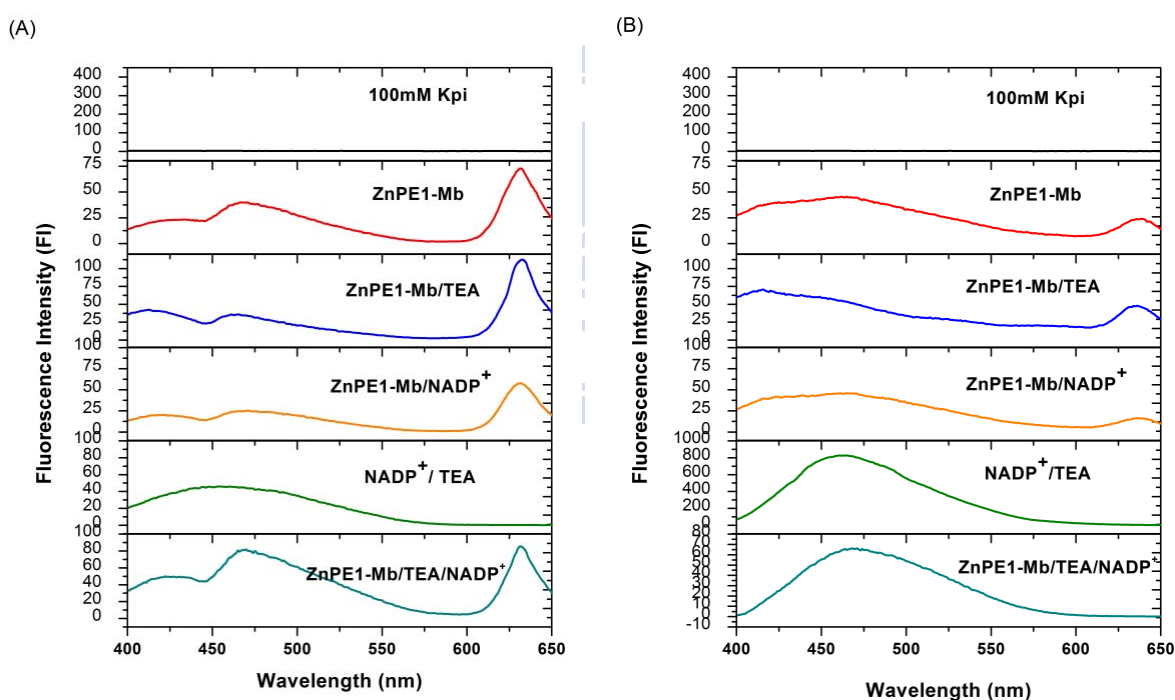
Table 4-7	Continued Photoirradiation	Photoirradiation & Dark reaction	Photoirradiation & Dark reaction (NADP <sup>+</sup> was added after 5hr photoirradiation)	Continued Dark reaction
ZnPE1		44%		0.46%
ZnPE1-Mb	85.2%	90%	82.6%	4.8%
H <sub>2</sub> PE1		44.8%		0.48%
H <sub>2</sub> PE1-Mb	84.6%	83.2%	81.2%	4.2%
CoPE1		16.6%		0.3%
CoPE1-Mb	30%	28%	18.8%	3.4%
NiPE1		4.4%		0.2%
NiPE1-Mb	4%	4.4%	5.2%	3%
CuPE1		24%		0.32%
CuPE1-Mb	54%	41.6%	34.2%	3.8%

Table 4-7 showed the summary results of NADPH formation for MtPE1-Mbs and MtPE1 in different conditions, every value in the table was the average value for three times repeat. Therefore, ZnPE1-Mb and H<sub>2</sub>PE1-Mb had the better conversion efficiency, but NiPE1 and NiPE1-Mb perform very poorly. Based on these results, reconstituted MtPE1-Mbs enhanced about 2-folds of conversion efficiency than MtPE1. The higher conversion efficiency of MtPE1-Mbs might be due to the electrostatic interaction between Mb and NADP<sup>+</sup>, increasing the opportunity to be reduced. In addition, MtPE1 reconstituted with Mb could avoid self-aggregation and prolong the lifetime of excited state.



## 4.6 Fluorescence analysis of ZnPE1-Mb before and after irradiation

We tried to analyze the variation of variety condition before and after photoirradiation with fluorescence analysis. In this experiment, we tried to find out the evidence of the MtPE1-Mb\*/TEA complex or the oxidized form of MtPE1-Mb. Comparing before and after photoirradiation with  $\lambda_{\text{ex}} = 340$  nm, the emission of Soret band decreased and the emission at 470 nm attributed to NADPH. (Fig. 4-38) Fluorescence emission comparison of variety condition were shown in figure 4-39, including 100 mM KPi, 1M TEA, 2.5 mM NADP<sup>+</sup>, 2.5 mM NADPH, NADP<sup>+</sup>+TEA. And we also compared the emission intensity of different NADPH concentrations. (Fig.4-40)



**Figure 4-38 The difference of fluorescence emission spectra for ZnPE1-Mb in variety condition: before (A) and after (B) photoirradiated with  $\lambda_{\text{ex}} = 340$  nm.**

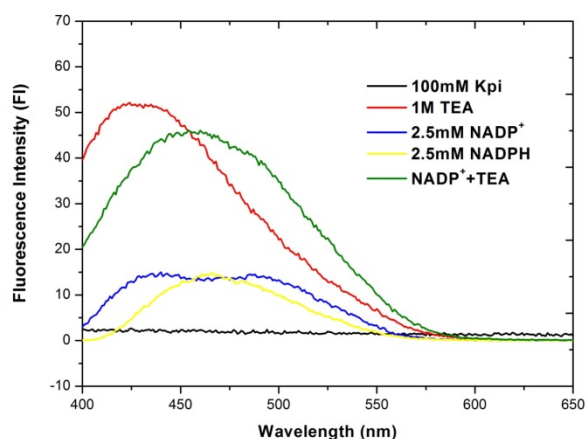


**Figure 4-39** Fluorescence emission comparison of variety condition, including 100 mM KPi, 1M TEA, 2.5 mM NADP<sup>+</sup>, 2.5 mM NADPH, NADP<sup>+</sup>+TEA.

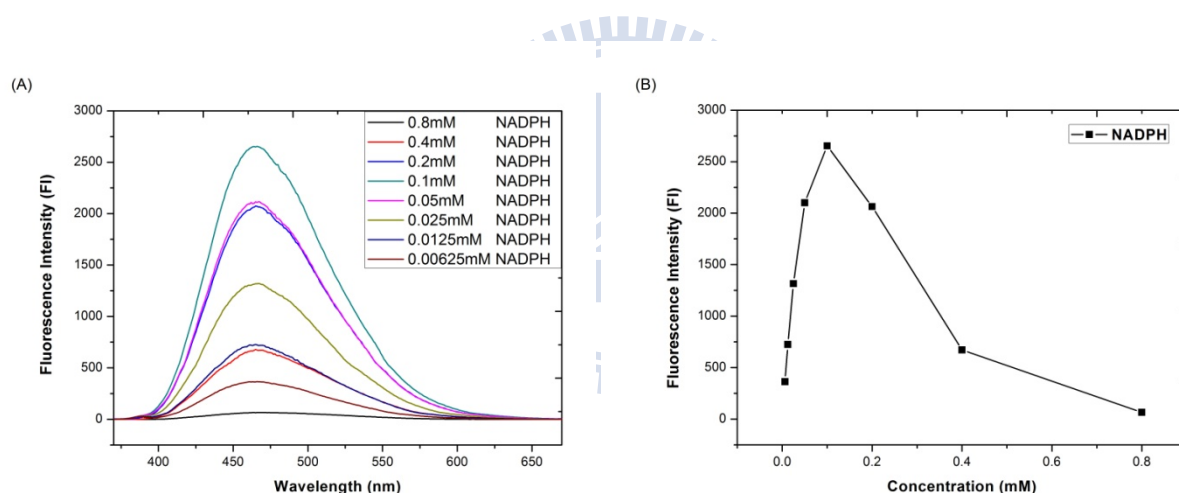


**Figure 4-40** The emission intensity of different concentration NADPH.

From this fluorescence analysis of ZnPE1-Mb in different conditions, there is no conspicuous change between different conditions with  $\lambda_{ex} = 340$  nm. A possible reason is the MtPE1-Mb<sup>\*</sup>/TEA complex or the oxidized form of MtPE1-Mb can't be excited at 340 nm. We need to try full-wavelengths scan of fluorescence analysis to see if there is any specific peak.

## 4.7 Photocurrent assay result

The components of our photocurrent setup could be separated into photoactivated-dye (MtPE1-Mbs), mesoporous dye-sensitized semiconductor ( $\text{TiO}_2$ ), electrolyte (100 mM Tris base, 0.5 M KCl, 0.03 M  $\text{I}_2$ , 0.1 M lithium iodide, pH 6.0), conducting glass (FTO) and cathode (Pt). Protein immobilization was achieved by immersing the  $\text{TiO}_2$  films ( $0.16 \text{ cm}^2$ ) in the  $5 \mu\text{M}$  MtPE1-Mbs solution (at  $4 \text{ }^\circ\text{C}$ ) for 2~3 days. UV-Vis absorption spectra of MtPE1-Mbs on  $\text{TiO}_2$  film were showed in figure 4-41. Besides the raising baseline of UV-Vis spectra caused by the scattering of  $\text{TiO}_2$  nanoparticles, the hypsochromic shift of the Soret bands in MtPE1-Mbs on  $\text{TiO}_2$  film indicated that MtPE1 might reside in a relatively hydrophobic site.

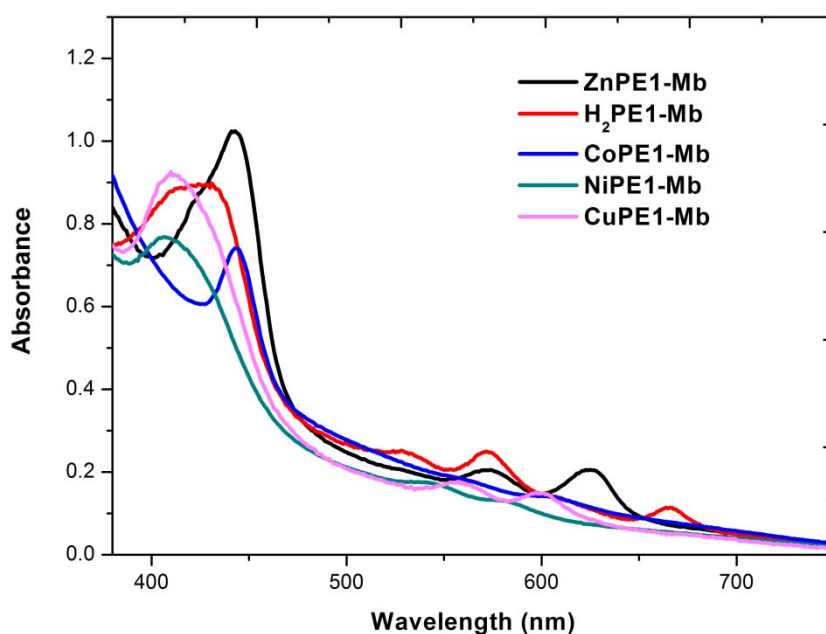
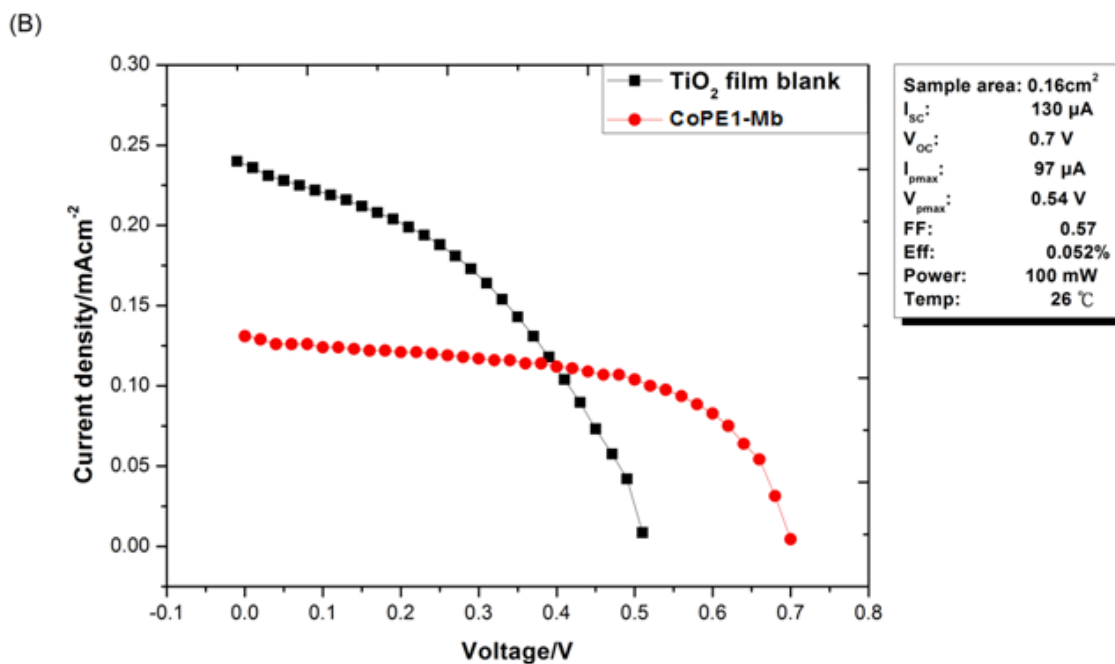
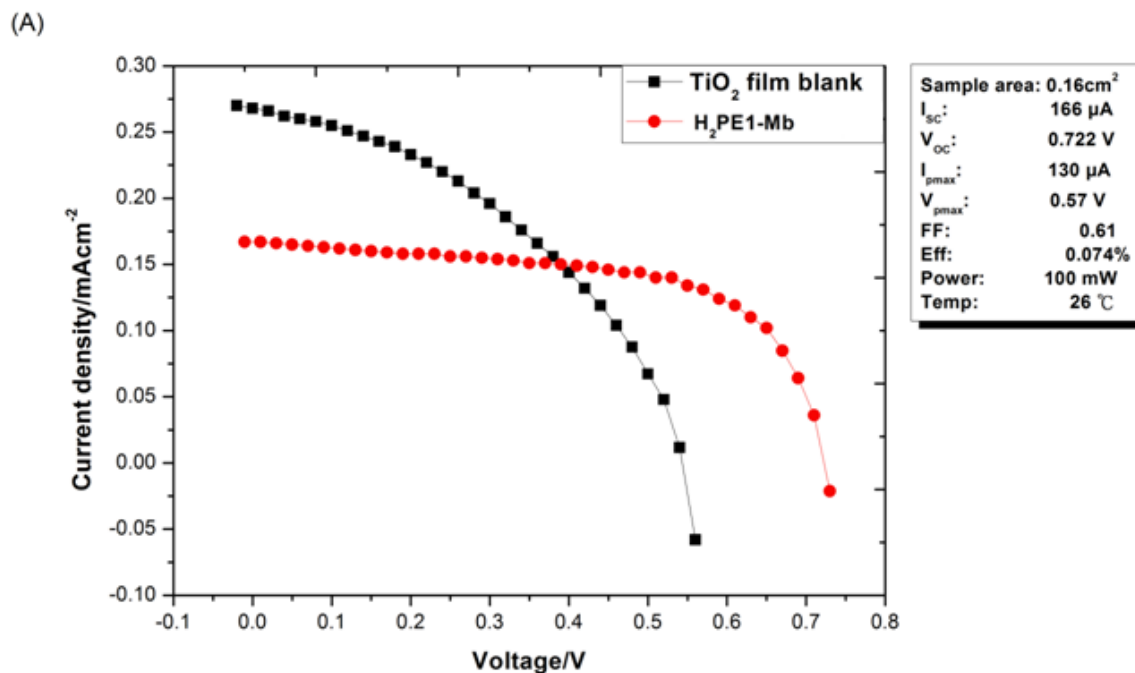


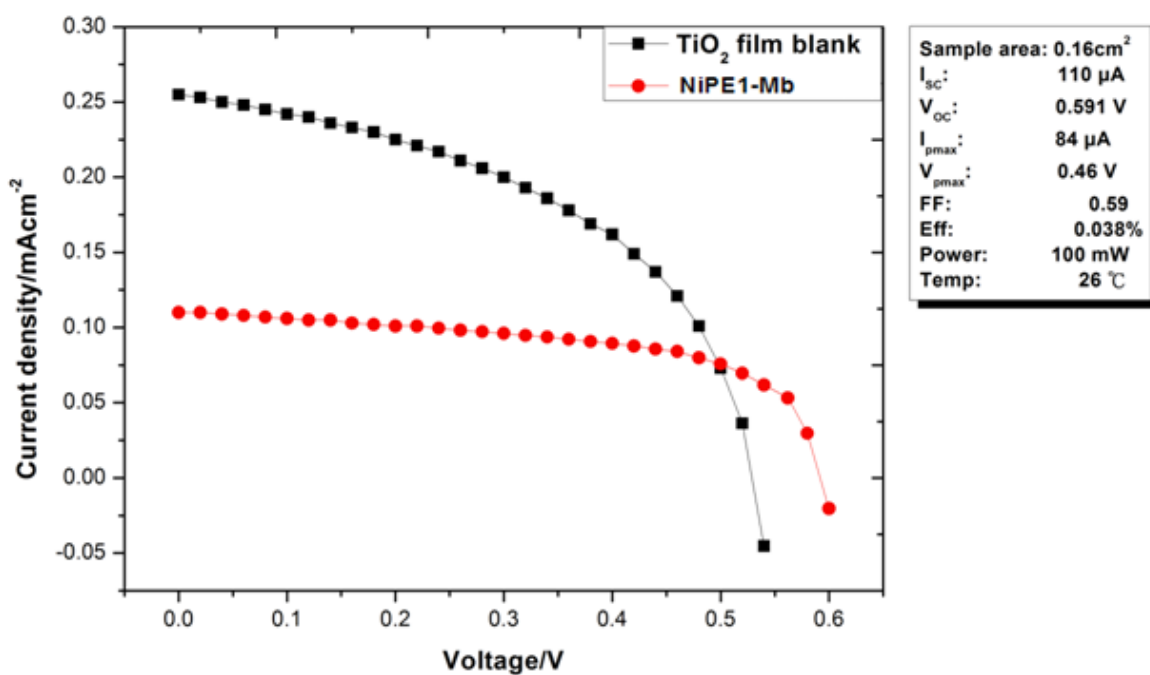
**Figure 4-41 UV-Vis absorption spectra of MtPE1-Mbs on  $\text{TiO}_2$  film**

The working electrode (FTO/ $\text{TiO}_2$ /MtPE1-Mbs), electrolyte (100 mM Tris base, 0.5 M KCl, 0.03 M  $\text{I}_2$ , 0.1 M lithium iodide, pH 6.0) and counter electrode (FTO/Pt) were sandwiched together for

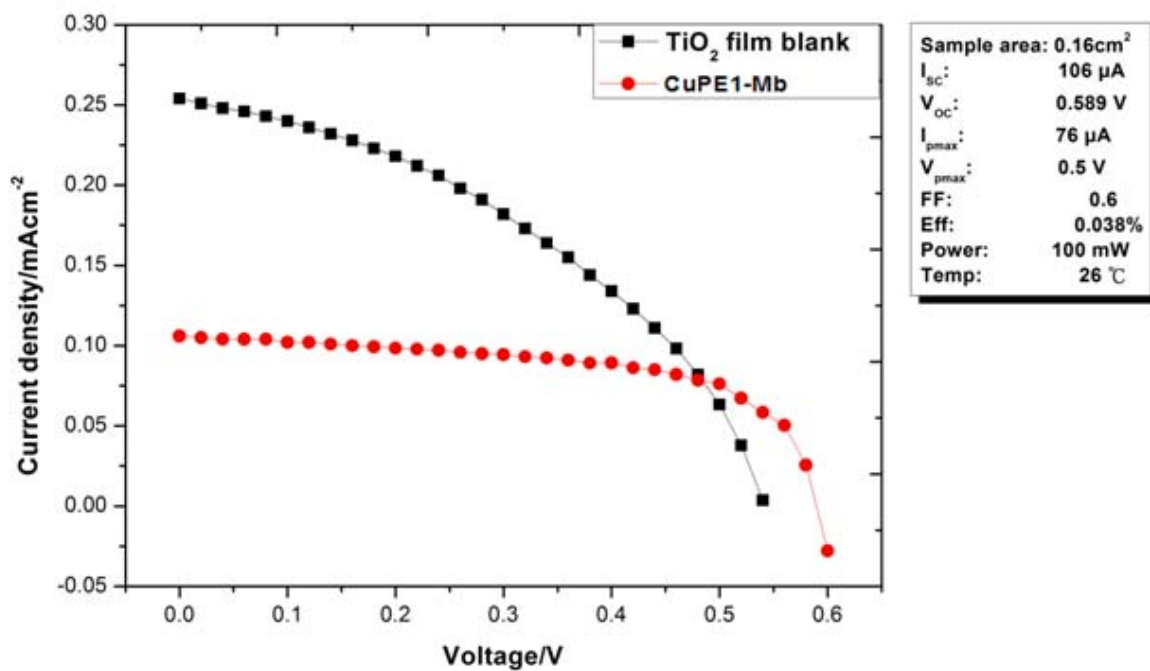
photocurrent measurement. And another cell which was used as blank was constructed in a similar process except that MtPE1-Mb was not involved (Working electrode has only FTO/TiO<sub>2</sub> and used as control). Then we detected photocurrent and compared their photovoltaic activity.



(C)



(D)



(E)

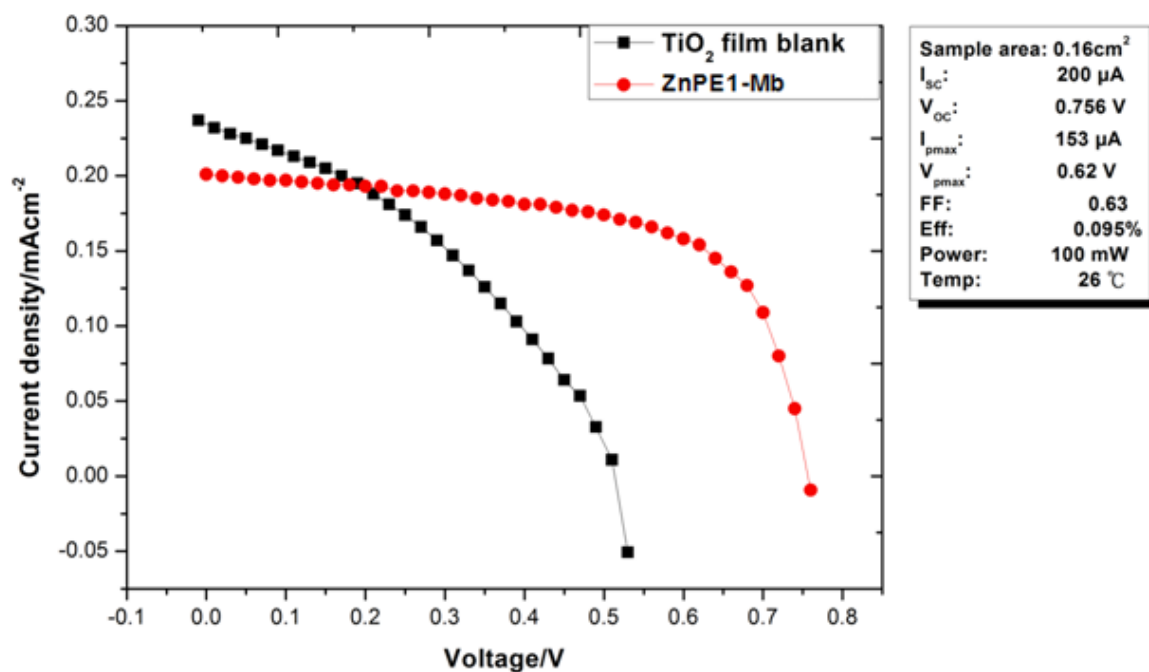


Figure 4-42 The photovoltaic characteristics of (A)H<sub>2</sub>PE1-Mb, (B)CoPE1-Mb, (C)NiPE1-Mb, (D)CuPE1-Mb, and (E)ZnPE1-Mb –sensitized solar cells. All measurements were performed under AM1.5 illumination (100 mW cm<sup>-2</sup>). For comparison, the individual blank TiO<sub>2</sub> films before sensitization are shown as red curves.



**Table 4-8**  
**Photovoltaic parameters of bio-sensitized solar cells under AM1.5 illumination (power 100 mW cm<sup>-2</sup>) with active area 0.16 cm<sup>2</sup>. For comparison, the values in parenthesis are the cell performances of the blank TiO<sub>2</sub> films measured before sensitization.**

Sensitizers	J <sub>sc</sub> /μA cm <sup>-2</sup>	V <sub>oc</sub> / V	FF	η (%)
H <sub>2</sub> PE1-Mb	166(270)	0.722(0.543)	0.61(0.41)	0.074(0.059)
CoPE1-Mb	130(240)	0.7(0.51)	0.57(0.41)	0.052(0.05)
NiPE1-Mb	110(255)	0.591(0.528)	0.59(0.48)	0.038(0.064)
CuPE1-Mb	106(254)	0.589(0.54)	0.6(0.41)	0.038(0.055)
ZnPE1-Mb	200(237)	0.756(0.513)	0.63(0.37)	0.095(0.045)

Based on the IV curve results shown in table 4-8, the conversion efficiencies (η) of ZnPE1-Mb absorbed on nanocrystalline TiO<sub>2</sub> film is little higher than other MtPE1-Mbs (H<sub>2</sub>, Co, Ni, Cu) like the result of photoreduction experiment, but the conversion efficiency is still low. By comparison, J<sub>sc</sub> of MtPE1-Mb-sensitized film are lower than TiO<sub>2</sub> blank, but the V<sub>oc</sub> and FF are higher than TiO<sub>2</sub> blank. And the conversion efficiency of MtPE1-Mb-sensitized films is higher than TiO<sub>2</sub> blank, except NiPE1-Mb and CuPE1-Mb. We conjectured that protein is easy to fall off because protein absorbed on TiO<sub>2</sub> film just by static electricity and aqueous phase electrolyte is also a factor to dissolved protein from TiO<sub>2</sub> film, so the electron can't transfer to TiO<sub>2</sub> efficiently. The first importance of future perspective is to find an ideal conductor for us to fix protein on it and don't destroy the protein structure.

## 5. Conclusion and future perspectives

We have gotten apo-Mb by MEK method and reconstituted apo-Mb with free-base and MtPE1 successfully. Comparison of reconstituted MtPE1-Mbs and MtPE1 in phosphate buffer (100 mM KPi, pH 6.8) and tetrahydrofuran (THF) to make sure that MtPE1 were successfully reconstituted with apo-Mb were analyzed by UV-Vis spectra. MtPE1 cannot be dissolved in phosphate buffer directly, so there is no absorption in UV-Vis spectrum. Reconstituted MtPE1 with apo-Mb can enhance the solubility in KPi buffer.

We also investigated steady-state emission fluorescence spectra of MtPE1-Mbs by exciting at 435 nm. This spectral feature provided strong evidence for the MtPE1 monomer reconstituted with the apo-Mb to form MtPE1-Mb in buffer solution. It also shows that metal ion in the center of porphyrin would cause the shift of emission peak.

Picosecond fluorescence transient spectra have been analyzed by time-correlated single-photon-counting system (TCSPC). The results show that ZnPE1-Mb and H<sub>2</sub>PE1-Mb in buffer have longer lifetime than ZnPE1 and H<sub>2</sub>PE1 in THF. CoPE1-Mb, NiPE1-Mb, and CuPE1-Mb in buffer have similar lifetime with CoPE1, NiPE1-Mb and CuPE1 in THF. The results show that reconstituted MtPE1-Mbs could retain MtPE1 in monomer when they were in buffer solution.

The redox properties of reconstituted MtPE1-Mbs have been studied by using cyclic voltammetry (CV). For CV study, all proteins have been adsorbed on the surface of working electrode (glass carbon electrode, GCE) which is modified with didodecyldimethylammonium bromide (DDAB), an electron shuttle to support the electron transfer between electrode and protein. We can use the reduction potential, oxidation potential, and cooperate with UV-Vis analysis to calculate the LUMO, HOMO, and band gap. Based on the CV data, we suggested that the electron transfer from TEA and MtPE1-Mb\* to NADP<sup>+</sup> successfully, except CoPE1-Mb.

A simple artificial photosynthetic system has been constructed by four major parts: light source (419 nm), photosensitizer (apo-Mb, MtPE1, MtPE1-Mbs), substrate (NADP<sup>+</sup>) and sacrificial electron donor (TEA). The hypothetical mechanism of photoinduced NADPH reduction is supposed that photosensitizer and sacrificial electron donor are photoirradiated to form some unknown catalysts which can further donate electron to substrate to cause the reduction reaction. Four kinds of reaction conditions have been used to elucidate the effect of photosensitizer and comparing the conversion efficiency of different photosensitizers: (1) continued photoirradiation, (2) photoirradiation and dark reaction, (3) photoirradiation (without substrate) and dark reaction (with substrate), and (4) continued dark reaction. The condition of photoirradiation and dark reaction has the best photo-induced NADPH conversion efficiency by using ZnPE1-Mb as photosensitizer. There has been approximately 100% of the NADP<sup>+</sup> converted to NADPH. It is interesting that we irradiated the complex of photosensitizers/TEA for 5 hours then added NADP<sup>+</sup> and kept the sample in the dark, could also induce the formation of NADPH. ZnPE1-Mb could be an ideal photosensitizer for us to further study catalyst formation and photoinitiation mechanism.

From this fluorescence analysis of ZnPE1-Mb in different condition, we tried to find out the evidence of the MtPE1-Mb<sup>\*</sup>/TEA complex or the oxidized form of MtPE1-Mb with  $\lambda_{\text{ex}} = 340$  nm. But there is no conspicuous change between different conditions with  $\lambda_{\text{ex}} = 340$  nm. A possible reason is the MtPE1-Mb<sup>\*</sup>/TEA complex or the oxidized form of MtPE1-Mb can't be excited at 340nm. We need to try full-wavelengths scan.

Based on the IV curve results, the conversion efficiencies ( $\eta$ ) of ZnPE1-Mb absorbed on nanocrystalline TiO<sub>2</sub> film is little higher than other MtPE1-Mbs (H<sub>2</sub>, Co, Ni, Cu), but the conversion efficiency is still low. We conjectured that protein is easy to fall off because protein absorbed on TiO<sub>2</sub> film just by static electricity and buffer phase electrolyte is also a factor to dissolved protein from TiO<sub>2</sub> film, so the electron can't transfer to TiO<sub>2</sub> efficiently. The first importance of future perspective is to find an ideal conductor for us to fix protein on it and don't destroy the protein structure.

Therefore, the present study provides the first practical example to make BSSC devices using artificial proteins as potential photosensitizers. Although the conversion efficiency remains improvable when compared to the typical DSSC, improvement for the cell performance is predictable. Work is in progress to further improve the cell performance of the BSSCs under investigation by increasing the adsorption of the proteins on TiO<sub>2</sub> films in a better experimental condition and by looking for more appropriate bio-related electrolytes. And we also try to find a more ideal protein conductor.



## 6. References

- (1) [http://en.wikipedia.org/wiki/Solar\\_energy](http://en.wikipedia.org/wiki/Solar_energy).
- (2) Morton, O. *Nature* 2006, 443, 19-22.
- (3) Gra"tzl, M. *Chem. Lett.* 2005, 34, 8.
- (4) Hu, X.; Damjanovic, A.; Ritz, T.; Schulten, K. *Proc Natl Acad Sci U S A* 1998, 95, 5935-41.
- (5) Lu, Y.; Xu, J.; Liu, B.; Kong, J. *Biosens Bioelectron* 2007, 22, 1173-85.
- (6) Raven, P. H.; Evert, R. F.; Eichhorn, S. E. *Biology of Plants* 2005, 124-127.
- (7) Chen, X. H.; Zhang, L.; Weng, Y. X.; Du, L. C.; Ye, M. P.; Yang, G. Z.; Fujii, R.; Rondonuwu, F. S.; Koyama, Y.; Wu, Y. S.; Zhang, J. P. *Biophys J* 2005, 88, 4262-73.
- (8) Suemori, Y.; Fujii, K.; Ogawa, M.; Nakamura, Y.; Shinohara, K.; Nakagawa, K.; Nagata, M.; Iida, K.; Dewa, T.; Yamashita, K.; Nango, M. *Colloids Surf B Biointerfaces* 2007, 56, 182-7.
- (9) Lam, K. B.; Irwin, E. F.; Healy, K. E.; Lin, L. *Sensors and Actuators B* 2006, 117, 480-487.
- (10) Das, R.; Kiley, P. J.; Segal, M.; Norville, J.; Yu, A. A.; Wang, L. *Nano Letters* 2004, 4, 1079-1083.
- (11) Katterle, M.; Prokhorenko, V. I.; Holzwarth, A. R.; Jesorka, A. *Chem. Phys. Lett.* 2007, 447, 284-288.
- (12) Yidong Lu, J. X., Baohong Liu, Jilie Kong *Biosensors and Bioelectronics* 2007, 22, 1173-1185.
- (13) Lu, Y.; Yuan, M.; Liu, Y.; Tu, B.; Xu, C.; Liu, B.; Zhao, D.; Kong, J. *Langmuir* 2005, 21, 4071-6.
- (14) Ordway, G. A.; Garry, D. J. *J Exp Biol* 2004, 207, 3441-6.
- (15) Kendrew, J. C.; Bodo, G.; Dintzis, H. M.; Parrish, R. G.; Wyckoff, H.; Phillips, D. C.

*Nature* 1958, 181, 662-6.

(16) Takano, T. *J Mol Biol* 1977, 110, 569-84.

(17) Takafumi Ueno, T. K., Satoshi Abe, Norihiko Yokoi, Masataka Ohashi, Hiroshi Nakajima, Yoshihito Watanabe *Journal of Organometallic Chemistry* 2007, 692, 142-147.

(18) Zahavy, E.; Willner, I. *J. Am. Chem. Soc.* 1996, 118, 12499-12514.

(19) Abe, S.; Ueno, T.; Reddy, P. A.; Okazaki, S.; Hikage, T.; Suzuki, A.; Yamane, T.; Nakajima, H.; Watanabe, Y. *Inorg Chem* 2007, 46, 5137-9.

(20) Immoos, C. E.; Di Bilio, A. J.; Cohen, M. S.; Van der Veer, W.; Gray, H. B.; Farmer, P. J. *Inorg Chem* 2004, 43, 3593-6.

(21) Heleg-Shabtai, V.; Gabriel, T.; Willner, I. *J. Am. Chem. Soc.* 1999, 121, 3220-3221.

(22) Hayashi, T.; Hisaeda, Y. *Acc Chem Res* 2002, 35, 35-43.

(23) Luo, L.; Lo, C. F.; Lin, C. Y.; Chang, I. J.; Diao, E. W. *J Phys Chem B* 2006, 110, 410-9.

(24) Hu, Y.-Z.; Tsukiji, S.; Shinkai, S.; Oishi, S.; Hamachi, I. *J. Am. Chem. Soc.* 2000, 122, 241-253.

(25) Katsuhiko Nishiyama, Y. M., Midori Kishita, Chiho Yamada, Rumiko Kitagawa, Isao Taniguchi *Chemistry Letters* 2005, 34, 1032.

(26) Katsuhiko Nishiyama, M. U., Yasuhiro Mie, Isao Taniguchi *Chemistry Letters* 1999, 28, 357.

(27) Teale, F. W. *Biochim Biophys Acta* 1959, 35, 543.

(28) Andrew W. Axup, M. A., Stephen L. Mayo, Robert J. Crutchley, Harry B. Gray *J. Am. Chem. Soc.* 1988, 110, 435-439.

(29) Shen-Ming Chen, C.-C. T. *Journal of Electroanalytical Chemistry* 2005, 575, 147-160.

(30) Nassar, A.-E. F.; Bobbitt, J. M.; Stuart, J. D.; Rusling, J. F. *J. Am. Chem. Soc.* 1995, 117, 10986-10993.

(31) Peterson M. Guto, J. F. R. *Electrochemistry Communications* 2006, 8, 455-459.

(32) Ribo, J. M.; Crusats, J.; Farrera, J.-A.; Valero, M. L. *Chem. Commun.* 1994, 681-682.

(33) Choi, M. Y.; Pollard, J. A.; Webb, M. A.; McHale, J. L. *J. Am. Chem. Soc.* 2003, 125, 810.

(34) Okada, S.; Segawa, H. *J. Am. Chem. Soc.* 2003, 125, 2792.

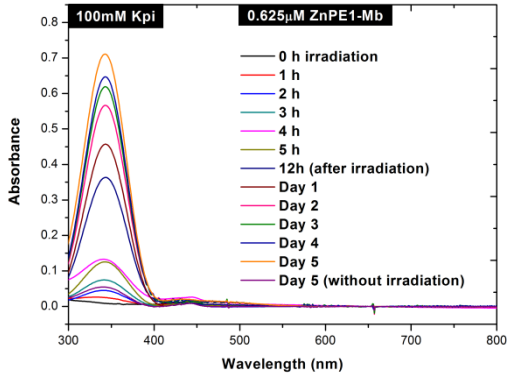
(35) Qingwen Li, G. L., Jun Feng *Electroanalysis* 2001, 13, 359-363.



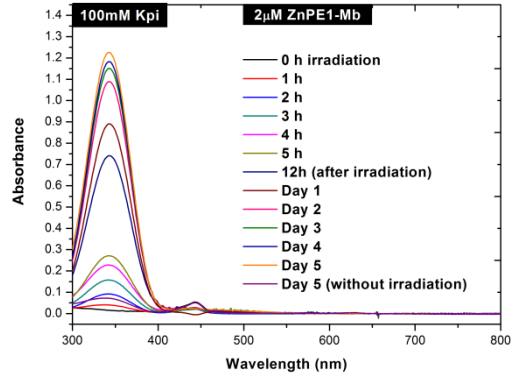
# 7. Appendix

## 1. Different concentration ZnPE1-Mb

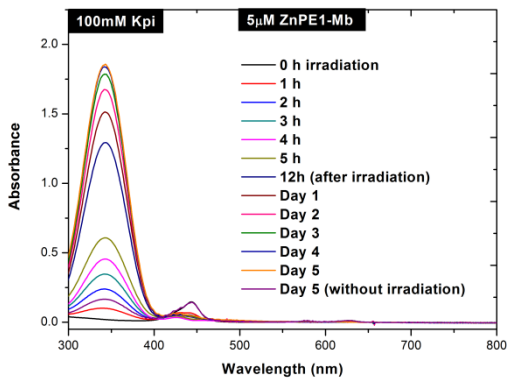
(A)



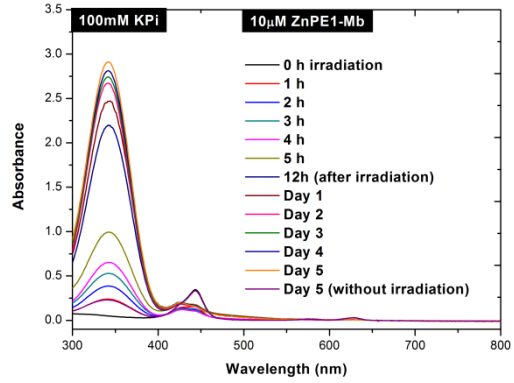
(B)



(C)



(D)





## 2. Dfferent concentration TEA

